Data-driven model reference control in the frequency-domain From model reference selection to controller validation

Pauline Kergus

ONERA
THE FRENCH AEROSPACE LAB

THÈSE

En vue de l'obtention de l'

DOCTORAT DE L'UNIVERSITÉ DE TOULOUSE

Délivrée par : *l'Institut National Polytechnique de Toulouse (INP Toulouse)*

Présentée et soutenue le *18/10/2019* **par :**

PAULINE KERGUS

Data-driven model reference control in the frequency-domain
From model reference selection to controller validation

JURY

MARCO CAMPI	Professeur, University of Brescia	Rapporteur
ALIREZA KARIMI	Professeur, EPFL	Rapporteur
HÅKAN HJALMARSSON	Professeur, KTH	Examinateur
GÉRARD SCORLETTI	Professeur, École Centrale de Lyon	Examinateur
SIMONE FORMENTIN	Assistant professeur, Politecnico di Milano	Examinateur
MARTINE OLIVI	Chargée de Recherche, INRIA	Examinateur
FABRICE DEMOURANT	Ingénieur de recherche, ONERA	Directeur de thèse
CHARLES POUSSOT-VASSAL	Ingénieur de recherche, ONERA	Directeur de thèse

---

École doctorale et spécialité :
EDSYS : Automatique 4200046
Unité de Recherche :
ONERA, The French Aerospace Lab, F-31055 Toulouse, France
Directeurs de Thèse :
Fabrice Demourant Charles Poussot-Vassal
Rapporteurs :
Marco Campi et Alireza Karimi

Data-driven model reference control in the frequency-domain

From model reference selection to controller validation

Pauline Kergus

Acknowledgements

First of all, I would like to thank my thesis advisors, Charles Poussot-Vassal and Fabrice Demourant for giving me the chance to pursue this thesis. I also thank the doctoral school EDSYS for having granted me the necessary funding from the Ministry of Higher Education and Research, but also for the fellowship I obtained to go for a mobility during my thesis.

I would like to thank Marco Campi and Alireza Karimi for their reviews of this manuscript but also for their interesting feedback on my work. I also thank all the members of the committee for having accepted to be a part of my defence which was a very special and wonderful day for me.

I especially thank Simone Formentin and Martine Olivi for hosting me in their respective teams at Politecnico di Milano and INRIA Sophia Antipolis. I would not have such a wide range of scientific interests without you. Our collaborations, that I hope to maintain in the future, were fruitful experiences.

I am very grateful to Charles Poussot-Vassal for putting me in touch with Martine Olivi and Simone Formentin. Thank you also for your guidance, your patience, your interest and your constructive feedbacks. But mostly, I would like to thank you for having always treated me as a colleague. I would also like to thank Pierre Vuillemin for his help during my thesis and for giving me the opportunity to supervise my first master student. Then, I thank Basile Bouteau who was an excellent master student and made this experience significant and enjoyable. Finally, I would like to thank all the people in the DTIS department at ONERA who helped me during my thesis on different levels, with a particular thought for Valérie Cassignol who made administrative tasks much easier, and for Claire Saurel, who supported me and encouraged me to stand up for my convictions.

I would also like to thank Bruno Sareni for giving me the opportunity to teach at ENSEEIHT. I also thank all the people with whom I worked at ENSEEIHT.

Obviously, these past three years would have been much less enjoyable without all the people I met in the department. First, I am very grateful to all the people with whom I shared the office during my thesis: Adèle, Guillaume, Mathieu, Manu, Matteo, Gustav, Sovanna, Cédric and Edouard. Thank you for your help when I needed some, for your support, your jokes, etc... I also have a special thought for Mehdi and Vincent who started their PhDs at the same time and got through with it alongside with me. A special thank also for Sébastien and Valentin for taking all of us to almost forced coffee breaks (but we all needed them). You are also the ones who made me play futsal, and this is a considerable achievement. Thanks also to Charles, Pierre, Cédric, Mario and all those I forget for the numerous afterworks.

Adèle, these acknowledgements would not be complete without a special word for

you: your friendship filled my days with joy and happiness while you were there.

I would also like to thank Swann for introducing me to his nice group in LAAS (better late than never). Of course, I am especially grateful to Victor, who has demonstrated an unfailing support in these last complicated months, it means a lot to me. Thanks also to his family and particularly to his brothers for keeping an eye on my cat while I travel around.

I would like to thank my family and friends for their encouragements all along my thesis. I cannot cite all of you but I am very grateful to all the people who have been a part of my life during this PhD.

The downside of all this is that these three years went way too fast, but I will cherish these precious memories.

Résumé

Dans de nombreuses applications, aucun modèle physique du système n'est facilement disponible, il s'agit alors de contrôler le système uniquement à partir de mesures entrées-sorties. Deux types d'approches sont envisageables : identifier un modèle du système puis l'utiliser afin de synthétiser un contrôleur, ce sont les méthodes indirectes, ou identifier le contrôleur directement à partir des données du système, ce sont les méthodes directes. Cette thèse se concentre sur les méthodes directes : l'objectif du travail présenté est de mettre en place une nouvelle méthode directe basée sur des données fréquentielles du système à contrôler.

Après un tour d'horizon des méthodes directes existantes, la méthode proposée est introduite. Il s'agit de résoudre un problème de suivi de modèle de référence dans lequel le problème d'identification est déporté du système vers le contrôleur. Dans ce cadre, deux techniques d'identification sont considérées dans cette thèse : l'interpolation de Loewner et l'approche des sous-espaces. De plus, une analyse préliminaire des données fréquentielles disponibles permet de connaître les limites en performances du système et, par conséquent, de choisir des spécifications atteignables. Enfin, une analyse de la stabilité en boucle fermée permet d'obtenir un contrôleur stabilisant d'ordre réduit. Tout au long de ce travail, les différentes étapes de la méthode sont appliquées progressivement sur des exemples numériques. Pour finir, la méthode proposée est appliquée sur deux systèmes irrationnels, décrits par des équations aux dérivées partielles: un cristalliseur continu et un canal de génération hydroélectrique. Ces deux exemples sont représentatifs de la catégorie de systèmes pour lesquels utiliser une méthode de contrôle directe est plus pertinent.

Abstract

In many applications, no physical description of the plant is easily available and the control law has to be designed on the basis of input-output measurements only. Two control strategies can then be considered : one can either identify a model of the plant and then use any kind of model-based technique (indirect methods) to obtain a control law, or use a data-driven strategy that directly compute the controller from the experimental data (direct methods). This work focuses on data-driven techniques : the objective of this thesis is to propose a new data-driven control technique based on frequency-domain data collected from the system to be controlled.

After recalling some basics in feedback control, an overview of data-driven control is given. Then, the proposed method is introduced. It is a model reference technique where the identification problem is moved from the plant to the controller. In this work, two identification techniques are used to that purpose: the Loewner framework and the subspace approach. In addition, a preliminary analysis of the available frequency-domain data allows determining the performance limitations and selecting achievable specifications. Finally, a stability condition, already known in data-driven control, is used during the reduction of the controller to ensure closed-loop internal stability. Along this thesis, the different steps of the method are progressively applied on two numercial examples. In the end, the proposed technique is applied on two irrational systems described by partial differential equations: a continuous crystallizer and an open-channel for hydroelectricity generation. These two examples illustrate the type of applications for which using a data-driven control method is indicated.

Notations and acronyms

Notations

$\imath$	Complex variable $\imath = \sqrt{-1}$
$\imath\mathbb{R}$	Imaginary axis
s	Laplace variable
I_n	Identity matrix of size n
A^*	Transpose and complex conjugate of A
†	Moore-Penrose inverse
$A \cdot B$	Entry-by-entry multiplication

Acronyms

LTI	Linear Time Invariant
pLTI	parametric-LTI
RHP	Right-Half Plane
NMP	Non-Minimum Phase
SISO	Single Intput - Single Output
MIMO	Multi Intput - Multi Output
BIBO	Bounded Input - Bounded Output
SVD	Singular Value Decomposition
SNR	Signal to Noise Ratio
FRF	Frequency Response Function
FFT	Fast Fourier Transform
CbT	Correlation-based Tuning
IFT	Iterative Feedback Tuning
VRFT	Virtual Reference Feedback Tuning
MFAC	Model-Free Adaptive Control
ILC	Iterative Learning Control
I4C	Identification for Control

Contents

Part I

Introduction

Chapter 1

Introduction to data-driven control

1.1 Context and motivations

For many applications, a mathematical description of the system, derived from physical laws, is not available. In this case, the controller has to be designed on the basis of experimental measurements. Given some input-output data collected on a system, two different strategies can be employed to design a controller. The first one consists in identifying a model of the plant and then using any kind of model-based technique to obtain a control law, and is called **indirect methods**. On the other side, the data-driven strategy directly computes the controller from the experimental data. Such techniques are also called **direct methods**. Data-driven and model-based control are two parts of control theory that do not address the same classes of problems.

1.1.1 Model-based control and data-driven control

Concerning the model-based strategy, the control performances directly depend on the amount of under-modelling of the true system. However, modeling errors are inevitable when it comes to identify a process on the basis of experimental data. To address this issue in model-based theory, robust control theory emerged and proposed to consider noise and uncertainties in the model or the parameters. Therefore, this type of approach is indicated for problems where a reliable model with bounded modeling errors is available. Considering descriptions of modeling errors, it is then possible to guarantee that the obtained controller is robust enough in case the model does not represent exactly the actual system, as long as the true system stays in the defined set of uncertainties around the nominal model. The main challenge is then to correctly describe the model uncertainties, which is not a trivial question since in most cases, identification techniques do not give enough information regarding the error between the obtained model and the actual plant to construct such a model. It should also be noted that an accurate model often has an important order, which complicates the resolution of the control design problem. Depending on the employed model-based technique, the complexity of the obtained controller may increase with the order of the identified model of the plant. From a control perspective, structured model-based control have been developed to address this problem and to be able to limit the order of the designed controller by structuring it. It should be noted that the area of system

identification grew a lot to be able to expand the fields of applications for model-based control technique for applications where a model cannot be derived from first principles. For this reason, identification for control (I4C) emerged: the objective of I4C is to design a model appropriate for control design, instead of looking for the true system. I4C often consists in iterating the identification and control steps to improve the quality of the model regarding the control performances. However, the obtained control-oriented models are uncertain and one of the major issue was to identify these models uncertainty to study the robustness of the resulting controllers. Finally, finding a model that is accurate and at the same time simple enough to design a controller, and finding appropriate bounds for the associated uncertainties, can still be too time-consuming, too complex or too costly, for some applications.

For this type of applications, data-driven techniques should be considered. Direct data-driven methods are not sensitive to modelling errors since the selection of the controller is done directly from the experimental data. They are also less conservative. Moreover, they are less time-consuming since the modelling and/or identification steps are skipped and the resulting control law is tailored to the actual system. In [Hjalmarsson, 2005], it is recalled that modelling represents 75% of the efforts in control projects. Of course, one could argue that the model of the plant considered in model-based strategy can be used for other purposes (stability and robustness analysis, simulation, etc...). However, recent developments of data-driven techniques allow to deal with robust control design specifications. Furthermore, different techniques have been proposed to handle stability considerations in different data-driven frameworks. Finally, when it comes to simulation purposes, the models employed to this aim are often too complex to be used for controller design through model-based approaches.

Nevertheless, data-driven approaches suffer some drawbacks. The first one is that, as said in [Safonov and Tsao, 1994], experimental data only represent a subset of the physical system's behaviour. Only the dynamics exhibited by the available data will be controlled by such techniques while robust control techniques will consider a set of plant's dynamics. Furthermore, since no plant model is available in a data-driven framework, it is not possible to have any closed-loop simulations or any stability and/or robustness guarantees. The advantage of model-based techniques such as robust control is to address these problems by considering a nominal model and a surrounding envelope containing the possible plant's behaviour. The definition of a model set in indirect control approaches is based on an upper bound for the modelling error: this bound can be chosen to be conservative or on the basis of the available data. In this last case, it should be noted that, as said in [Safonov and Tsao, 1994], the data can only provide a lower bound on the plant uncertainty since it does not represent the complete system's behaviour. This is why it is said in [Brozenec et al., 2001]:

"*Control theory makes no claims about the performance or stability of physical systems; only about their models.*"

The same stands for data-driven control: direct techniques cannot go further than the available data.

The conclusion of these remarks is that these two strategies, model-based and data-driven, are complementary in the sense that they do not address the same categories of

problems. If a reduced-order and accurate model, suitable for model-based control, is available, then a model-based approach should be considered. This is also the case if the model is uncertain but these uncertainties can be simply and accurately described. If it is not the case because the identification step is too complicated compared to the stakes of the considered application, data-driven control stands as the perfect alternative. It should be noted that the complexity of model identification depends on the considered application: is it a critical system? what is at stake when using this system (human lives, expensive experimental set-ups, etc...)? The answers to these questions are important to determine the importance of system identification. A survey of data driven control techniques, and the trends and challenges regarding data-driven control in general, is proposed in [Hou and Wang, 2013]. The complementarity of these two types of control theory is perfectly expressed in this paper as follows:

"*[Model-based control] starts and ends with the model. To some extent, it may be called model theory rather than control theory.*".

Another comparison between a model-based and a data-driven technique has been proposed in [Formentin et al., 2014b] and emphasize that using data-driven techniques implies a larger variance of the controller parameters than model-based control design, but it also can lead to a lower control cost.

1.1.2 Developments of the data-driven control community

Numerous direct methods have been proposed in the literature. The first known direct control technique is the data-driven design of PID controllers proposed in the pioneer work of Ziegler and Nichols in the 40's [Ziegler and Nichols, 1942]. This work allows to set the parameters values of a PID controller according to experimental measurements. For the first time, a technique answers the need for a practical tuning method that does not involve a too difficult step of system analysis and identification. In the 90's, other direct techniques to tune PID controllers have been proposed, see [Åström and Hägglund, 1995]. At the same time, the Unfalsified Control (UC, [Safonov and Tsao, 1995]), Iterative Feedback Tuning (IFT, [Hjalmarsson et al., 1994]), Model-Free Adaptive Control (MFAC, [Hou, 1999]) and Iterative Learning Control (ILC, [Moore, 1996]) were developed. More recently, other data-driven techniques have been proposed, such as the VRFT (Virtual Reference Feedback Tuning, [Campi et al., 2002]), the Correlation-based Tuning (CbT, [Karimi et al., 2002]), or the ones proposed in [Karimi and Kammer, 2017], [Hori et al., 2016], [Apkarian and Noll, 2018] and [Karimi et al., 2018].

Even though the literature offers numerous data-driven techniques to design controllers, the community is still growing and has many challenges to face in the various related fields of research. To begin with, data-driven theory still needs tools to analyze stability and robustness. In particular, it implies to propose new definitions of robustness when it comes to data-driven theory, as pointed out in [Hou and Wang, 2013]. As a matter of fact, in model-based theory, a control system is said to be robust if it can endure variations of the considered model due to unmodelled dynamics. In data-driven control, no model of the plant is used and, therefore, the concept of unmodelled dynamics does not apply to direct control design techniques. When it comes to stability, some data-driven techniques have proposed ways to analyze or enforce closed-loop stability,

see [Van Heusden et al., 2009] for example. Some of them rely on data-driven optimization or data-driven estimation of the $\mathcal{H}_\infty$ norm of dynamical systems: data-driven theory still needs to develop tools in these two areas. In addition, it is important to find a way to evaluate the performances of the designed closed-loops in a data-driven framework.

1.1.3 Motivating applications

In [Hou and Wang, 2013], it is recalled that data-driven control has emerged with the development of large-scale industrial processes for which obtaining of a model through system identification is a complicated task. In fact, data-driven framework is more indicated to process the huge amounts of data made available in this kind of control problems. A good example is the power grid, treated in [Kammer, 2018] with a data-driven control technique. In order to increase the part of renewable energy, the structure of the power grid moves from a centralized one to a distributed one with a great number of generation units, increasing its complexity. Regarding this evolution of the electrical grid, the challenge is to ensure stability and power quality. This requires new control methodologies since the electrical parameters are uncertain, and sometimes unknown: finding a parametric model of the grid would be really complicated. At the same time, the availability of real-time measurement data has increased significantly. For these reasons, a data-driven strategy is indicated in this case.

More generally, data-driven techniques allows to treat numerous modern control applications in which a model is too complex to obtain while experimental data is easily available. This is the case for modern industry, as highlighted in [Yin et al., 2014] and [Yin et al., 2015], for which no sufficient knowledge regarding the involved complex processes is available. As explained in [Bonvin et al., 2006], this is the case for batch processes. In [Formentin et al., 2014a], the data-driven technique presented in [Formentin et al., 2012] has been applied to a gravimetric blender, which is a typical batch process in the plastic industry: the obtained control performances allow to ensure the quality of the produced material, to reduce plastic wastes and therefore to increase the efficiency of the process. For the MFAC framework only, more than 70 applications are cited in [Hou et al., 2017], including industrial processes, but also power systems and motion systems.

The recent profusion of the literature in the area of data-driven control highlights the fact the data-driven control community has to grow to face challenging modern applications as the ones mentioned before.

1.2 Overview of the contributions and thesis organization

1.2.1 Proposed method in a glimpse

This study is focused on the data-driven design of controllers for Linear Time-Invariant (LTI) systems on the basis of frequency-domain data. To address this topic, a new data-driven technique is proposed in the frequency-domain. As the IFT, the VRFT or the CbT, it is a model reference technique: the specifications are expressed through a reference transfer function denoted $\mathbf{M}(s) \in \mathcal{RH}_\infty$ that represents the desired closed-loop behaviour.

The general problem formulation for model-reference control is summed up on Figure 1.1. The objective is to design a controller $\mathbf{K}$ on the basis of frequency-domain data from the plant $\mathbf{P}$ so that the corresponding closed loop behaviour is as close as possible from the objective closed-loop $\mathbf{M}$, e.g. to minimize ε for any reference signal $\mathbf{r}$.

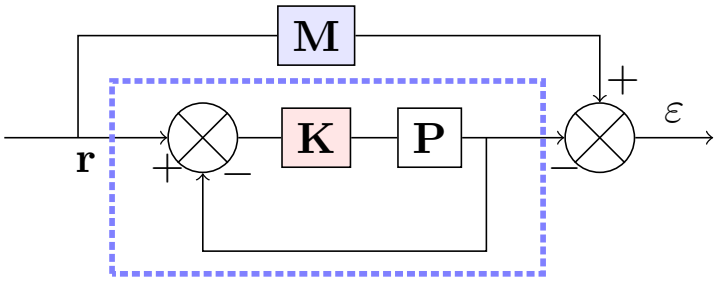

Figure 1.1: Problem formulation: $\mathbf{M}$ is the desired closed-loop, $\mathbf{P}$ is the plant and $\mathbf{K}$ the controller to be designed.

While the IFT, the CbT and the VRFT are based on time-domain data, the method proposed in this thesis is based on frequency-domain data from the plant. The data consists in samples of the frequency-response of the system $\mathbf{P}$, denoted $\{\Phi_i\}_{i=1}^N$, given on a discrete frequency-grid $\{\omega_i\}_{i=1}^N$. The couple $\{\omega_i, \Phi_i\}_{i=1}^N$ is the required data.

Then, the proposed method to solve the reference-model problem relies on two steps:

1. Based on the available data $\{\omega_i, \Phi_i\}_{i=1}^N$ and the reference model $\mathbf{M}$, compute the frequency-response of the ideal controller $\mathbf{K}^\star$ at the frequencies $\{\omega_i\}_{i=1}^N$. The ideal controller $\mathbf{K}^\star$ is the one that would exactly give the objective transfer $\mathbf{M}$ if inserted in the closed-loop during the experiment.

2. Identify a reduced order model $\hat{\mathbf{K}}$ of the ideal controller on the basis of its frequency-domain data. To this aim, two frequency-domain identification methods have been largely used in this manuscript:

   - The Loewner interpolation framework [Mayo and Antoulas, 2007] [Antoulas et al., 2015], usually employed for data-driven model approximation;
   - A subspace-based algorithm [McKelvey et al., 1996], which is a well known frequency-domain identification method;

This method has been introduced in this original form in [Kergus et al., 2017], where only the Loewner approach was presented for controller identification. The main advantage of the proposed method is its simplicity:

- The user does not have to choose a structure for the controller, unlike the CbT or the VRFT approaches where the poles of the controller are fixed *a priori*.

- The order of the controller may become a tunable parameter allowing to find a compromise between complexity and reliability. It may also be selected automatically through the Loewner framework and the subspace approach.

- As for other data-driven techniques, this method is appealing for engineers for applications when a controller should be synthesized quickly and for which it would be too costly or too complex to identify a model.

- It can be applied from SISO (Single Input-Single Output) to MIMO (Multi Inputs-Multi Outputs) plants.

1.2.2 Thesis overview

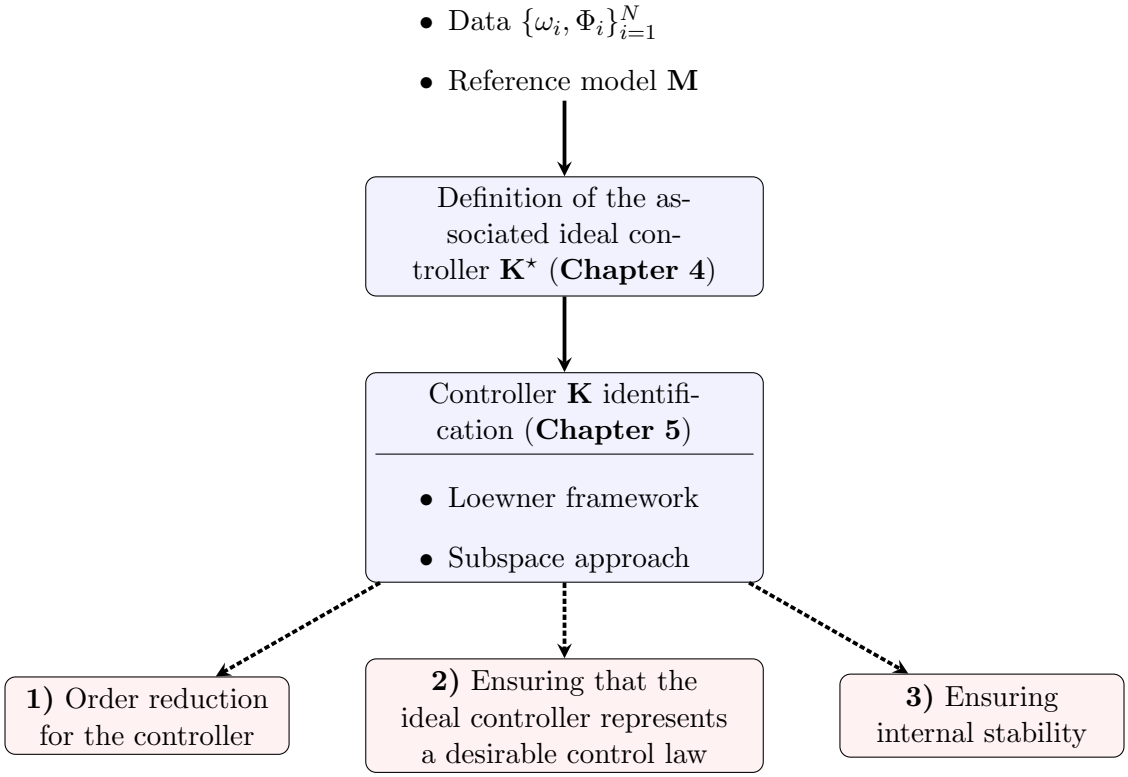

Figure 1.2: Original form of the proposed method (blue block) and the associated challenges (red blocks).

The main steps of the overall proposed method, as introduced in [Kergus et al., 2017], are represented on Figure 1.2. The problem formulation is further detailed in Chapter 4 while the identification methods are detailed in Chapter 5. Numerical applications are also provided in Chapter 4, highlighting the three major challenges explicited on Figure 1.2 and detailed hereafter.

1) **Order reduction for the controller**
The identification of the controller **K** is the core of the proposed method. Therefore, it will be treated in the first place, see Chapter 5. The order reduction is done through the proposed identification techniques. On that topic, the emphasis has

been put on exploring the abilities of the Loewner framework and the subspace approach in a data-driven control perspective. The main concern is to handle noisy data and to ensure the stability of the identified controller, see [Kergus et al., 2018b].

2) Ensuring that the ideal controller represents a desirable control law
As explained in [Bazanella et al., 2011], one of the main challenges for reference-model techniques is to determine the specifications. This is particularly highlighted when it comes to the particular cases of non-minimum phase or unstable plants: if the instabilities of the plant are not taken into account, they will be compensated by the ideal controller, which then destabilizes the plant. One of the first contribution, detailed in Chapter 6, is to propose a method to choose the objective $\mathbf{M}$ that takes into account the instabilities of the plant, see [Kergus et al., 2019b]. This is a common problem for all model-reference data-driven techniques.

3) Ensuring internal stability
Finally, in the initial form presented above, the proposed method does not give any information regarding closed-loop stability. The choice of the reference model $\mathbf{M}$ is then coupled with a stability analysis technique in order to predict if the designed closed-loop will be internally stable. This step will also limit the reduction of the controller order. This technique is detailed in Chapter 7.

To tackle these three challenges, the method proposed in [Kergus et al., 2017] has been modified. The new form of the method is now summed up in Figure 1.3. It includes two additional steps:

- The choice of the reference model $\mathbf{M}$: the objective is to answer problem **2)** by taking into account the intrinsic performance limitations of the plant when choosing a reference model. The choice of the reference model is now lead by a preliminary data-driven stability analysis of the plant's data, allowing to estimate its instabilities, both poles and zeros, which define what dynamics the plant can reach in closed-loop.

- A data-driven stability analysis: the last step of the method now consists in studying the internal stability of the resulting closed-loop, based on the controller modelling error. Consequently, this step will also bound the reduction of the controller in order to match the stability requirement.

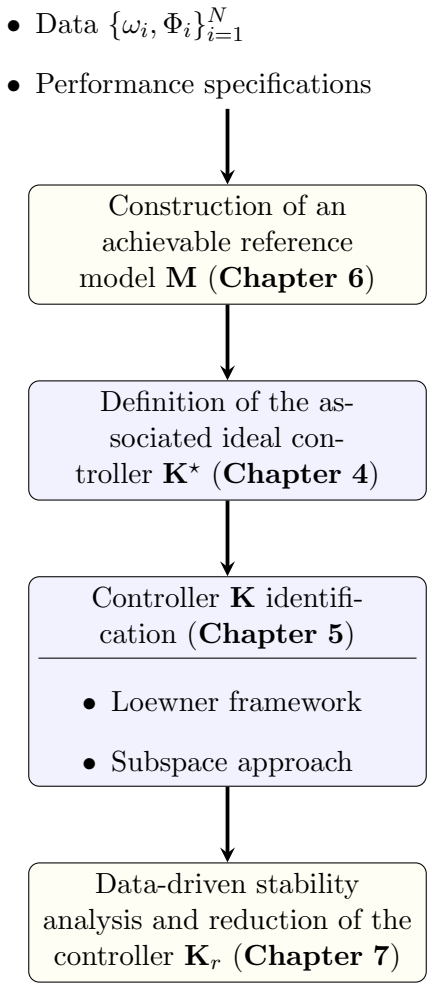

Figure 1.3: Final version of the proposed method.

1.2.3 Applications

Along this work, numerical examples will be used to illustrate the proposed method. Each one demonstrates some specific features. For example, the different natures of the plant will illustrate how instabilities affect the control performances. In the end, two industrial applications will be presented in Chapter 8.

i) A stable and minimum phase plant: the DC motor

The first considered example is the control of a DC motor's speed. The electric equivalent circuit is represented on Figure 1.4. It is a common actuator providing rotary motion. Its input is the voltage u and the output to be controlled is the rotational speed ω.

The following equation is obtained by applying Kirchoff's law:

$$L\frac{di}{dt} + Ri = u - v, \tag{1.1}$$

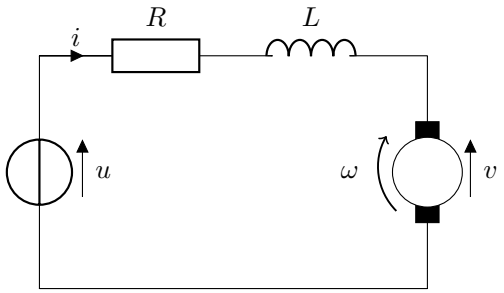

Figure 1.4: Armature circuit and DC motor.

where v is the back electromotive force, given by $v = K_{emf}\omega$ with $K_{emf} = 0.01V.(rad.s^{-1})^{-1}$ the electromotive force constant of the motor. $L = 0.5H$ is the inductance of the armature while $R = 1\Omega$ is its resistance. By applying Newton's 2^{nd} law on the motor, we have:

$$J\dot{\omega} + b\omega = T, \tag{1.2}$$

where $T = K_t i$ is the torque generated by the motor, proportional to the armature current i through the motor torque constant $K_t = 0.01N.m.A^{-1}$. $J = 0.01kg.m^2$ is the moment of inertia of the rotor and $b = 0.1N.m.s$ is the friction constant of the motor. By applying the Laplace transform, the following transfer function of the system is obtained:

$$\mathbf{P}(s) = \frac{\omega(s)}{u(s)} = \frac{K_t}{(Js+b)(Ls+R) + K_{emf}K_t} = \frac{0.01}{0.005s^2 + 0.06s + 0.1001}. \tag{1.3}$$

For this application, the control objective is to fasten the response of this actuator and to have a zero tracking error. The proposed method will be applied on this example in Chapter 4 in order to illustrate the original form of the proposed method (see Figure 1.2 and [Kergus et al., 2017]). Its purpose is mainly to apply the controller identification step using different reference models in order to understand the impact of the order reduction and of the specifications on the design process. In Chapter 5, this example will be used on the basis of noisy data in order to demonstrate the improvements of the controller identification step. In Chapter 7, a data-driven closed-loop stability analysis is also performed.

ii) A non-minimum phase stable plant: the flexible transmission

This application has been used as a benchmark for robust digital control in [Landau et al., 1995] and for different data-driven control techniques: the IFT in [Hjalmarsson et al., 1995], the VRFT in [Campi et al., 2002] and [Sala and Esparza, 2005], and in [Karimi et al., 2007] and [Van Heusden et al., 2011b] for the non-iterative CbT. The considered flexible transmission is composed of three pulleys, see Figure 1.5. It is a SISO system: its input is the angle θ_1 which can be controlled, and its output is the angle θ_3.

In the original application in [Landau et al., 1995], three discrete transfer functions are given for different loads of the third pulley, for a sampling period $T_s = 0.05s$. Here,

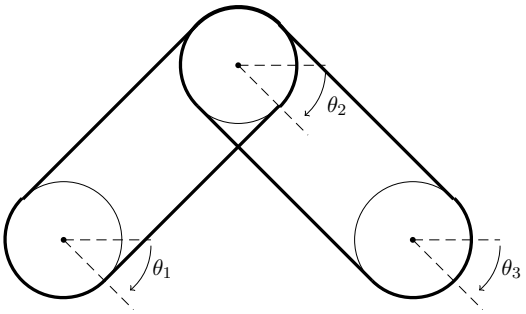

Figure 1.5: Flexible transmission system.

we consider the unloaded case only. The transfer of the plant is given by:

$$\mathbf{P}(z) = \frac{\theta_3(t)}{\theta_1(t)} = \frac{0.2821z + 0.5067}{z^4 - 1.418z^3 + 1.589z^2 - 1.316z + 0.8864}.$$

Applying a bilinear transform with the given sampling period, the continuous time model $P(s)$ is obtained:

$$\mathbf{P}(s) = \frac{\theta_3(s)}{\theta_1(s)} = \frac{0.03616(s - 140.5)(s - 40)^3}{(s^2 + 1.071s + 157.9)(s^2 + 3.172s + 1936)}. \tag{1.4}$$

This transfer function has four zeros in the Right-Half Plane (RHP). This application will be used in Chapter 4 to illustrate the difficulty of choosing an appropriate reference model and how, in practice, if no attention is paid, it is possible to identify a destabilizing controller. In Chapter 5, this example is used to detail the controller identification step. In Chapter 6, the RHP zeros of the system are estimated in a data-driven way and used to build an achievable model reference. In Chapter 7, closed-loop stability is analyzed.

iii) Industrial applications

In Chapter 8, two industrial applications that show the relevance of using data-driven control techniques are considered:

1. The control of the water depth in an open-channel: this system is presented in [Dalmas et al., 2016] and was controlled using the original method in [Kergus et al., 2017];

2. The control of a continuous crystallizer: this process is widely used in the chemical industry. The partial differential equations describing its behaviour are studied in [Rachah et al., 2016]. This control problem has been treated in [Vollmer and Raisch, 2001] using a model-based technique and in [Apkarian and Noll, 2018] using a data-driven one.

In these applications, the system is irrational, which makes the frequency-domain approach very interesting. Indeed, time-domain simulations are not easily accessible. However we still can estimate samples of the frequency response of the system $\{\omega_i, \Phi_i\}_{i=1}^N$, from which the ideal controller's frequency response can be deduced. For this reason, these two applications illustrate the strengths of data-driven control since there is no need to find a reduced-order model of the system to design the controller. These examples are treated in Chapter 8 using all the tools proposed in this work and recalled in Figure 1.3. These two applications are also presented in [Kergus et al., 2019a].

1.2.4 Thesis organization

The manuscript is divided in three parts. The present one consists in an introduction to data-driven control. The contribution of this thesis, which is the proposal of a new data-driven reference model technique, is presented in the second part. Finally, the third one is composed of the conclusions and outlooks of this work.

Chapter 2: Preliminaries on LTI systems and feedback control

This chapter aims at introducing various concepts regarding dynamical systems and feedback control that will be used all along this work. Notations are also introduced.

Chapter 3: Data-driven control

This chapter recalls the definition of data-driven control and the main differences with model-based control design. Then, a brief survey of existing data-driven control design techniques is proposed.

Part II: Data-driven control in the frequency domain

Chapter 4: General problem formulation

In this chapter, the general formulation of the method proposed in this thesis is exposed in its original form, as in [Kergus et al., 2017]. First, the new data-driven paradigm to design controllers for LTI systems is introduced. The key notions and the steps of the method are exposed. This first version of the method is then applied to the control of the DC motor and of the flexible transmission systems. These use-cases underline the challenges that any model reference technique has to tackle: the identification of the controller, the choice of achievable specifications and closed-loop stability analysis, see Figure 1.2. These problems will be treated in the following dedicated chapters. This chapter plays a pivotal role and provides the main idea of the manuscript.

Chapter 5: Controller identification in the frequency-domain

In this chapter, the Loewner framework and the subspace approach are recalled. These are the two identification techniques in the frequency-domain used in the proposed method to identify a controller. They are applied to the identification of the so-called ideal controller $\mathbf{K}^\star$. As said earlier, the properties of the considered identification techniques are explored to enforce the stability of the identified controller and to improve the robustness of the proposed method to noisy data. These contributions were exposed in [Kergus et al., 2018b].

Chapter 6: Choice of an achievable reference model

In this chapter, the difficulty to choose the reference model $\mathbf{M}$ in data-driven techniques is addressed. The definition of the achievable closed-loop behaviours is defined according to the plant's instabilities. A technique to build an achievable reference model is proposed. It relies on a data-driven estimation of the plant's instabilities uniquely on the basis of its frequency-response samples. This contribution is presented in [Kergus et al., 2019b] and applications are given in [Kergus et al., 2019a].

Chapter 7: Closed-loop stability analysis and enforcement

This chapter exposes a data-driven stability analysis of the closed-loop obtained with the identified controller. To this aim, the small-gain theorem is applied in the data-driven case. The conditions of its applications are met thanks to the steps detailed in the Chapters 4, 5 and 6. Internal stability is ensured until a certain controller modelling error. Therefore, this internal stability consideration plays a key role in the order reduction of the controller.

Chapter 8: Application to an hydroelectricity generation channel

In this chapter, the proposed data-driven method is applied on the two industrial examples introduced earlier: the open-channel for hydroelectricity generation and the continuous crystallizer. The objective is to furnish data-driven oriented applications: contrary to the numerical examples used along the thesis as a proof of concept, a reduced-order model, suited for model-based design, would be complicated to obtain. These examples are also presented in [Kergus et al., 2019a].

Part III: Conclusion

Chapter 9: Discussion

In this Chapter, the proposed data-driven control technique is summarized in one algorithm and its different steps are briefly summed up. The results on the different applications are discussed, as for the main strengths and limitations of the proposed technique. Finally, different ways to improve the method proposed during this thesis are presented and suggested for future research.

Chapter 2

Preliminaries on LTI systems and feedback control

The objective of this Chapter is to introduce various concepts regarding the modeling and control of dynamical systems that will be used all along this work. In this thesis, we consider the control of Linear Time-Invariant (LTI) continuous systems. For more information on this general topic, the reader should refer e.g. to [Zhou et al., 1996] and [Zhou and Doyle, 1998].

Contents

2.1 Generalities on LTI systems

As indicated by its name, a LTI system is linear and defines the relationship between the inputs and the outputs of the system as a linear map. Time invariance means that the output does not depend on the particular time the input is applied. Therefore, the main property of LTI systems is that they can be characterized entirely by their impulse response in the time-domain and equivalently, by their Frequency Response Function (FRF) in the frequency-domain.

2.1.1 Representations of LTI models

State-space representation and transfer functions

A rational LTI system $\mathbf{H}$ of order n, with n_u inputs and n_y outputs, can be represented by a state-space model $\mathbf{H} = (A, B, C, D)$ as in (2.1) in the time-domain:

$$\mathbf{H} : \begin{cases} \dot{\mathbf{x}}(t) = A\mathbf{x}(t) + B\mathbf{u}(t) \\ \mathbf{y}(t) = C\mathbf{x}(t) + D\mathbf{u}(t) \end{cases}, \tag{2.1}$$

where $A \in \mathbb{R}^{n\times n}$, $B \in \mathbb{R}^{n\times n_u}$, $C \in \mathbb{R}^{n_y\times n}$ and $D \in \mathbb{R}^{n_y\times n_u}$. Then, $\mathbf{x}(t) \in \mathbb{R}^n$ is the state vector, $\mathbf{u}(t) \in \mathbb{R}^{n_u}$ is the input vector and $\mathbf{y}(t) \in \mathbb{R}^{n_y}$ the output vector. It can also be represented in frequency-domain by its associated transfer function, as follows:

$$\mathbf{H}(s) = C(sI_n - A)^{-1}B + D, \tag{2.2}$$

where I_n is the identity matrix of size $n \times n$.

Considering a matrix transfer function $\mathbf{H}(s)$, a state-space model (A, B, C, D) satisfying $\mathbf{H}(s) = (A, B, C, D)$ is a **realisation** of $\mathbf{H}(s)$.

Definition 2.1.1. Minimal realisation
A state-space realisation (A, B, C, D) of a rational transfer matrix $\mathbf{H}(s)$ is a **minimal realisation** if the dimension of the matrix A is the smallest possible.

For proper systems, the order of a minimal state-space realisation of a matrix transfer function is also called the **McMillan degree**.

Remark 2.1.1. It is also possible for a dynamical system to be characterized by a descriptor state-space representation $\mathbf{H} = (E, A, B, C, D)$:

$$\mathbf{H} : \begin{cases} E\dot{\mathbf{x}}(t) = A\mathbf{x}(t) + B\mathbf{u}(t) \\ \mathbf{y}(t) = C\mathbf{x}(t) + D\mathbf{u}(t) \end{cases}, \tag{2.3}$$

where $E \in \mathbb{R}^{n\times n}$. Its associated transfer function is given by (2.4).

$$\mathbf{H}(s) = C(sE - A)^{-1}B + D. \tag{2.4}$$

The first interest of this type of representation is that the matrix E can be singular or complicated to invert for large-scale systems for example. As said in [Luenberger, 1977] and [Duan, 2010], many systems are naturally described by a descriptor state-space model. Furthermore, some systems cannot be described by traditional state-space models as the ones described by Differential Algebraic Equations (DAE), see [Sjöberg, 2005] on that topic and for examples of systems dirscribed by DAEs. While a state-space system can only have finite modes, a descriptor system can exhibit both finite and infinite modes. Therefore, descriptors models allow to consider impulsive dynamics and more complex models including polynomials for example. In addition, the D-term may be embedded in the E matrix as an infinite mode. Indeed, any rational matrix has a descriptor realization in the form of (2.4) as said in [Duan, 2010].

A descriptor representation is said to be minimal if its dimension n is the smallest possible. When considering such a realisation, the McMillan degree is given by the rank of the E matrix.

It should be noted that the classic state-space representation is only a particular case of the descriptor state-space one, for which $E = I_n$.

Poles and zeros

LTI systems are also characterized by their poles and zeros. On this aspect, the reader should refer to [MacFarlane and Karcanias, 1976] for more information. However, as in [Zhou et al., 1996] or [Zhou and Doyle, 1998], the poles and zeros are defined by putting the considered system in the Smith form. Here, the poles and zeros are defined directly according to the transfer matrix $\mathbf{H}(s)$ of a system $\mathbf{H}$, as in [Havre and Skogestad, 1996] and [Havre and Skogestad, 2001].

Let us consider a rational LTI system $\mathbf{H}$ equipped with a state-space representation (A, B, C, D). Its poles and zeros are defined as follows.

Definition 2.1.2. Zeros
$z_i \in \mathbb{C}$ is a zero of the system $\mathbf{H}$ if the rank of $\mathbf{H}(z_i)$ is less than the maximal rank of the transfer matrix $\mathbf{H}(s)$. There exists non-zero vectors $\mathbf{y}_{z_i} \in \mathbb{C}^{n_y}$ and $\mathbf{u}_{z_i} \in \mathbb{C}^{n_u}$, respectively called the output zero direction and the input zero direction, which satisfy:

$$\mathbf{y}_{z_i}^T \mathbf{H}(z_i) = 0 \qquad \mathbf{H}(z_i)\mathbf{u}_{z_i} = 0 \tag{2.5}$$

Definition 2.1.3. Poles
The poles $\{p_j\}_{j=1}^{n_p} \in \mathbb{C}$ of the system $\mathbf{H}$ are the eigenvalues of the matrix A. They are the roots of the characteristic equation:

$$\det(sI - A) = 0.$$

For each pole p_j, there exist non-zero vectors, the output directions $\mathbf{y}_{p_j}$ and the input directions $\mathbf{u}_{p_j}$, which represents the directions in which $\mathbf{H}(p_j)$ is infinite.

Considering a state-space representation $\mathbf{H} = (A, B, C, D)$, for a pole p_j of $\mathbf{H}$, the associated input and output directions, $\mathbf{u}_{p_j}$ and $\mathbf{y}_{p_j}$ respectively, can be computed as follows:

$$\begin{array}{l} \mathbf{u}_{p_j} = B^T \mathbf{x}_L \\ \mathbf{y}_{p_j} = C\mathbf{x}_R \end{array}, \tag{2.6}$$

where $\mathbf{x}_L$ and $\mathbf{x}_R$ are respectively left and right eigenvectors of A associated to p_j:

$$\begin{array}{l} \mathbf{x}_L^T A = \mathbf{x}_L^T p_j \\ A\mathbf{x}_R = p_j \mathbf{x}_R \end{array}. \tag{2.7}$$

Pole-residue expansion

Another representation that will used in this work is the pole-residue expansion of the transfer function. When the system has semi-simple poles (A is diagonalisable), the pole-residues expansion is given by:

$$\mathbf{H}(s) = \sum_{i=1}^{n} \frac{R_i}{s - \lambda_i}, \tag{2.8}$$

where $\{\lambda_i\}_{i=1}^{n}$ are the poles of the considered system, which are the eigenvalues of the matrix A, considering the state-space realisation in (2.1). Each matrix $R_i \in \mathbb{C}^{n_y \times n_u}$ is the residue associated to the pole λ_i, they are computed as follows:

$$\forall i = 1 \dots n, R_i = (C\mathbf{x}_i)\left(\mathbf{y}_i^T B\right), \tag{2.9}$$

with, for all $i = 1 \dots n$, $\mathbf{x}_i$ and $\mathbf{y}_i$ are the right and left eigenvectors associated with the eigenvalue λ_i of the matrix A. The norm of the residues will be used in Chapter 5 as a measure if the importance of the associated poles in the system's dynamics.

Remark 2.1.2. For a descriptor state-space model as in (2.3), the poles λ_i of the system are the eigenvalues of the matrix pencil (A, E). They are defined along with the associated right and left eigenvectors in (2.10). The residues are then computed according to (2.11).

$$\forall i = 1 \dots n, \ \begin{cases} A\mathbf{x}_i = \lambda_i E\mathbf{x}_i \\ \mathbf{y}_i^T A = \lambda_i \mathbf{y}_i^T E \end{cases} \tag{2.10}$$

$$\forall i = 1 \dots n, \ R_i = (C\mathbf{x}_i)\left(\mathbf{y}_i^T E\mathbf{x}_i\right)^{-1}\left(\mathbf{y}_i^T B\right) \tag{2.11}$$

Remark 2.1.3. As said earlier, LTI systems are completely characterized by their frequency-response. Consequently, people may refer to frequency response measurements from such plants as non-parametric models.

From now on, if not said otherwise, we will consider state-space realisations (2.1) and their transfer functions (2.2).

2.1.2 Properties of LTI models

Observability and controlability

These notions are particularly relevant to understand the identification techniques recalled in Chapter 5 and used to obtain a controller model. They will also be used in the data-driven estimation of instabilities presented in Chapter 6.

Definition 2.1.4. Observability
A system described by a state-space realisation as in (2.1), and its pair (A, C), is said to be **observable** if the initial state $x_0 = x(0)$ of the system can be determined from the input and output signals $u(t)$ and $y(t)$ in a given time interval $[0, t_f]$, for any $t_f > 0$.

Therefore, if the system is observable, it means that the entire system's behaviour is characterized by the system's output y, for any input signal u. On the contrary, for an unobservable plant, the state vector cannot be determined through outputs measurements.

The observability matrix, introduced in (2.12) for a system of order n, allows to test if a system is observable. The system is observable if and only if $\mathcal{O}$, as given in (2.12), has full-column rank, meaning rank($\mathcal{O}$)$= n$.

$$\mathcal{O} = \begin{pmatrix} C \\ CA \\ CA^2 \\ \vdots \\ CA^{n-1} \end{pmatrix} \in \mathbb{R}^{n_y n \times n} \tag{2.12}$$

Since the observability of a system is determined by the A and C matrices only, it is also said that the pair (C, A) is observable.

Definition 2.1.5. Controllability
A system described by a state-space realisation as in (2.1), or the pair (A, B), is said to be **controllable** if, for any initial state x_0 and final state x_f, and for any $t_f > 0$, there exists a piecewise continuous input signal $u(t)$ defined on the interval $[0, t_f]$ such that $x(t_f) = x_1$.

The controllability matrix, introduced in (2.13) for a system of order n, allows to test if a system is controllable. The system is controllable if and only if $\mathcal{C}$, as given in (2.13), has full-row rank, meaning rank($\mathcal{C}$)$= n$.

$$\mathcal{C} = \begin{pmatrix} B & AB & A^2B & \dots & A^{n-1}B \end{pmatrix} \in \mathbb{R}^{n \times n_u n} \tag{2.13}$$

A realisation of a transfer matrix $\mathbf{H}(s)$ is minimal if and only if it is both controllable and observable.

Remark 2.1.4. These notions of controlability and observability can be extended to descriptor state-space models. A realisation (E, A, B, C, D) of order n is said to be controllable if rank$(A - \lambda E, B) = n$ and rank$(E, B) = n$ for all $\lambda \in \mathbb{C}$. This is equivalent with rank$(\mathcal{C}_g) = n$, where $\mathcal{C}_g$ is the generalized controlability matrix, defined as follows:

$$\mathcal{C}_g = \begin{pmatrix} (\lambda_1 E - A)^{-1}B & \dots & (\lambda_n E - A)^{-1}B \end{pmatrix} \in \mathbb{R}^{n \times n n_u} \tag{2.14}$$

with $\{\lambda_i\}_{i=1}^n \in \mathbb{C}$ a set of distinct values which are not eigenvalues of the pencil (A, E).

The same way, a realisation (E, A, B, C, D) of order n is said to be observable if rank$(A^T - \mu E^T, C^T) = n$ and rank$(E^T, C^T) = n$ for all $\mu \in \mathbb{C}$. This is equivalent with rank$(\mathcal{O}_g) = n$, where $\mathcal{O}_g$ is the generalized observability matrix, defined as follows:

$$\mathcal{O}_g = \begin{pmatrix} C(\mu_1 E - A)^{-1} \\ \vdots \\ C(\mu_n E - A)^{-1} \end{pmatrix} \in \mathbb{R}^{n_y n \times n} \tag{2.15}$$

with $\{\mu_i\}_{i=1}^n \in \mathbb{C}$ a set of distinct values which are not eigenvalues of the pencil (A, E).

As for state-space realisations, a descriptor state-space realisation is minimal if it is controllable and observable. This will be useful when introducing the Loewner framework in Chapter 5.

Stability and the $\mathcal{H}_\infty$ and $\mathcal{H}_2$ spaces

As mentioned in the introduction chapter, analyzing closed-loop stability is an important challenge for any data-driven control technique. It is then important to recall the definition of a stable system.

Definition 2.1.6. BIBO stability
A system $\mathbf{H}$ is said to be Bounded-Input Bounded-Output (BIBO) stable if, for any bounded input, it produces a bounded output.

Given a continuous state-space realisation $\mathbf{H} = (A, B, C, D)$, the plant $\mathbf{H}$ is stable if and only if all its poles, the eigenvalues of A, have negative real values. More generally, a system is stable if and only if its transfer function is analytic in the Right-Half Plane

(RHP). The notion of stability leads us to introduce the following spaces, representing important classes of functions.

$\mathcal{L}_\infty$ is the space of functions bounded on the imaginary axis $\imath\mathbb{R}$. It means that the functions in $\mathcal{L}_\infty$ have no poles on the imaginary axis. $\mathcal{RL}_\infty$ is the rational subspace of $\mathcal{L}_\infty$, containing all the proper and real rational functions bounded on the imaginary axis. $\mathcal{L}_\infty$ is equipped with the following norm:

$$\forall \mathbf{H} \in \mathcal{L}_\infty,\ \|\mathbf{H}\|_\infty = \sup_{\omega\in\mathbb{R}} \overline{\sigma}\left(\mathbf{H}(\imath\omega)\right), \tag{2.16}$$

where $\overline{\sigma}(\cdot)$ denotes the maximal singular value of a matrix. This norm, called the $\mathcal{H}_\infty$-norm, is important for stability and robustness analysis, as explained in Section 2.2.1. The closed-loop stability test proposed in Chapter 7 for the proposed data-driven control technique relies on the estimation of the $\mathcal{H}_\infty$-norm of a system from its FRF.

$\mathcal{H}_\infty$ is the subspace of $\mathcal{L}_\infty$ that are analytic and bounded in the open RHP. $\mathcal{RH}_\infty$ is the subspace of proper real rational functions of $\mathcal{H}_\infty$.

$\mathcal{L}_2$ is the set of square integrable functions defined on the imaginary axis. It is equipped with the following norm:

$$\forall \mathbf{H} \in \mathcal{L}_2, \|\mathbf{H}\|_2 = \sqrt{\frac{1}{2\pi}\int_{-\infty}^{\infty} \mathrm{trace}\left(\mathbf{H}^*(\imath\omega)\mathbf{H}(\imath\omega)\right) d\omega}, \tag{2.17}$$

where trace$(\cdot)$ denotes the trace of a matrix and $(\cdot)^*$ is the complex conjugate transpose of a matrix. $\mathcal{RL}_2$ is the subspace of $\mathcal{L}_2$ containing the real rational and proper functions with no poles on the imaginary axis.

$\mathcal{H}_2$ is the subspace of $\mathcal{L}_2$ of stable functions, in sense that they admit an analytic continuation in the open RHP. $\overline{\mathcal{H}}_2$, the orthogonal of $\mathcal{H}_2$, is the subspace of $\mathcal{L}_2$ containing the anti-stable functions, analytic in the open left-half plane. These spaces will be mostly used for the data-driven stability analysis performed in Chapter 6. $\mathcal{RH}_2$ and $\mathcal{R}\overline{\mathcal{H}}_2$ respectively and proper functions of $\mathcal{H}_2$ and $\overline{\mathcal{H}}_2$.

2.1.3 Towards parametric models

If identification techniques are well-established for LTI systems in both time and frequency-domain, the obtained models are valid only for a single operating point. Extension to continuum of operating points have been developed in the area of Linear Parametrically Varying (LPV) modelling and identification, as detailed in [Tóth, 2010]. LPV models can be represented by a state-space model where the matrices depends on a time-varying vector $\mathbf{p}(t)$, as in (2.18):

$$\mathbf{H}(\mathbf{p}(t)) : \left\{ \begin{array}{rcl} \dot{\mathbf{x}}(t) & = & A(\mathbf{p}(t))\mathbf{x}(t) + B(\mathbf{p}(t))\mathbf{u}(t) \\ \mathbf{y}(t) & = & C(\mathbf{p}(t))\mathbf{x}(t) + D(\mathbf{p}(t))\mathbf{u}(t) \end{array} \right. . \tag{2.18}$$

To obtain such a model, global approaches in the area of LPV modelling require a single experiment, where the parameters entering the model vary in a known sequence. In this type of experiment, frequency-domain data are absolutely not relevant.

Nevertheless, in many applications, as explained in [Lovera and Mercere, 2007], a parameter-dependent model, as given in (2.19), is identified on the basis of local experiments or simulations in which the parameter is frozen. When the operating point remains unchanged during a local experiment, it is possible to use frequency-domain data to characterize the system.

$$\mathbf{H}(\mathbf{p}) : \begin{cases} \dot{\mathbf{x}}(t) &= A(\mathbf{p})\mathbf{x}(t) + B(\mathbf{p})\mathbf{u}(t) \\ \mathbf{y}(t) &= C(\mathbf{p})\mathbf{x}(t) + D(\mathbf{p})\mathbf{u}(t) \end{cases}, \tag{2.19}$$

Note that, because of the lack of information regarding the time variation of the scheduling parameter, this scenario is different from the traditional LPV framework and can be designated as parametric-LTI (p-LTI).

It should be noted that a classical way to model LPV systems is to identify local LTI frozen models at different operating points and to interpolate them. This type of techniques, like gain scheduling for example, are called local approaches. The line between the p-LTI case and the LPV one is usually crossed by assuming that the parameters are slowly varying. It allows to transpose the obtained p-LTI model to the LPV case with a bounded error, like in [Alkhoury et al., 2017].

In this work, identifying a parametric model of a controller can be useful. A variant of the classic Loewner framework already tackles the identification of p-LTI models, see [Ionita and Antoulas, 2014] and [Rapisarda and Antoulas, 2016]. In the subspace approach, a one technique has been proposed during this thesis to identify such models, see [Kergus et al., 2018a].

2.2 The feedback control problem

Given a system $\mathbf{P}$, feedback control consists in designing a controller $\mathbf{K}$ so that the feedback structure visible on Figure 2.1 is internally stable and allows to meet the performance specifications. The different involved signals are $\mathbf{u}$ and $\mathbf{y}$, the input and output vectors of the plant, the measurement noise $\mathbf{w}$, the disturbance $\mathbf{d}$, the reference signal $\mathbf{r}$, which should be reproduced, and the associated tracking error $\varepsilon = \mathbf{r} - \mathbf{y}$. The following relations between the different signals of the closed-loop are the basis of

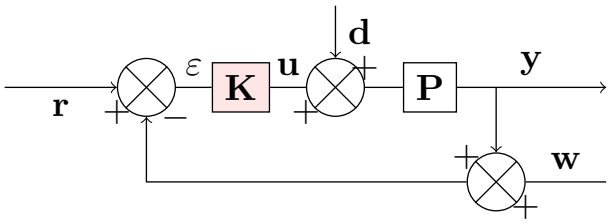

Figure 2.1: Considered feedback structure.

stability enforcement and performance specifications for feedback control design:

$$\mathbf{y} = (I_{n_y} + \mathbf{PK})^{-1}\mathbf{PKr} - (I_{n_y} + \mathbf{PK})^{-1}\mathbf{Pd} - (I_{n_y} + \mathbf{PK})^{-1}\mathbf{PKw}; \tag{2.20}$$

$$\varepsilon = (I_{n_y} + \mathbf{PK})^{-1}\mathbf{r} - (I_{n_y} + \mathbf{PK})^{-1}\mathbf{Pd} + (I_{n_y} + \mathbf{PK})^{-1}\mathbf{w}; \tag{2.21}$$

$$\mathbf{u} = (I_{n_u} + \mathbf{KP})^{-1}\mathbf{Kr} - (I_{n_u} + \mathbf{KP})^{-1}\mathbf{KPd} - (I_{n_u} + \mathbf{KP})^{-1}\mathbf{Kw}. \tag{2.22}$$

Considering the closed-loop of Figure 2.1, the sensitivity function $\mathbf{S}$ is the transfer from the reference signal $\mathbf{r}$ to the tracking error ε. It is given by:

$$\mathbf{S}(s) = (I_{n_y} + \mathbf{P}(s)\mathbf{K}(s))^{-1}. \tag{2.23}$$

The closed-loop transfer $\mathbf{T}$ from the reference signal $\mathbf{r}$ to the output $\mathbf{y}$, is defined by:

$$\mathbf{T}(s) = (I_{n_y} + \mathbf{P}(s)\mathbf{K}(s))^{-1}\mathbf{P}(s)\mathbf{K}(s). \tag{2.24}$$

It is also called the complementary sensitivity function since it satisfies $\mathbf{T} + \mathbf{S} = I_{n_y}$.

Assuming that the plant $\mathbf{P}$ and the controller $\mathbf{K}$ are proper, let us consider that this closed-loop interconnection is realisable, meaning that all the transfers mentioned above are well-defined and proper. As recalled in [Zhou and Doyle, 1998], this is the case if and only if $I + K(\infty)P(\infty)$ is invertible.

The considerations concerning the transfer functions appearing in (2.20), (2.21) and (2.22) and the stability of the interconnection visible on Figure 2.1 will play an important role in Chapter 6. The choice of the specifications and their impact on the proposed design process can be well understood thanks to the notions presented in this section.

2.2.1 Internal stability

Internal stability is the first requirement for any feedback system: it guarantees that, for bounded input signals, all the signals in the closed-loop stay bounded.

Definition 2.2.1. Internal stability
The closed-loop system of Figure 2.1 is internally stable if bounded inputs $\mathbf{r}$, $\mathbf{d}$ and $\mathbf{w}$ produce bounded outputs ε and $\mathbf{u}$. This is the case if the six following transfer functions are stable: $\mathbf{S}$, $\mathbf{T}$, $\mathbf{SP}$, $(I_{n_u} + \mathbf{KP})^{-1}$, $(I_{n_u} + \mathbf{KP})^{-1}\mathbf{KP}$ and $(I_{n_u} + \mathbf{KP})^{-1}\mathbf{K}$.

Remark 2.2.1. In the SISO case, the matrices $\mathbf{P}(s)$ and $\mathbf{K}(s)$ commute and then, only four transfer functions need to be stable to ensure internal stability.

Instead of checking the stability of all the mentioned transfer functions, the following theorem introduces another condition as in [Zhou and Doyle, 1998] that will be used in this work.

Theorem 2.2.1. The closed-loop visible on Figure 2.1 is internally stable if and only if $\mathbf{S}$ is stable and if the number of RHP poles of the open-loop $\mathbf{PK}$ is equal to $n_K + n_P$, n_K and n_P being the number of RHP poles of $\mathbf{K}$ and $\mathbf{P}$ respectively.

From a practical point of view, Theorem 2.2.1 means that there should not be any instabilities cancellation in the open-loop.

2.2.2 Performances

In addition to the stability requirement, the control design should ensure that the feedback system shown on Figure 2.1 meets some performance objectives: the output $\mathbf{y}$ should follow the reference signal $\mathbf{r}$ with a certain speed, a limited overshoot, while the system may be submitted to disturbances $\mathbf{d}$ and measurement noise $\mathbf{w}$. The command signal $\mathbf{u}$ should also be reasonable to avoid any problem with the actuators. These specifications can be divided in four categories: tracking, disturbance rejection, noise attenuation and moderate command.

These four performance specifications and the way they are expressed for control design purposes are detailed in the following paragraph. The inherent limitations of the system, due to its instabilities, are finally discussed. These considerations will help the reader to understand how critical the choice of the reference model is in the proposed method, which is an important topic in Chapters 4 and 6.

A. Performance specifications in the frequency-domain

As explained in [Zhou and Doyle, 1998], the mentioned performance objectives means that the signals ε and $\mathbf{u}$ should be in a given class of signals. This implies to understand the relation between the inputs of the feedback system, the signals $\mathbf{r}$, $\mathbf{d}$ and $\mathbf{w}$, and its outputs ε, $\mathbf{y}$ and $\mathbf{u}$. To that extent, it is needed to define the specifications in the frequency-domain through the transfer functions appearing in (2.21) and (2.22).

Tracking performances are defined by the relation between the reference signal $\mathbf{r}$ and the tracking error signal ε. Then, according to (2.21), the tracking performances are determined by the sensitivity function $\mathbf{S}$ in the frequency-domain:

- The tracking error in permanent regime is determined by the value of $|\mathbf{S}(\imath\omega)|$ in the low frequency-range.
- The response time of the closed-loop system is determined by the bandwidth ω_0 of the sensitivity function $\mathbf{S}$: the greater ω_0 is, the faster the closed-loop is.
- The overshoot of the time-response is determined by the $\mathcal{H}_\infty$-norm of $\mathbf{S}$.

Therefore, this is why this problem is called sensitivity minimization, since it can be written as follows:

$$\begin{cases} |\mathbf{S}(\imath\omega)| \leq \gamma & \forall \omega \leq \omega_0 \\ |\mathbf{S}(\imath\omega)| \leq M & \forall \omega > \omega_0 \end{cases}, \tag{2.25}$$

where γ, M and ω_0 represents the tracking performance objectives and are fixed by the user.

Disturbance rejection is characterized in the frequency-domain by the transfer $\mathbf{SP}$, see (2.21). This transfer should be designed as a bandstop filter for the frequency ranges where the Fourier transform of the disturbance signal $\mathbf{d}$ is important.

Noise attenuation is determined by the transfer $\mathbf{T}$. Since measurement noise is usually mostly important in the high frequency range, $\mathbf{T}$ should be designed as a lowpass filter. Since $\mathbf{T} + \mathbf{S} = I$, a trade-off is necessary between the tracking performances and

the noise attenuation ones: indeed, increasing the cutoff frequency ω_0 of the closed-loop transfer $\mathbf{T}$ fasten the closed-loop but does not prevent the noise to affect the tracking error ε.

Moderate command objectives are given on the transfers appearing in (2.22). The gain of the transfer $(I_{n_u} + \mathbf{KP})^{-1}\mathbf{K}$ should be limited to have a reasonable command signal $\mathbf{u}$. To limit the influence of the noise, its gain should also be limited in the high frequency-range.

Remark 2.2.2. Weighted $\mathcal{H}_2$ and $\mathcal{H}_\infty$ performance
In robust control design, the specifications are expressed through weighting functions that represent the desired shapes for the different transfers and the desired performances. For example, the sensitivity minimization problem becomes:

$$\|\mathbf{W_1 S}\|_\infty \leq 1, \tag{2.26}$$

where $\mathbf{W_1}^{-1}$ represents the desired highpass filter behaviour for the sensitivity function. The moderate command objective is also classically written as follows:

$$\|\mathbf{W_2 KS}\|_\infty \leq 1, \tag{2.27}$$

where $\mathbf{W_2}^{-1}$ allows to bound the gain of transfer function $\mathbf{KS}$.

B. Performance limitations

The possible performances of the feedback system of Figure 2.1 are limited by two factors: the necessary trade-off between the different design objectives and the eventual presence of instabilities in the plant. These two aspects are detailed hereafter.

Performance trade-off must be performed among the different performance objectives mentioned in the previous paragraph. A classic example is that the faster one wants the closed-loop to be, the higher the command signal will be. Furthermore, as explained in [Zhou et al., 1996] and [Zhou and Doyle, 1998], the loop design in the frequency-domain, associated with the performances objectives, actually consists in achieving high loop gains in a desired frequency range. However, it is not possible to achieve an arbitrarily high gain over an arbitrarily wide frequency range: the closed-loop stability feature gets less robust to model uncertainty and, at some point, the system may be destabilized.

The presence of instabilities, RHP poles or zeros in the system limits the possible closed-loop performances. Indeed, as said in Theorem 2.2.1, a necessary condition for the closed-loop to be internally stable is that there should not be any cancellation of instabilities in the open-loop. Therefore, as detailed in [Havre and Skogestad, 1996], to preserve internal stability, for a given RHP zero z_i of the plant $\mathbf{P}$, associated with an output direction $\mathbf{y}_{z_i}$, the sensitivity function $\mathbf{S}$ and the complementary sensitivity function $\mathbf{T}$ must satisfy:

$$\begin{cases} \mathbf{y}_{z_i}^T \mathbf{T}(z_i) = 0 \\ \mathbf{y}_{z_i}^T \mathbf{S}(z_i) = \mathbf{y}_{z_i}^T \end{cases}. \tag{2.28}$$

The same way, considering a given RHP pole p_j of the plant $\mathbf{P}$, associated with an output direction $\mathbf{y}_{p_j}$, the sensitivity function $\mathbf{S}$ and the complementary sensitivity function $\mathbf{T}$ must satisfy (2.29) to preserve internal stability.

$$\begin{cases} \mathbf{T}(p_j)\mathbf{y}_{p_j} = \mathbf{y}_{p_j} \\ \mathbf{S}(p_j)\mathbf{y}_{p_j} = 0 \end{cases} \tag{2.29}$$

The analyticity constraints on $\mathbf{S}$ and $\mathbf{T}$ given in (2.28) and (2.29) limit the possible performances of the closed-loop, see [Zhou and Doyle, 1998] or [Havre and Skogestad, 2001]. To highlight this point in the SISO case, let us introduce the Blaschke products $\mathbf{B}_z$ and $\mathbf{B}_p$ defined respectively by the RHP zeros $\{z_i\}_{i=1\dots n_z}$ and poles $\{p_j\}_{j=1\dots n_p}$ of the plant:

$$\mathbf{B}_z(s) = \prod_{i=1}^{n_z} \frac{s - z_i}{s + z_i} \qquad\qquad \mathbf{B}_p(s) = \prod_{j=1}^{n_p} \frac{s - p_j}{s + p_j}. \tag{2.30}$$

These two functions, $\mathbf{B}_z$ and $\mathbf{B}_p$, are stable and satisfy $|\mathbf{B}_z(\imath\omega)| = 1$ and $|\mathbf{B}_p(\imath\omega)| = 1$ for all frequencies $\omega \in \mathbb{R}$.

Thanks to (2.29) and (2.28), the functions $\mathbf{B}_p^{-1}\mathbf{S}$ and $\mathbf{B}_z^{-1}\mathbf{T}$ are in $\mathcal{H}_\infty$ and the following relations can be written:

$$\begin{cases} \forall z \in \mathbb{C},\ \|\mathbf{S}(s)\|_\infty = \left\|\mathbf{B}_p^{-1}(s)\mathbf{S}(s)\right\|_\infty \geq \left|\mathbf{B}_p^{-1}(z)\mathbf{S}(z)\right| \\ \forall p \in \mathbb{C},\ \|\mathbf{T}(s)\|_\infty = \left\|\mathbf{B}_z^{-1}(s)\mathbf{T}(s)\right\|_\infty \geq \left|\mathbf{B}_z^{-1}(p)\mathbf{T}(p)\right| \end{cases} \tag{2.31}$$

By considering the RHP zeros $\{z_i\}_{i=1\dots n_z}$ and poles $\{p_j\}_{j=1\dots n_p}$ of the system, it is shown that the peak in $\mathbf{S}$ and $\mathbf{T}$ have a lower bound determined by the plant's RHP poles and zeros:

$$\begin{cases} \|\mathbf{S}(s)\|_\infty \geq \max\limits_{i=1\dots n_z} \left|\mathbf{B}_p^{-1}(z_i)\right| \\ \|\mathbf{T}(s)\|_\infty \geq \max\limits_{j=1\dots n_p} \left|\mathbf{B}_z^{-1}(p_j)\right| \end{cases}. \tag{2.32}$$

Similar results are obtained in the MIMO case in [Zhou and Doyle, 1998] or [Havre and Skogestad, 2001].

The instabilities of the system also limit the cutoff frequencies of the closed-loop transfer functions $\mathbf{S}$ and $\mathbf{T}$. As explained in the previous paragraph, in the SISO case, one wants to have $\mathbf{T}(\imath\omega) = 1$ for low frequencies while $\mathbf{T}(z_i) = 0$ for any RHP zero z_i. Consequently, the bandwidth of the closed-loop must be much smaller than the smallest RHP zero frequency.

In the general MIMO case, a good overview of the limitations of closed-loop performances is available in [Seron et al., 1997]. As in the SISO case, these limitations are induced by the analyticity constraints given in (2.28) and (2.29), determined by the RHP poles and zeros of the system.

2.2.3 Robustness

In practice, models are associated with uncertainties since it cannot represent the true plant behaviour. The uncertainties are the errors between the model and the reality.

Usually, model sets are used to represents the uncertainties, by putting bounds in the frequency domain for example.

The notion of robustness has been introduced in control theory to take into account model uncertainty. The robustness of a closed-loop feedback system denotes the ability of the controller to stabilize and/or ensure performances for the whole model set instead of doing it for the nominal model only.

Results regarding the robust stability are mainly obtained thanks to the small gain theorem, recalled in Theorem 2.2.2 as given in [Zhou and Doyle, 1998]. It requires to write the uncertain system as another interconnection, visible on Figure 2.2. The block $\mathbf{\Delta}$ represents the uncertainties.

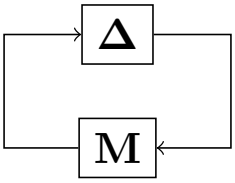

Figure 2.2: $\mathbf{M} - \mathbf{\Delta}$ interconnection for stability analysis using the small-gain theorem.

Theorem 2.2.2. Small-gain theorem
Suppose $\mathbf{M} \in \mathcal{RH}_\infty$ and let $\gamma > 0$. Then the interconnected system shown on Figure 2.2 is well-posed and internally stable for all $\mathbf{\Delta} \in \mathcal{RH}_\infty$ with:

(a) $\|\mathbf{\Delta}\|_\infty \leq \frac{1}{\gamma}$ if and only if $\|\mathbf{M}\|_\infty < \gamma$

(b) $\|\mathbf{\Delta}\|_\infty < \frac{1}{\gamma}$ if and only if $\|\mathbf{M}\|_\infty \leq \gamma$

As said in [Zhou and Doyle, 1998], Theorem 2.2.2 still holds when $\mathbf{M}$ and $\mathbf{\Delta}$ are infinite dimensional: they only need to be in $\mathcal{H}_\infty$. The small-gain theorem will be used in Chapter 7 to study the stability of the closed-loop.

Chapter 3

State of the art: Data-driven control

The objective of this chapter is to introduce data-driven control and the related challenges and difficulties. The differences and the relations between data-driven control theory and model-based control theory will be exposed in Section 3.1. A survey of the existing data-driven control techniques is proposed in Section 3.2.

Contents

3.1 Data-driven control theory

Model-based control and data-driven control are two different parts of control theory. However, model-based control techniques may have been called data-driven in the past. This was mostly the case with model-based techniques where the model is obtained from the plant's measurements (the identification of the model is data-driven). For example, in [Kostic, 2004], these techniques are called "*Model-based data-driven control design*". The terms "model-based control" and "data-driven control" can therefore be confusing. This section aims at recalling their definitions before recalling the differences between these two types of methods.

3.1.1 Definition of data-driven control

Different definitions of data-driven control have been proposed in the literature. All of them emphasize the key aspect of data-driven control which is the direct use of input-output data from the plant. In [Xu and Hou, 2009], the definition of data-driven control includes the analysis and the guarantee of the results. In [Van Helvoort, 2007],

it is said that data-driven control uses the plant's data directly to adapt the controller. In [Van Heusden, 2010], data-driven control is defined as the minimization of a control criterion. In [Hou and Wang, 2013], these three definitions are regrouped in only one. In this work, the following definition of data-driven control is proposed.

Definition 3.1.1. Data-driven control
A control technique is said to be data-driven when the measured data of the plant is used directly for the design of the controller. No parametric model of the system is necessary.

This definition includes all the *direct* control approaches, even the ones that are not adaptive or not relying on the resolution of an optimization problem. Furthermore, analyzing the stability and the robustness of the obtained closed-loop is still a challenging issue for many data-driven control techniques, but they still should be classified as data-driven methods. In contrast, model-based control can be defined as in [Van Heusden, 2010].

Definition 3.1.2. Model-based control
A control technique is said to be model-based when it can be decomposed in two distinct steps. The first step consists in obtaining a model of the plant. During the second step, the controller is designed on the basis of the model of the system.

3.1.2 Relations and differences with model-based control theory

As explained in [Hou and Wang, 2013], real-world systems can be divided in four categories:

1. Plants for which an accurate model is available;
2. Those for which a model with a good accuracy and moderate uncertainties is available;
3. Those for which a model is available but not adapted to control design because of a too high order for example;
4. Those for which a model is unavailable or too difficult to obtain.

Here, the models can be obtained either by first principle or system identification. Model-based control theory allows to tackle the problems where plants are in the first two classes.

For systems in the third category, model or controller reduction is inevitable for control design purposes. As a matter of fact, this type of models complicates the resolution of the control design problem and/or leads to high order controllers, which are too complex to implement. However, robust control or adaptive control can address such problems to some extent. It should be noted that non-linear systems might be catalogued in this category when the non-linearities are too important to be tackled by nonlinear model-based control techniques.

The last category of systems cannot be treated by model-based control techniques. Finally, data-driven control techniques are developed to address the control design for systems in this category, but also for some very complex plants of the third category.

3.2 Overview of data-driven control techniques

The objective of this section is to give an overview of data-driven techniques. They are classified according to their type of problem formulation: (i) model-reference control, (ii) robust control and (iii) predictive and learning control. Since the method introduced in this work is a model-reference one, the corresponding part is more detailed in order to put in perspective the results to be exposed. Other possible classifications of data-driven control techniques will be discussed in 3.2.4.

3.2.1 Model reference control

Model-reference control consists in finding a controller that achieves a desired closed-loop behaviour, called the reference model, denoted **M**. Here, only the data-driven model reference techniques are presented.

Virtual Reference Feedback Tuning (VRFT)

The VRFT is one of the most popular one-shot data-driven technique. It was first proposed in [Campi et al., 2002] for SISO plants. It relies on a single batch of time-domain data $\{u(t_k), y(t_k)\}_{k=1}^{N}$ from the plant **P**. The problem is shown on Figure 3.1.

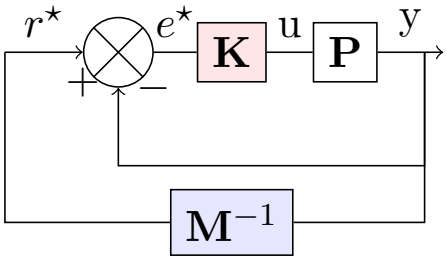

Figure 3.1: Principle of the VRFT.

The VRFT is based on the *fictive reference* $r^\star$, represented on Figure 3.1. It is the reference signal that would give the experimental output if the closed-loop were defined by the objective transfer function **M**. By definition, its expression is given by:

$$r^\star(t) = \mathbf{M}(z)^{-1} y(t). \tag{3.1}$$

The fictive error $e^\star(t) = r^\star(t) - y(t)$ is then introduced. This signal would be the input of the controller in the ideal case, when the obtained closed-loop is equal to the objective during the experiment. The design task then becomes an identification problem: the controller must fit the dynamical relationship between $e^\star$ and u.

A class $\mathcal{K}$ of linearly parametrized controllers is selected *a priori*:

$$\mathcal{K} = \left\{ \mathbf{K} : \mathbf{K}(z, \theta) = \beta^T(z)\theta \right\}, \tag{3.2}$$

where $\beta(\mathbf{z})$ is a vector of given transfer functions, fixing the poles of the controller and constituting the basis of $\mathcal{K}$, and $\theta \in \mathbb{R}^n$ are the controller's tunable parameters. Choosing a linear parametrization of the admissible controllers makes the problem convex and

the global solution can be found. It is a global method, there is no problem with the initialization of θ or local minimas.

The objective is to solve (3.3). However, it is not possible without having a model of the plant $\mathbf{P}$.

$$\begin{aligned} \theta^\star &= \arg\min_{\theta\in\mathbb{R}^n} J(\theta), \\ J(\theta) &= \left\| \left(\frac{\mathbf{P}(z)\mathbf{K}(z,\theta)}{1+\mathbf{P}(z)\mathbf{K}(z,\theta)} - \mathbf{M}(z) \right) W(z) \right\|_2^2, \end{aligned} \tag{3.3}$$

For this reason, to avoid the identification of a model, the VRFT minimizes the following criteria instead:

$$J_{VRFT}(\theta) = \|u - \mathbf{K}(z,\theta) r^\star\|_2^2 . \tag{3.4}$$

Since only a finite amount of measurements is available, $J_{VRFT}(\theta)$ is approximated by $J^N_{VRFT}(\theta)$:

$$J^N_{VRFT}(\theta) = \frac{1}{N} \sum_{k=1}^{N} \left(u_F(t_k) - \mathbf{K}(z,\theta) e^\star_F(t_k) \right)^2 , \tag{3.5}$$

where N is the number of measurements. It satisfies:

$$\lim_{N\to\infty} J^N_{VRFT}(\theta) = J_{VRFT}(\theta). \tag{3.6}$$

In (3.5), $e^\star_F(t) = \mathbf{F}(z)e^\star(t)$ and $u_F(t) = \mathbf{F}(z)u(t)$ are filtered signals. As explained in [Campi et al., 2002], the filter $\mathbf{F}(z)$ is chosen so that $J(\theta)$ and $J_{VRFT}(\theta)$ shares the same minimizer $\theta^\star$. This is possible when $J(\theta^\star) = 0$. It implies that the ideal controller, the one that would have given the model reference $\mathbf{M}$ during the experiment, is contained by the selected class of controllers $\mathcal{K}$.

In [Campi et al., 2002], noisy data are handled by introducing an instrumental variable. The VRFT has been extended to MIMO plants in [Formentin et al., 2012] and to non-linear systems in [Campi and Savaresi, 2006], the main changes concern the design of the filter $\mathbf{F}$. In [Formentin and Savaresi, 2011] and [Formentin et al., 2013], gain-scheduled controllers are obtained through the VRFT framework for LPV plants. It is also possible to change the reference function, and the associated criterion, in order to perform sensitivity minimization as in [Hori et al., 2016] or disturbance rejection as in [Eckhard et al., 2018]. Applications of the VRFT can be found in the previous references or in [Panzani et al., 2012] and [Passenbrunner et al., 2012].

The main strength of the VRFT, in addition to not requiring a model of the plant, is to be a one shot technique requiring a single experiment. Its main drawback is the difficulty to choose the reference model, as highlighted in [Bazanella et al., 2011], mostly when the plant is non-minimum or unstable. To that extent, a flexible criterion has been introduced in [Campestrini et al., 2011] to design the reference model $\mathbf{M}$ along with the controller for non-minimum phase systems. This has been done in [Selvi et al., 2018]. Even once the specifications are chosen, the choice of a class $\mathcal{K}$ of controllers is a difficult task without any other prior knowledge of the plant. To tackle this issue, a technique has been proposed in [Formentin et al., 2015]. Finally, in order to analyze closed-loop stability, two techniques have been proposed in [Van Heusden et al., 2009], relying on the small-gain theorem, and in [Dehghani et al., 2009], based on the winding number and the Nyquist diagram.

Correlation-based Tuning (CbT)

CbT was introduced in [Karimi et al., 2002]. It is an iterative algorithm: each iteration requires an experiment to update the controller's parameters using time-domain data. The principle of CbT is exposed on Figure 3.2. The method is based on the correlation approach, also used in system identification. CbT is applicable to SISO LTI plants.

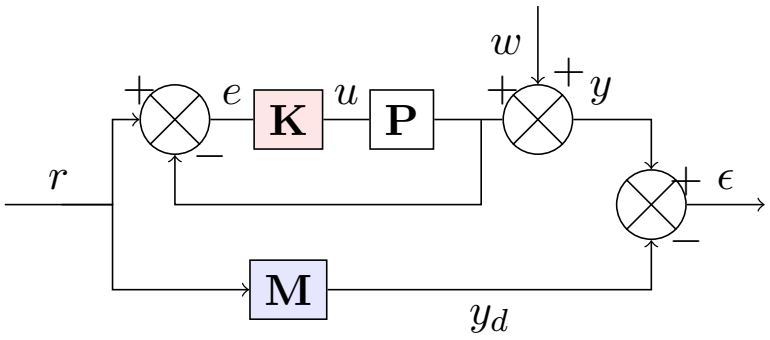

Figure 3.2: Principle of the CbT.

The objective is to design a controller $\mathbf{K}$ so that the resulting closed-loop reproduces the reference model $\mathbf{M}$ behaviour for a reference signal r. Therefore, according to the expression of the output error ϵ, see (3.7), minimizing the error between the closed-loop and the reference model boils down to decorrelate ϵ from the reference signal r.

$$\epsilon(s) = \left(\mathbf{M}(s) - \frac{\mathbf{P}(s)\mathbf{K}(s)}{1+\mathbf{P}(s)\mathbf{K}(s)}\right) r(s) + \frac{1}{1+\mathbf{P}(s)\mathbf{K}(s)} w(s) \tag{3.7}$$

A class $\mathcal{K}$ of admissible controllers is selected, using the following parametrization:

$$\begin{gathered} \mathbf{K}(\theta, s) = \frac{B(s)}{A(s)} = \frac{b_0 + b_1 s + \cdots + b_{n_b} s^{n_b}}{1 + a_1 s + \cdots + a_{n_a} s^{n_a}} \\ u(t) = \phi(\theta, t)^T \theta \\ \phi^T(\theta, t) = [-u(t-1) \cdots - u(t-n_a), e(t) \ldots e(t-n_b)] \\ \theta^T = [a_1 \ldots a_{n_a} b_0 \ldots b_{n_b}] \end{gathered} \tag{3.8}$$

where e is the tracking error and u is the command signal in the closed-loop obtained with $\mathbf{K}(\theta)$. For a given parameter vector θ, the correlation between r and ϵ is given by:

$$\xi(\theta) = \frac{1}{N} \sum_{k=1}^{N} \zeta(\theta, t_k) \epsilon(\theta, t_k) \tag{3.9}$$

where ζ is an instrumental variable correlated with r but decorrelated from the measurement noise w. If contained in the set $\mathcal{K}$, the ideal controller is obtained for $\xi(\theta) = 0$. Otherwise, the controller's parameters are chosen by minimizing the correlation function ξ. This is done using an iterative gradient-based algorithm. In the ideal case, the

instrumental variable should be chosen as the gradient of the correlation function. This can be done through the identification of a plant model, or using the output y_d. In this case, the regressor vector $\phi(\theta, t)$, defined in (3.8), is approximated as if the closed-loop was the desired one $\mathbf{M}$. This implies that the distance to the optimal solution can be made small.

In [Karimi et al., 2007], a non-iterative version of this method has been proposed. The main improvement resides in the fact that this version only requires a single experiment. It is still based on the correlation function ζ. The criterion to be minimized is given in (3.10), with l a sufficiently large integer:

$$J_c(\theta, l) = \sum_{\tau=-l}^{l} R^2_{\epsilon u_F}(\tau), \tag{3.10}$$

where $R_{\epsilon u_F}$ is the cross correlation function between ϵ and u_F, the filtered command signal:

$$R_{\epsilon u_F}(\tau) = \sum_{t=1}^{N} \epsilon(\theta, t) u_F(t - \tau) \tag{3.11}$$

with N the number of available samples.

The command signal u is filtered using weighting filter designed as in the VRFT, so that (3.12) holds and that the resulting closed-loop is as close as possible to the desired one $\mathbf{M}$. The design of this filter, as for the VRFT, assumes that the sensitivity function obtained with $\mathbf{K}(\theta)$ can be assimilated to $1 - \mathbf{M}$, the one corresponding to the ideal case.

$$\lim_{l \to \infty} J_c(\theta, l) = \left\| \mathbf{M} - \frac{\mathbf{PK}(\theta)}{1 + \mathbf{PK}(\theta)} \right\|_2^2. \tag{3.12}$$

In [Van Heusden et al., 2011a], the data-driven stability criteria introduced in [Van Heusden et al., 2009] is used to constraint the optimization problem and enforce closed-loop stability. This is done using a stabilizing controller. In practice, this assumption might be a strong one, depending on the considered application.

In [Formentin et al., 2014b], the CbT is compared to a model-based control technique. It emphasizes that using data-driven techniques implies a larger variance of the controller parameters than model-based control design, but it also can lead to a lower control cost.

Iterative Feedback Tuning

Iterative Feedback Tuning (IFT) was introduced in [Hjalmarsson et al., 1994]. More information and some applications can be found in [Hjalmarsson et al., 1998] and the references therein.

The class $\mathcal{K}$ of admissible controllers is linearly parametrized by a parameter vector θ as in the VRFT and CbT, see (3.2). As for the CbT, the objective is to find the controller's parameters $\theta^\star$ that minimize the error between the output $y(\theta)$ and the desired one y_d, see Figure 3.2. y_d is defined as the output of the reference closed-loop

$\mathbf{M}$, representing the expected behaviour, while $y(\theta)$ is the output of the closed-loop with $\mathbf{K}(\theta)$ as controller, see Figure 3.2. The minimization of the control criterion relies on the estimation of its gradient at each iteration, which requires two experiments. The collected measurements are in the time-domain. The algorithm converges to a local minimum of the control criterion.

The difference between CbT and IFT resides in the way they approximate the gradient of the output error $\epsilon = y(\theta) - y_d$. In CbT, the ideal case is used to tune an instrumental variable. In the IFT framework, a second experiment is performed to obtain the derivative of ϵ, using $r - y(\theta)$ a s a reference signal. This is justified by (3.13), obtained by deriving (3.7) with no disturbance term.

$$\frac{\partial \epsilon(\theta)}{\partial \theta} = \frac{1}{\mathbf{K}(\theta)} \frac{\partial \mathbf{K}(\theta)}{\partial \theta} \left(\frac{\mathbf{PK}(\theta)}{1 + \mathbf{PK}(\theta)} (r - y(\theta)) \right) \tag{3.13}$$

In [Hjalmarsson et al., 1998], it is also said that the choice of the reference model $\mathbf{M}$ is a "key design decision". Indeed, for unstable or NMP systems, the controller giving exactly the desired behaviour $\mathbf{M}$ in closed-loop may be unstable. The implementation of the IFT should be modified in order to estimate the gradient correctly: the collected signal y is filtered and the filter must compensate the RHP zeros of the plant to avoid this problem.

Obviously, the main drawback of this approach is the great number of experiments required for the control design. This is also the conclusion of the comparison between unfalsified control and IFT proposed in [Wang and Safonov, 2002]. This method has been extended to MIMO sytems in [Hjalmarsson, 1999]. In order to limit the error of the gradient estimation due to noise, a pre-filtering step is proposed in [Hildebrand et al., 2005]. Other extensions of the IFT have been proposed to tackle the control of nonlinear systems. In [Hjalmarsson, 1998], it is shown that the original algorithm can be applied to nonlinear systems only if they can be assimilated to their first-order Taylor expansion. Most of these improvements are summed up in [Hjalmarsson, 2002], which also contain a list of applications of the IFT. Other work either require even more experiments per iterations as in [Sjöberg et al., 2003], or on the identification of linearized time-varying models at each iteration, see [Sjöberg et al., 2009]. In [De Bruyne and Kammer, 1999], a sufficient condition for closed-loop internal stability, introduced in [Vinnicombe, 1993], is used to choose the step size of the algorithm such that closed-loop internal stability is guaranteed.

Unfalsified control

Unfalsified Control (UC) was introduced in [Safonov and Tsao, 1995]. It relies on the idea that a control law is validated if its ability to meet the desired specifications is not falsified by the data. Given a set of controllers $\mathcal{K}$, parametrized by a vector θ, and measurements data in the time-domain, it constructs the set $\mathcal{K}_{UF} \subset \mathcal{K}$ of unfalsified controllers, the ones for which the desired performances would have been reached if inserted in the closed-loop during the experiment. This falsification procedure relies on the concept of virtual reference, defined according to the controller as follows:

$$\tilde{r}(t) = \mathbf{K}^{-1}(\theta, z) u(t) + y(t). \tag{3.14}$$

The main difference with the VRFT is that the virtual reference is obtained by inversing the controller at the current iteration, instead of inversing the reference model $\mathbf{M}$.

When implemented in real-time, a controller in $\mathcal{K}_{UF}$ is chosen at each iteration. The controller changes according to the data of the plant. Therefore, it constitutes an adaptive control scheme. Different switching mechanisms have been proposed in the literature to choose a controller at each iteration. In [Van Helvoort et al., 2007], the performances are expressed as reference closed-loop behaviour and the set of unfalsified controllers is described by an ellipsoid, allowing to compute analytically the updated controller. In [Jun and Safonov, 2002], a gradient-based approach is proposed to minimize a performance objective in $\mathcal{K}_{UF}$. The stability of these schemes are studied in [Battistelli et al., 2010]. Applications can be found in [Van Helvoort et al., 2005] for a motion system, in [Safonov, 2006] for a robot arm control and a missile guidance problem, and in [Demourant et al., 2002] for an aircraft autopilot.

In [Battistelli et al., 2018], a new data-driven technique based on the unfalsified control framework is proposed. It requires a single experiment only. Instead of using one reference model, two transfer functions representing the closed-loop behaviour are used: the reference closed-loop $\mathbf{M}$, between the reference signal r and the output y, and $\mathbf{W}_u$, the transfer one wants to achieve between the reference signal r and the command signal u. The scheme of this method is represented on Figure 3.3. The signals u_θ and y_θ are the ones that should be obtained if the controller $\mathbf{K}(\theta)$ is ideal.

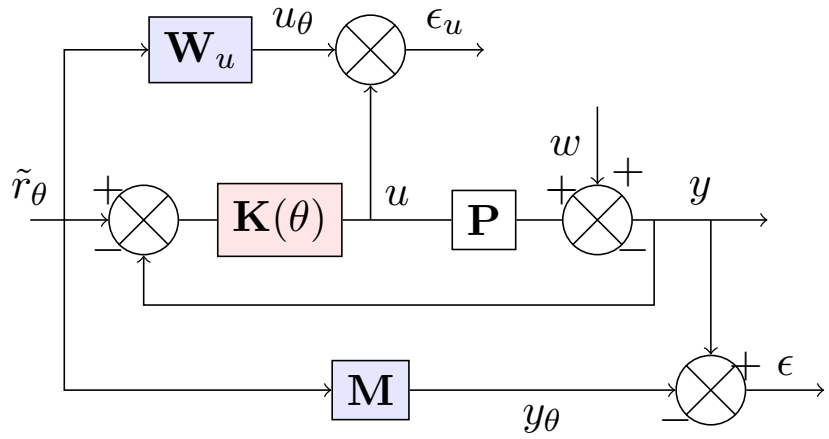

Figure 3.3: Principle of the non-iterative data-driven controller falsification.

The controller's final parameters $\theta^\star$ are obtained by solving the problem given in (3.15). δ is a scalar in $[0, 1]$ used to weight the two criterias associated with the two objective transfers $\mathbf{M}$ and $\mathbf{W}_u$.

$$\begin{aligned} \theta^\star = \arg\min_\theta \ & \delta J_N(\theta) + (1-\delta) V_N(\theta), \\ & J_N(\theta) = \|y - y_\theta\|_2^2, \\ & V_N(\theta) = \|u - u_\theta\|_2^2. \end{aligned} \tag{3.15}$$

The initialisation of the algorithm is done by taking θ_0, defined according to (3.16), as the initial set of parameters for the controller. It corresponds to the resolution of

(3.15) for $\delta = 0$. $\mathbf{K}(\theta_0)$ stabilizes the plant internally, even for non-minimum phase plants.

$$\theta_0 = \arg\min_{\theta} \; V_N(\theta) \tag{3.16}$$

Then, δ is progressively decreased. For each value of δ, $\mathbf{K}(\theta)$ is obtained and a stability test is performed, as in [Van Heusden et al., 2009]. If this test is not satisfied, the controller is falsified. The algorithm stops when it reaches the minimal value of δ such that the controller given by (3.15) stabilizes the plant internally.

3.2.2 Robust data-driven control

In model-based control, robust control is one of the most popular category of techniques since it deals with uncertainties, noise and disturbances. Unlike adaptive control where changes in the system imply changes in the controller, robust control designs a controller that will be valid in a bounded set of uncertainties around a nominal model. However, frequency-domain data have been used to directly tune controllers since the development of Quantitative Feedback Theory, see [Horowitz, 1982]. This technique uses graphical tools based on the Nyquist chart to design robust controllers and highlighted the performance limitations recalled briefly in Chapter 2 and the necessary trade-offs for control design. It was then replaced by the more general framework of $\mathcal{H}_\infty$-synthesis, still in the frequency-domain.

Since then, various data-driven techniques based on frequency-domain data have been proposed to design controllers that ensure robust stability and performances. The first approach consists in using convex optimization for data-driven robust control design. In [Karimi and Galdos, 2010], a technique to tune linearly parametrized controllers given a loop-shaping objective and $\mathcal{H}_\infty$ performance criteria is proposed for SISO LTI systems. The robust performance conditions are expressed as linear or convex constraints around the desired open-loop on the Nyquist diagram. In [Saeki et al., 2010], these constraints are linearized around an initial stabilizing controller. In [Karimi and Kammer, 2017], an extension of this technique is propose and is not limited to linearly parametrized controllers and is applicable to MIMO systems. For SISO systems, [Karimi et al., 2018] proposed a technique to achieve the same goal without any initial stabilizing controller. Contrary to the previous mentionned methods, it converges to the global solution of the optimization problem, not only a local minima. An application to a power converter is available in [Nicoletti et al., 2017].

Some techniques based on non-convex optimization have also been proposed. In [Den Hamer et al., 2009], a fixed-order controller is tuned to ensure stability and optimize closed-loop stability. The admissible controllers are defined using Youla Q-parametrisation. The parameters appear in a non-convex way in the $\mathcal{H}_\infty$-norm of the closed-loop system, which is the criteria used in the minimisation. This technique requires to be initialized by a stabilizing controller. In [Khadraoui et al., 2013], a fixed-order controller is designed so that the closed-loop frequency response fits a desired frequency response. This is done by solving as a nonlinear programming problem based on the concept of bounded error. This technique is applicable to SISO systems only. In [Apkarian and Noll, 2018], a technique based on the computation of the winding number is proposed. A non-smooth trust region method is employed to tune the parameters of

the controller. The admissible controllers are arbitrarily parametrized. It is applied to infinite-dimensional LTI systems.

3.2.3 Predictive and learning data-driven control

The last category of data-driven techniques rely on the prediction of the plant behaviour. This is the case for the **Self-Tuning Regulators** (STR). This technique is presented in [Åström et al., 1977]: the parameters of the plant are estimated, a linear controller is deduced. It is an adaptive technique: when new data from the system are available, the estimation of the plant's parameters is updated and so is the control law.

Model-Free Adaptative control (MFAC) was introduced in [Hou, 1999] is another online technique. At each iteration, a local and compact model, relying on the concept of *pseudo partial derivative*, is obtained. It consists in a dynamic linearization of the plant's behaviour. The command signal u is then updated so that the system's output converge to the desired signal y_d.

Model-Free Control (MFC) was introduced in [Fliess, 2009]. More insights can be found in [Fliess and Join, 2013]. It proposes to tune intelligent PIDs controllers (iPID). As MFAC, it relies on local models, but expressed in a different form. The gains of the iPID are tuned according to the ultra local model identified at each step. This technique relies on numerical differentiation.

Another technique is the so called data-driven Model Predictive Control (MPC), see [Huang and Kadali, 2008], which is a derivative of the traditional model-based MPC framework [Lee, 2011]. This technique is also called the **subspace approach** since the main idea is that the plant's behaviour is represented as a subspace of finite dimension. The basis of this subspace is given by dynamic matrices, which can be obtained from input-output data. The command signal is then obtained at each time through the traditionnal MPC framework.

Local models can also be obtained through supervised machine learning. This is the concept of the **lazy learning** control approach, see [Bontempi et al., 1999]. At every instant, a linear local model of the plant is obtained. Then, the controller can be obtained using an optimal control method for example. The main drawback of this approach is to be computationally demanding.

Iterative Learning Control (ILC) is different from the other methods presented in this paragraph since it does not identify local models of the system's dynamic. ILC has been developped to control systems doing a repetitive task in a finite amount of time. The basic idea behind ILC is to iteratively find a command sequence u such that the tracking error converges to zero. At each iteration, the current controller is inserted in the closed-loop and the collected data are used offline to update the control law. ILC does not tune a controller, it directly compute the optimal command signal u. Different types of control laws can be considered. Although ILC does not make any assumptions regarding the system dynamics, in the end, the system is inverted, see [Markusson et al., 2001]. The main drawback of ILC is to require plenty of experiments. An overview of ILC techniques, applications and research developments can be found in [Ahn et al.,

2007].

3.2.4 Classification of data-driven control methods

In this section, the data-driven techniques are categorized according to the nature of the resolution of the control design problem. However, different classifications may also pertinent.

Online and offline data

In [Hou and Wang, 2013], a survey of data-driven control techniques is proposed. The data-driven control methods are classified according to the type of data: online, offline or hybrid. Indeed, contrary to offline techniques, online techniques also require to study the convergence of the proposed schemes. Moreover, the tools used to study closed-loop stability are rather different in both cases. When it comes to offline techniques, most stability criteria are based on the winding number or the small-gain theorem. These conditions are useless in online approaches where BIBO stability has to be studied.

Structure of the controller

Most techniques presented in Section 3.2 require to define a class $\mathcal{K}$ of admissible controllers. This choice is a key design decision. As a matter of fact, for model-reference techniques, the ideal controller is assumed to be contained in $\mathcal{K}$. For some techniques, the chosen structure is just a maximal order for the controller. This is the case for the CbT, the IFT or the non iterative UC algorithm: this assumption is then less limitating than for the VRFT where the poles of the controller are fixed in order to convexify the problem. To sum up, the class of admissible controllers, when required, should be large enough to allow to meet the performance specifications.

Knowledge of the system used in data-driven control

It should be noted that not all the techniques require the same knowledge of the system. For example, for reference model control, it is often required to know the unstable zeros of the system or to have access to an initial stabilizing controller. These two information are crucial when studying closed-loop stability. An initial stabilizing controller is also needed for most data-driven robust control techniques.

Finally, the techniques having the least knowledge of the plant are the predictive and learning ones. Paradoxically, they are the ones producing most information on the plant dynamics by identifying local models, or by inverting the plant for ILC techniques. On this last point, it should be noticed that the concept of ideal controller, which is central in model reference control, also needs to invert the system. This is exactly why some problems happen for non-minimum phase plants, and it makes the choice of the reference model a critical step.

Part II

Data-driven control in the frequency domain

Chapter 4

General problem formulation

In this chapter, a direct data-driven design method, based on frequency-domain data, is proposed. The identification of the plant is skipped and the controller is designed directly from the available measurements. The identification task is reported on the controller, using for the first time the Loewner approach, known for model approximation and reduction, and a subspace approach, known in system identification. The problem formulation is given in Section 4.1 and the main lines of the method are defined. The proposed technique is then illustrated through numerical examples in Section 4.2.

The purpose of this chapter is to illustrate the steps of the method, and the associated challenges, that will be further detailed in the next chapters. The proposed method has been introduced in its first version in [Kergus et al., 2017]. Successive improvements were added in [Kergus et al., 2018b] and [Kergus et al., 2018a] concerning the controller identification and in [Kergus et al., 2019b] concerning the reference model selection and the data-driven stability analysis. Applications can be found in [Kergus et al., 2019a].

Contents

4.1 Problem formulation

4.1.1 The model reference problem

As recalled in Chapter 3, the objective of data-driven techniques is to design a controller on the basis of experimental data from the plant, without having to identify a parametric model of the system to be controlled. The proposed method is a model reference one, like the techniques presented in Section 3.2.1: the specifications are expressed as a reference transfer function which represents the desired closed-loop behavior.

The problem is shown on Figure 4.1. The goal is to find a controller $\mathbf{K}$ for an unknown plant $\mathbf{P}$ so that $\mathbf{K}$ gives a closed-loop as close as possible to the reference transfer $\mathbf{M}$. The proposed method can be used for SISO plants as well as for MIMO plants. The number of inputs and outputs of the system to be controlled are respectively denoted n_u and n_y.

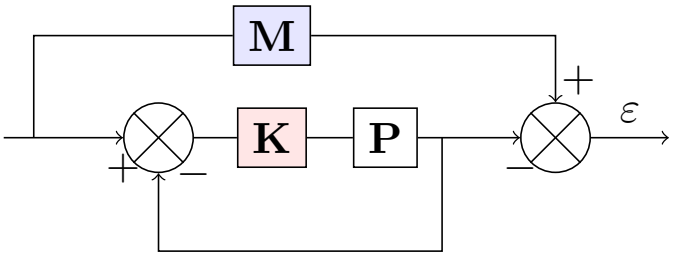

Figure 4.1: Problem formulation: $\mathbf{M}$ is the desired closed-loop, $\mathbf{P}$ is the plant and $\mathbf{K}$ the controller to be designed.

The proposed formulation is very close from the one of the CbT, see Figure 3.2. However, while the VRFT or the CbT are based on time-domain data, in this work, the controller is designed on the basis of frequency-domain data. The data is given as samples of the frequency response of the plant $\{\omega_i, \Phi_i\},\ i = 1 \dots N$, where $\Phi_i \in \mathbb{C}^{n_y \times n_u}$ and $\omega_i \in \mathbb{R}_+$. The method proposed in this work is closer to the VRFT in sense that it is a one-shot technique: the main idea for both methods is to find a controller that matches the ideal case for a given set of input-output data from the plant.

The direct data-driven control design technique proposed in this work, as introduced in [Kergus et al., 2017], relies on two steps:

1. The obtention of the frequency response $\mathbf{K}^\star(\imath\omega_i)$ of the *ideal* controller, the one that would give the desired reference model $\mathbf{M}$ if inserted in the closed-loop;
2. The identification of a model $\hat{\mathbf{K}}$ of this ideal controller through the Loewner framework or the subspace approach, in the frequency-domain.

This approach is rather different from the VRFT and the CbT since the proposed method identify a controller instead of formulating an optimization problem. Moreover, in this work, there is no need for an a priori selection of a class of controllers: the user does not have to determine the poles of the controller, which makes it really appealing for engineers. Indeed, for the VRFT, this is a difficult task that do not guarantee the selected poles optimality for a given reference model. It should be noted that the second step of the proposed method allows to obtain a reduced-order controller model. Therefore, it is possible for the user to fix a maximal order for the controller, which constitutes a sort of structuration.

4.1.2 Relying on the data

The proposed technique does not require a plant model. The only assumption is that the considered system is LTI and causal so that it can be characterized by its frequency

response. The main drawback of this type of model-free approach is that it is impossible to check the validity of the data, as explained in [Den Hamer, 2010]. Consequently, the data should reflect the dynamics to be controlled and be reliable, not too biased by noise or disturbances. To sum up, the data should be as close as possible to the true system behaviour. The same constraints also apply when using any black-box identification technique, the resulting model being used for control purposes most of the time.

This question of how much trust can be put in the data is directly related to the way they are obtained. As recalled in [Pintelon and Schoukens, 2012], a Frequency Response Function (FRF), which consists of transfer function measurements on a discrete frequency grid, contains a lot of information but not in a small set of parameters like a model: it is also called a non-parametric model. In [Pintelon and Schoukens, 2012], the quality of FRF measurements is analyzed. It depends on different factors including the experiment design, the sampling, the Fast Fourier Transform (FFT), but also the use of post-processing techniques on the raw measurements.

Remark 4.1.1. The measurements can be given as a time-domain data-set $\{\mathbf{u}(t_k), \mathbf{y}(t_k)\}_{k=1}^{N_k}$, where $\mathbf{u}(t_k) \in \mathbb{R}^{n_u}$ and $\mathbf{y}(t_k) \in \mathbb{R}^{n_y}$. A Fourier transform of the input and output signals is done and samples of the plant frequency response are estimated:

$$\Phi_i = \frac{Y(\imath\omega_i)}{U(\imath\omega_i)} = \frac{\mathcal{F}(\mathbf{y}(t_k))}{\mathcal{F}(\mathbf{u}(t_k))}. \tag{4.1}$$

Obviously, the signal $\mathbf{u}$ should sufficiently excite the system to get rich-enough information in terms of frequencies. Most often, this is how FRF measurements are obtained, the Fourier transform being obtained by applying a FFT to the collected time-domain signals. However, in some cases, like in electronics for example, the FRF measurements are directly obtained by a frequency analyser.

For system modelling as much as for data-driven control, the quality of the data plays a pivotal role in the performance of the employed technique. For this reason, experiment design is an important field of research in the area of system identification. In [Hjalmarsson, 2005], the close relation between system identification and closed-loop control performances is studied: it is concluded that "*experiment design is the most important design variable for a successful application*". The references therein contains plenty of experiment design techniques. The objective of experiment design is to maximize the information content of the measurements. The essential concepts and the premices of experiment design can be found in [Goodwin and Payne, 1977]. A review of different experiment design concepts and tools is available in [Gevers and Bombois, 2006]. A survey is available in [Pronzato, 2008] where special attention is given to non-parametric models, which is more pertinent in the present case.

When it comes to the obtention of good FRF measurements, specific advice can be found in [Phillips and Allemang, 2003] where an overview of excitation methods is proposed and the influence of averaging and post-processing techniques is discussed. Finally, considering the perspective of this work, the reader should refer to [Pintelon et al., 2010a] and [Pintelon et al., 2010b]: a technique to estimate the noise and obtain reliable FRF measurements of multivariable systems is proposed.

The objective of this thesis is not to study or improve the quality of FRF measurements. Assuming that a good experiment design was done, it is possible to filter the obtained FRF to obtain reliable data with a limited noise influence. However, the problem of noisy data can be addressed through the identification of the ideal controller. This topic is more detailed in Chapter 5.

4.1.3 The ideal controller

As for other model reference data-driven control techniques, see Section 3.2.1, the concept of ideal controller is central in the control design. As a matter of fact, it is the one LTI controller that would give exactly the objective transfer function $\mathbf{M}$ if inserted in the closed-loop. Each process and reference model pair corresponds to one ideal controller. Thanks to this key notion, the problem of identifying a model of the plant is moved to the identification of the controller.

The first step of the method proposed in this thesis consists in characterizing this ideal controller. The closed-loop objective transfer $\mathbf{M}$ and the open-loop experimental data of the plant are used to get the frequency response of the ideal controller $\{\omega_i, \mathbf{K}^\star(\imath\omega_i)\}_{i=1}^N$ for a limited frozen set of frequency values. Therefore, by definition, the frequency response samples of the ideal controller are computed according to (4.2):

$$\forall\ i = 1 \dots N,\ \mathbf{K}^\star(\imath\omega_i) = \Phi_i^{-1}\mathbf{M}(\imath\omega_i)(I_{n_y} - \mathbf{M}(\imath\omega_i))^{-1}. \tag{4.2}$$

The ideal controller is also important in the VRFT or CbT even though it is not used expressively during the design of the controller, see Chapter 3. Both techniques assume that, in the ideal case, the selected class of controllers $\mathcal{K}$ contains the ideal controller $\mathbf{K}^\star$. This implies that the choice of $\mathcal{K}$ is a key step in the success of such techniques. This can be a complicated step in the case of the VRFT, since the admissible controllers are linearly parametrized to make the design problem convex. This is less important for the CbT or the IFT which design fixed-order controllers described by fully-parametrized transfer functions. Therefore, the first strength of our method is that it does not require to define a set $\mathcal{K}$ of admissible controllers other than the set of rational and linear models. The only possible structuration consists in the choice of a maximal order by the user.

The mismatched case happens when $\mathbf{K}^\star \notin \mathcal{K}$. Even in this case, it is assumed that the difference between $\mathbf{K}(\theta)$ and $\mathbf{K}^\star$ can be made small. For the VRFT or the non-iterative CbT, the sensitivity function $(1 + \mathbf{P}\mathbf{K}(\theta))^{-1}$ is then approximated by the ideal one $(1 + \mathbf{P}\mathbf{K}^\star)^{-1}$. It allows to make the model reference control criterion convex in the controllers parameters θ. Consequently, the class of admissible controllers should be chosen large enough so that this assumption is valid.

To sum up, the basic idea of model reference control is to get as close as possible to the ideal case. The underlying assumption is that the corresponding ideal controller represents the behaviour that the designed controller should reproduce. However, this assumption is not always true, as explained in [Bazanella et al., 2011]. For example, for NMP systems, the achievable dynamics are limitated by the RHP zeros of the plant. Therefore, if the reference model does not take into account these intrinsic limitations, the ideal controller may destabilize the plant internally. In this case, its behaviour is

disastrous in terms of closed-loop stability and should not be reproduced in the designed controller. This problem will be illustrated in Section 4.2 by applying the proposed method on numerical examples. This issue will be tackled in Chapter 6 by proposing a method to choose an achievable model reference.

4.1.4 Identification of the controller

Assuming that the specified reference model $\mathbf{M}$ is well chosen, obtaining a closed-loop as close as possible to $\mathbf{M}$ boils down to find a controller as close as possible to the ideal controller. Thanks to the concept of ideal controller, this can be done by moving the identification problem from the plant to the controller directly.

In the proposed method, the ideal controller $\mathbf{K}^\star$, known over a limited data samples, is approximated by $\mathbf{K}$, a linear time-invariant model defined by the following generalized state-space form:

$$\mathbf{K} : \left\{ \begin{array}{rcl} E\dot{\mathbf{x}}(t) & = & A\mathbf{x}(t) + B\mathbf{e}(t) \\ \mathbf{u}(t) & = & C\mathbf{x}(t) \end{array} \right. , \tag{4.3}$$

where $\mathbf{x}(t) \in \mathbb{R}^n$ the state vector, $\mathbf{e}(t) \in \mathbb{R}^{n_y}$ the input vector of the controller, which is the tracking error, $\mathbf{u}(t) \in \mathbb{R}^{n_u}$ the output vector (i.e. the control signal) and $E, A \in \mathbb{R}^{n\times n}$, $B \in \mathbb{R}^{n\times n_y}$ and $C \in \mathbb{R}^{n_u\times n}$. Its associated transfer function is $\mathbf{K}(s) = C(sE - A)^{-1}B$.

Remark 4.1.2. There is no D-term in (4.3) since it can be embedded in the E matrix.

The problem is to find a realization K of the ideal controller, through the following interpolatory conditions:

$$\forall i = 1 \dots N,\ \mathbf{K}(\imath\omega_i) = \mathbf{K}^\star(\imath\omega_i) \tag{4.4}$$

This is achieved through the Loewner framework or the subspace approach. These two techniques will be recalled in Chapter 5. The identification of the ideal controller allows to avoid structuring the controller, which makes this technique really easy to use compared to the VRFT. Indeed, the poles will be determined during the identification step and will therefore be adapted to the considered reference model $\mathbf{M}$. The order n of the designed controller $\mathbf{K}$ can be a tunable parameter in the method if one wants to reduce its complexity. However, it can be chosen automatically since the considered identification techniques both rely on an order revealing decomposition.

As said earlier, this step, not formulated as the minimization of a control criterion, distinguish the method proposed in this work from the other techniques described in Section 3.2.1. Nevertheless, it should be noted that the same objective is pursued: to minimize the norm of the error between the reference model $\mathbf{M}$ and the resulting closed-loop $\mathbf{H}$:

$$\mathbf{H} = \frac{\mathbf{PK}}{1 + \mathbf{PK}}.$$

Indeed, this error, known as $J(\theta)$ for other techniques presented in Section 3.2.1, can

be developed as follows (written in the SISO case):

$$\begin{aligned}\|\mathbf{M}-\mathbf{H}\| &= \left\| \frac{\mathbf{P}\mathbf{K}^\star}{1+\mathbf{P}\mathbf{K}^\star} - \frac{\mathbf{P}\mathbf{K}}{1+\mathbf{P}\mathbf{K}} \right\| \\ &= \left\| \frac{\mathbf{P}(\mathbf{K}^\star-\mathbf{K})}{(1+\mathbf{P}\mathbf{K}^\star)(1+\mathbf{P}\mathbf{K})} \right\| \\ &= \left\| \frac{\mathbf{P}(\mathbf{K}^\star-\mathbf{K})}{(1+\mathbf{P}\mathbf{K}^\star)^2-(1+\mathbf{P}\mathbf{K}^\star)\mathbf{P}(\mathbf{K}^\star-\mathbf{K})} \right\|.\end{aligned} \tag{4.5}$$

Therefore, according to (4.5), when the designed controller $\mathbf{K}$ tends to $\mathbf{K}^\star$, the error between $\mathbf{M}$ and $\mathbf{H}$ tends to zero. This is why, the interpolation and the order reduction of the ideal controller, because they minimize an $\mathcal{H}_2$-norm, goes in the same direction that solving an optimization problem as in other model reference control techniques.

4.2 Application to numerical examples

In this section, the proposed method is applied on the two numerical examples presented in Chapter1 in order to highlight the underlying challenges that will be addressed in the following chapters.

4.2.1 Application of the proposed direct control method: the DC motor

The first considered system is a DC motor, see Section 1.2.3. It is a SISO and stable second-order plant described by the following transfer function:

$$\mathbf{P}(s) = \frac{0.01}{0.005s^2+0.06s+0.1001} = \frac{2}{(s+9.997)(s+2.003)}.$$

In the first place, the data is noise-free, $N=100$ samples $\{\omega_i, \mathbf{P}(\imath\omega_i)\}_{i=1}^N$ of the frequency response of $\mathbf{P}$ are considered, for frequencies $\{\omega_i\}_{i=1}^N$ logarithmically spaced between 0.1 and 10^3rad.s^{-1}. In order to have no tracking error and to fasten the response of the system, the reference model is chosen as:

$$\mathbf{M}(s) = \frac{1}{\frac{s^2}{\omega_0^2}+\frac{2\xi}{\omega_0}s+1}, \tag{4.6}$$

with $\omega_0 = 10$rad.s^{-1} and $\xi = 1$. The corresponding ideal controller, calculated thanks to the expressions of $\mathbf{M}$ and of the true system $\mathbf{P}$, is:

$$\mathbf{K}^\star(s) = \frac{50s^2+600s+1001}{s^2+20s} = \frac{50(s+9.997)(s+2.003)}{s(s+20)}. \tag{4.7}$$

It should be noted that the expression of the ideal controller given in (4.7) is supposed to be unknown when applying a data-driven reference model technique. Nevertheless, samples of its frequency-response can be estimated at the frequencies $\{\omega_i\}_{i=1}^N$ without using the plant model, but only the data, according to Equation (4.2). Then, given the interpolatory conditions in (4.4), the ideal controller is interpolated through the Loewner framework, giving us the minimal realization $\mathbf{K}$ of $\mathbf{K}^\star$, also visible on Figure 4.2.

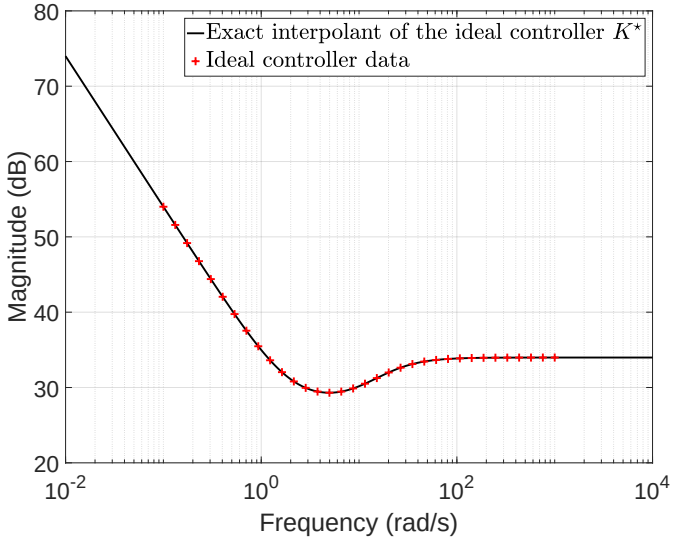

Figure 4.2: Interpolation of the ideal controller for the DC motor example.

Since the data is unbiased, the expression of the minimal realisation $\mathbf{K}$ has exactly the same expression than $\mathbf{K}^\star$, see (4.7). This is due to the properties of the Loewner framework that will be detailed in Chapter 5. The subspace approach also recover the exact expression of the ideal controller with a second-order model. This controller allows to achieve the desired closed-loop performances, as shown on Figure 4.3.

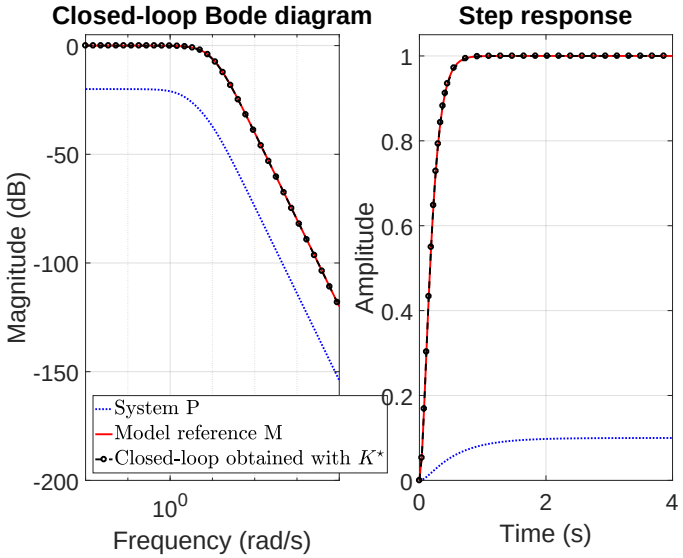

Figure 4.3: Closed-loop performances achieved in the DC motor example using the minimal realization of the ideal controller obtained through the Loewner framework.

However, this second-order controller would not be implemented to control a second-order system because it is as complex than the system itself. To that extent, the ideal controller is reduced to two first-order models: $\mathbf{K_l}$, obtained through the Loewner frame-

work, and $\mathbf{K_s}$, obtained by the subspace-based algorithm. Their frequency response are given in Figure 4.4.

$$\mathbf{K_l}(s) = \frac{49.828}{s - 1.074.10^{-5}}$$

$$\mathbf{K_s}(s) = \frac{33.403(s + 1.505)}{(s + 0.0126)}$$

The performances of the resulting closed-loops are shown on Figure 4.5. $\mathbf{K_l}$ is almost

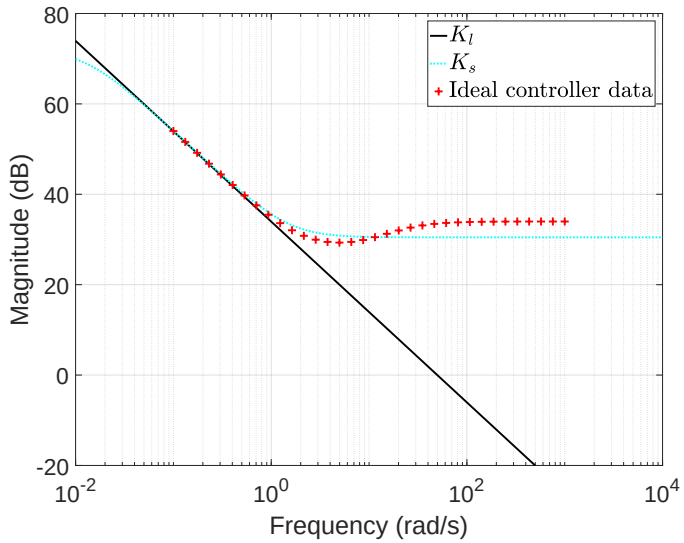

Figure 4.4: Identification of the first-order controllers $\mathbf{K_l}$ and $\mathbf{K_s}$, respectively through the Loewner framework and the subspace approach.

an integrator: therefore, the tracking error is made null in permanent regime. However, it creates an overshoot of 57% and a pseudo-periodic output signal: it takes 5.5 seconds for the tracking error to be lower than 5%. Indeed, the fact that $\mathbf{K}_l$ contains only an integrator tends to destabilize the feedback structure: it increases the overshoot and reduces closed-loop robustness. On the other side, this problem is avoided with the subspace approach: $\mathbf{K}_s$ is not a mere integrator but also contains a zero. The subspace-based controller $\mathbf{K_s}$ only creates an overshoot of 3% and its response time is 0.35s. In permanent regime, the associated closed-loop gives a tracking error of 0.5%. Considering that the original plant has a static gain of 0.01 and a response-time of 1.5s, $\mathbf{K_s}$ is the best controller between the two obtained by the proposed method. The main reason why $\mathbf{K_l}$ is less performing is that the Loewner framework identify a strictly proper model, contrary to the subspace approach.

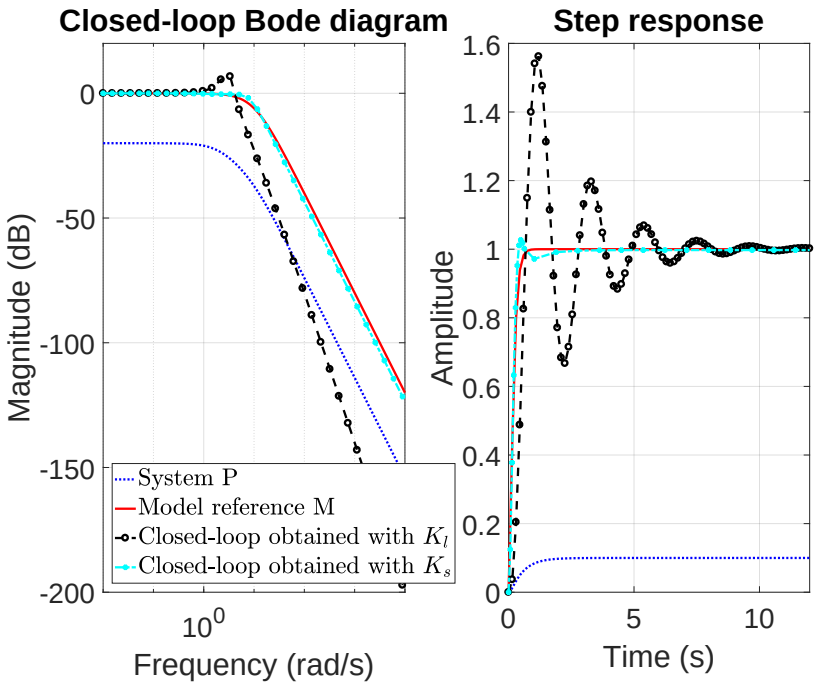

Figure 4.5: Closed-loop performances achieved in the DC motor example when inserting $\mathbf{K_l}$ and $\mathbf{K_s}$ in the closed-loop.

The synthesis of these two controllers illustrates the importance of the identification of the controller as well as its reduction. From the same data from the ideal controller, the Loewner framework and the subspace approach give two really different controllers when reducing the order. This aspect will be detailed in Chapter 5 in which the two mentioned approximation techniques are recalled and their application to the ideal controller is detailed.

This example also highlights the difficulty of choosing the reference model $\mathbf{M}$, even for a simple case like this one. It will be shown in Chapter 6 that the desired performances expressed in $\mathbf{M}$ have a great impact on the design process and the resulting closed-loop. It is actually the same issue of compromising between the complexity of the controller and the closed-loop performances, as in model-based control. For example, in the present case, by relaxing the performance specifications in terms of response time, the identified first-order controllers will produce less overshoot. For instance, by setting $\omega_0 = 1$ rad.s^{-1} in the reference model $\mathbf{M}$ instead of $\omega_0 = 10$rad.s^{-1}, see (4.6), the identified first-order controllers $\mathbf{K_l}$ and $\mathbf{K_s}$ allow to match the desired-closed loop behaviour almost perfectly, see Figures 4.6 and 4.7. Their expressions are given by:

$$\mathbf{K_l}(s) = \frac{5.0049}{s - 3.884.10^{-7}},$$

$$\mathbf{K_s}(s) = \frac{0.5(s + 10.01)}{(s - 2.758.10^{-5})}.$$

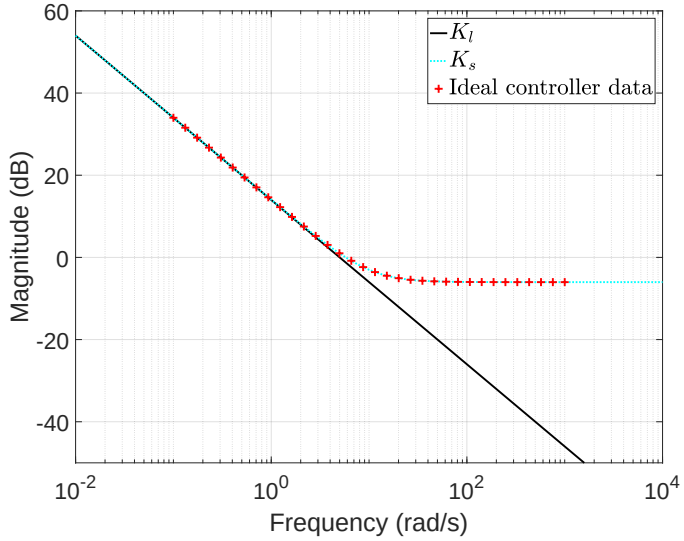

Figure 4.6: Identification of first-order controllers through the Loewner framework and the subspace approach for the DC motor for a reference model defined as in (4.6) with $\omega_0 = 1$ rad.s^{-1} and $\xi = 1$.

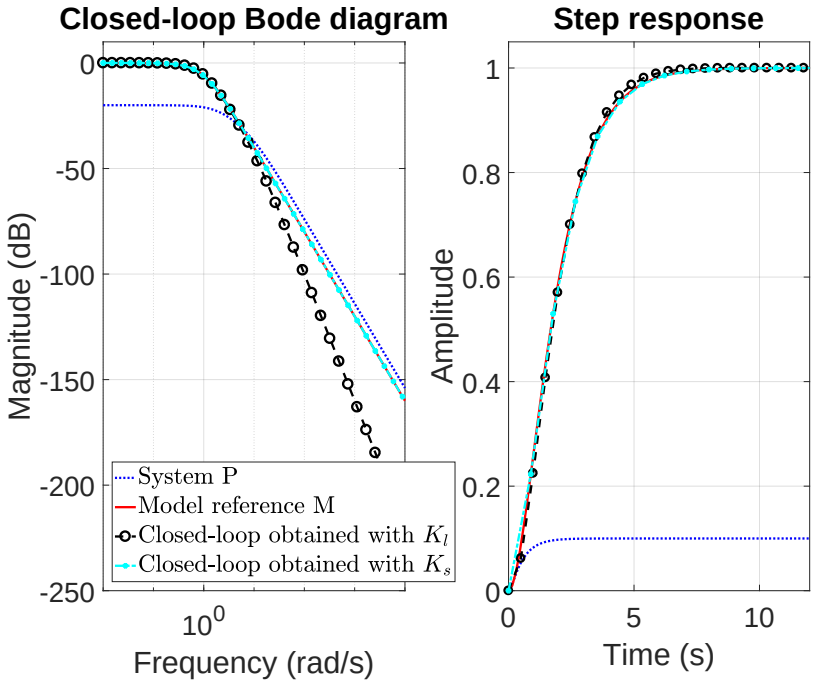

Figure 4.7: Closed-loop performances achieved in the DC motor example with first-order controllers designed using a reference model $\mathbf{M}$ defined as in (4.6) with $\omega_0 = 1$ rad.s^{-1} and $\xi = 1$.

4.2.2 The particular case of unstable and non-minimum phase system

Now let us move to a more challenging control design problem by considering a non-

minimum-phase plant through the flexible transmission benchmark, see Section 1.2.3 for the definition of the considered plant. The system is characterized by the following transfer function:

$$P(s) = \frac{0.03616(s - 140.5)(s - 40)^3}{(s^2 + 1.071s + 157.9)(s^2 + 3.172s + 1936)}.$$

The objective is to obtain a well-damped and faster closed-loop behaviour. In the first time, the reference model $\mathbf{M}$ is defined by a second-order transfer function as in the DC motor example, see (4.6), but with $\omega_0 = 10$ rad.s^{-1} and $\xi = 1$. In order to apply the proposed method, $N = 200$ samples of the frequency-response of the plant $\mathbf{P}$ are considered. The corresponding frequencies are logarithmically spaced between 1 and 10^3 rad.s^{-1}. For now, the considered data is noise-free.

The frequency-response samples of the corresponding ideal controller are computed according to Equation (4.2). The theoretical expression of the ideal controller is given in (4.10). As for the DC motor example, the transfer of the ideal controller is supposed to be unknown in a data-driven control framework.

$$\mathbf{K}^\star(s) = \frac{2765.5(s^2 + 1.071s + 157.9)(s^2 + 3.172s + 1936)}{s(s + 20)(s - 140.5)(s - 40)^3} \tag{4.8}$$

Since the reference model does not contain the RHP zeros of the plant, by definition, the ideal controller compensates them. Therefore, according to Theorem 2.2.1, it destabilizes the plant internally. The interpolation of the ideal controller through the Loewner framework gives the exact expression of the ideal controller. In this case, the ideal controller represents a behaviour that should not be identified. Even if the reduced-order controllers do not cancel the RHP zeros of the plant, trying to reduce the error between the designed controller and this internally destabilizing ideal controller is not a good strategy.

Here, the model of the plant is known, it is then possible to detect this problem. For an unknown plant however, this configuration is hard to detect. Indeed, in the present version of this method, no technique has been proposed to analyze internal stability of the resulting closed-loop. Most traditional tools to analyze or enforce closed-loop stability involve a model of the controlled plant. To tackle this issue in a data-driven framework, in Chapter 7, the stability criteria proposed in [Van Heusden et al., 2009], based on the small-gain theorem, is derived to identify a stabilizing controller.

It should be noted that the same type of problem occurs for unstable plants: for a poor choice of specifications, the ideal controller's zeros compensates the RHP poles of the system. This can be explained by the fact that the instabilities of the plant, its RHP poles or zeros, represents intrinsic closed-loop performances limitations that cannot be overcome. The only solution is to use an achievable model reference, which takes into account the instabilities of the system.

In [Campi et al., 2002], the VRFT is applied on this benchmark example. The reference model used is $\mathbf{M}_{VRFT}$, given by the following discrete-time transfer function:

$$\mathbf{M}_{VRFT}(z) = \frac{z^{-3}(1 - \alpha)^2}{(1 - \alpha z^{-1})^2}$$

with $\alpha = e^{-T_s\omega_0}$, $T_s = 0.05s$ and $\omega_0 = 10$ rad.s^{-1}. Applying a bilinear transform, the continuous reference model $\mathbf{M}_{VRFT}$ is obtained:

$$\mathbf{M}_{VRFT}(s) = \frac{-0.059985(s-40)^3}{(s+40)(s+9.797)^2}. \tag{4.9}$$

It contains the RHP zeros of the plant except the one at 140.5 rad.s^{-1}. This zero is introduced by the analogic-numeric converter and is situated beyond the maximal frequency $\omega_{max} = \frac{2\pi}{T_s} = 125.7$ rad.s^{-1}. Using this reference model, the ideal controller is now given by:

$$\mathbf{K}^{\star}_{VRFT}(s) = \frac{-1.565(s^2+1.071s+157.9)(s^2+3.172s+1936)}{s(s^2+49.43s+1102)(s-140.5)}. \tag{4.10}$$

The three RHP zeros of the plant at 40 rad.s^{-1} are not compensated by the ideal controller anymore, which represents a huge improvement. It should be noted that the unstable poles of $\mathbf{K}^{\star}$ will not affect the VRFT design process since it is not simulated during the experiment ($\omega_{max} = 125.7$ rad.s^{-1}). Therefore, using $\mathbf{M}_{VRFT}$ as a reference model does not induce any instability compensation in the open-loop in the ideal case.

This example highlights that the choice of the reference model has a major impact on the design process, even more for NMP or unstable plants. In the present case, $\mathbf{M}$ and $\mathbf{M}_{VRFT}$ present similar dynamics, see Figure 4.8, but the first one is not achievable by the plant. The choice of an achievable reference model is one of the contributions of this work: a method is proposed in Chapter 6. It requires to perform a preliminary analysis of the plant's FRF since, as illustrated in this example, the system's instabilities have to be known to define good closed-loop specifications.

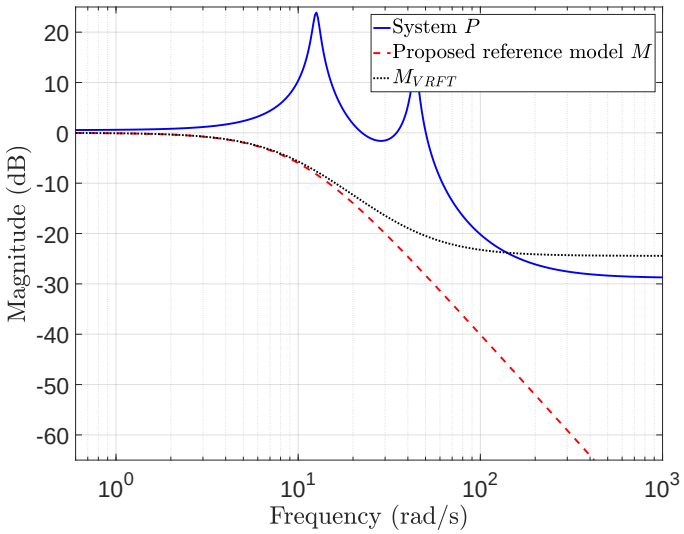

Figure 4.8: Frequency response of the plant and of the two reference models $\mathbf{M}$ and $\mathbf{M}_{VRFT}$.

4.3 Challenges in model-reference control

The application of the proposed method on these two examples, including a non-minimum phase plant, emphasizes the challenges in model-reference control. They are briefly recalled hereafter and each one of them is subject to a contribution detailed in the next chapters.

Identification of the controller

The first question that should be answered concerns the identification of the controller. The two frequency-domain techniques used in this work, the Loewner framework and the subspace approach, will be recalled in Chapter 5. They both allow to reduce the complexity of the controller. In order to prevent instability compensation in the open-loop and to avoid introducing unstable dynamics, the stability of the controller will be enforced during the identification of the controller.

Choice of an achievable reference model

As shown on the example of the flexible transmission, a poor choice of the reference model $\mathbf{M}$ can lead to the identification of a destabilizing controller. This problem has been underlined in [Bazanella et al., 2011], [Piga et al., 2018] and [Selvi et al., 2018]. Therefore, the choice of the reference model should be done wisely, by taking into account the plant's instabilities. As a matter of fact, the unstable poles and zeros of a system constitute the main limitations of the achievable closed-loop performances. In this thesis, a technique to choose the reference model is proposed in Chapter 6: the FRF is first used to estimate the plant's instabilities in a data-driven way and an achievable model-reference is built.

Towards data-driven closed-loop stability

The application of the proposed method on numerical examples has shown that, in its original form, it is not possible to assess whether the obtained closed-loop is internally stable or not. As for data-driven control techniques in general, studying closed-loop stability in a data-driven framework is a challenging problem. In Chapter 7, the technique proposed in [Van Heusden et al., 2009] is applied to the proposed method in order to study the stability of the resulting closed-loop and to validate the obtained controllers.

Summary

In this chapter, the main idea of the proposed method is introduced. Considering some frequency-domain data $\{\omega_i, \Phi_i\}_{i=1}^N$ from the plant $\mathbf{P}$ and a reference model $\mathbf{M}$ provided by the user, the proposed technique consists in two steps:

1. In the first place, the ideal controller, the one LTI controller that would have lead to the desired reference model during the considered experiment, is determined by samples of its frequency-response, computed according to (4.2).

2. The second step consists in identifying the ideal controller and reducing its order. Two methods are considered in this work: the Loewner interpolation framework and the subspace approach. This step will be detailed in the next chapter.

This initial version of the proposed technique is applied on two numerical examples, the DC motor and the flexible. The results highlight that the choice of the reference model $\mathbf{M}$ is crucial and should take into account the plant's performance limitations. This aspect will be detailed in Chapter 6. The proposed examples also show the need for a stability analysis. This point will be treated in Chapter 7.

Chapter 5

Controller identification in the frequency-domain

This chapter first aims at recalling the frequency-domain identification techniques used in the proposed data-driven framework in Section 5.1. These methods, namely the Loewner framework and the subspace approach, are then used in Section 5.2 to identify the ideal controller defined in Chapter 4. As in [Kergus et al., 2018b], the stability of the controller is enforced and special attention is given to the noisy case. Finally, numerical applications are provided in Section 5.3.

Contents

5.1 Preliminary: frequency-domain identification

The objective of this section is to give an overview of the developments of system identification in the first time. More attention is then drawn on the Loewner framework in Section 5.1.2 and on the subspace approach in Section 5.1.3 as these two methods will be used later on to identify a controller through the proposed data-driven control technique. These two identification techniques have been chosen because of their complementarity. Obviously, other frequency-domain techniques could be considered for controller identification purposes.

5.1.1 Brief overview of system identification

The history and developments of system identification are extensively exposed in [Deistler, 2002], [Ljung, 2010] and [Gevers, 2006]. Only the principal milestones in

relation with control theory of the area will be recalled here. The objective is mainly to show how control and system identification are related and intrinsically linked.

Development of system identification: history and techniques

As recalled in [Deistler, 2002], system identification began to develop in the late 18th century. The early work in system identification consists in time series analysis, with the harmonic analysis and the Fourier theory. The least square method, allowing to fit a model on measurement data, was developed at the beginning of the 19th century by Legendre and Gauss. In the early 20th century, Galton and Pearson made a significative contribution to statistics by conceptualizing the linear regression and the correlation analysis. Time series analysis kept growing during the last century, mainly because of the econometrics high demand.

As explained in [Gevers, 2006], the interest for system identification considerably increased due to the development of model-based control theory in the 1960s. Since, in a lot of applications, no mathematical description of the plant can be derived from physical laws, there was a need to obtain a model on the basis of measurements data in order to broaden the fields of application of these new model-based control techniques.

The state-space realization theory, which is the origin of subspace identification, and the maximum likelihood framework, the heir of time series analysis, were introduced during this period. Afterwards, system identification progressively became the search for the best approximation model, instead of looking for the true system inside a predefined model set. As explained in [Hjalmarsson, 2005], looking for a model of the true system is pointless since every model depends on the input used during the experiment. Therefore, the challenge is to choose wisely the input in order to make the system reveal its relevant properties. A good model will be an approximation of the true system that reflects these properties. These considerations gave birth to the field of experiment design. The latest developments of system identification focused also on the identification of non linear system, on model order reduction, the identification of model uncertainties and on identification for control.

Duality between control and system identification

These last two fields of interest, namely uncertainty modelling and identification for control, underline the connection between modelling and control, even if, at the beginning, these two steps were kept separate. This was possible by assuming that the considered model represents the true system: this is called the certainty equivalence principle. However, the actual modelling errors can lead to poor control performances or even to design a destabilizing controller. Therefore, the uncertainties have to be taken into account and this why adaptive control schemes and robust control ones have been developed.

As said in [Gevers, 2005], the control community introduced the idea that instead of looking for the true system, system identification should find its best approximation within a model set. This idea then gave birth to identification for control: the identification should be done in such a way that modelling errors does not affect the control

objective too much. Only the dynamics to be controlled need to be reflected in the model, and sometimes a simple model can be enough for control purposes.

To sum up, the latest developments of system identification were destined to control purposes. On one side, uncertain models allow to analyze the performances and the robustness of the designed closed-loops. On the other side, I4C provides models in a given set, suited for control design by their reflection of the dynamics to be controlled only.

Finally, the interplay between system identification and control design can be explained by different factors but the most important one is that the main motivation behind the identification of a model is often the control design. It should be noted that it is the case for model-based control but also for data-driven control thanks to the concept of ideal controller, see Section 4.2. What changes is only the object on which you apply an identification technique: you can identify either the plant or the controller directly.

Let us now briefly describe the Loewner framework and the subspace approach, used along this manuscript to identify a controller model $\mathbf{K}$ of the ideal controller $\mathbf{K}^\star$.

5.1.2 Loewner-based interpolation

The Loewner approach, exposed in [Mayo and Antoulas, 2007] and [Antoulas et al., 2015], is an interpolatory method initially used for model approximation and reduction. Since this method is one of the key tools in the proposed data-driven control design technique, the objective of this section is to recall its principle and its different properties. However, interested readers are invited to refer to the above references for details.

Considering a plant $\mathbf{G}$, the objective of the Loewner-based approach is to find a descriptor realization $\mathbf{H} = [E, A, B, C, 0]$ of an appropriate order n so that the corresponding transfer function $\mathbf{H}(s) = C(sE - A)^{-1}B$ matches data from the plant $\mathbf{G}$. The obtained model is a descriptor system, also called generalized state-space system, defined as follows:

$$\mathbf{H} : \left\{ \begin{array}{rcl} E\dot{\mathbf{x}}(t) & = & A\mathbf{x}(t) + B\mathbf{u}(t) \\ \mathbf{y}(t) & = & C\mathbf{x}(t) \end{array} \right. , \tag{5.1}$$

where $\mathbf{x}(t) \in \mathbb{R}^n$ the state vector, $\mathbf{u}(t) \in \mathbb{R}^{n_u}$ the input vector of the system, $\mathbf{y}(t) \in \mathbb{R}^{n_y}$ the output vector, and $\mathbf{E}, \mathbf{A} \in \mathbb{R}^{n \times n}$, $\mathbf{B} \in \mathbb{R}^{n \times n_u}$ and $\mathbf{C} \in \mathbb{R}^{n_y \times n}$. The pencil $s\mathbf{E} - \mathbf{A}$ needs to be regular, meaning that $det(s\mathbf{E} - \mathbf{A}) \neq 0$.

Remark 5.1.1. Omission of the D-term
The D-term of the descriptor state-space representation of (5.1) is omitted when looking for a minimal realisation through the Loewner framework. As explained in Chapter 2, if there is a D-term, it is embedded in the E matrix as an infinite mode.

The plant's data is given as a set of interpolation points, $\{\lambda_i\}_{i=1}^{\rho}$ and $\{\mu_j\}_{j=1}^{\nu}$, tangential directions, $\{\mathbf{r}_i\}_{i=1}^{\rho}$ and $\{\mathbf{l}_j\}_{j=1}^{\nu}$, and of measurements data, $\{\mathbf{w}_i\}_{i=1}^{\rho}$ and $\{\mathbf{v}_j\}_{j=1}^{\nu}$. This set is divided between:

- right interpolation data $\left\{(\lambda_i, \mathbf{r}_i, \mathbf{w}_i) \in \mathbb{C} \times \mathbb{C}^{n_u \times 1} \times \mathbb{C}^{n_y \times 1}\right\}_{i=1}^{\rho}$

- and left interpolation data $\left\{(\mu_j, \mathbf{l}_j, \mathbf{v}_j) \in \mathbb{C} \times \mathbb{C}^{1\times n_y} \times \mathbb{C}^{1\times n_u}\right\}_{j=1}^{\nu}$

The objective is to find $\mathbf{H}$ that interpolates both right and left constraints, given as (5.2).

$$\left\{ \begin{array}{lll} \forall i = 1 \dots \rho & \mathbf{H}(\lambda_i)\mathbf{r}_i & = \mathbf{w}_i \\ \forall j = 1 \dots \nu & \mathbf{l}_j\mathbf{H}(\mu_j) & = \mathbf{v}_j \end{array} \right. \tag{5.2}$$

This problem is called the generalized realization problem.

Let us first introduce the following compact notations:

$$\begin{array}{llll} \Lambda = \begin{bmatrix} \lambda_1 & & \\ & \ddots & \\ & & \lambda_\rho \end{bmatrix} \in \mathbb{C}^{\rho\times\rho} & R = [\mathbf{r_1} \dots \mathbf{r}_\rho] \in \mathbb{C}^{n_u\times\rho} & W = [\mathbf{w_1} \dots \mathbf{w}_\rho] \in \mathbb{C}^{n_y\times\rho} \\ M = \begin{bmatrix} \mu_1 & & \\ & \ddots & \\ & & \mu_\nu \end{bmatrix} \in \mathbb{C}^{\nu\times\nu} & L = \begin{bmatrix} \mathbf{l_1} \\ \vdots \\ \mathbf{l}_\nu \end{bmatrix} \in \mathbb{C}^{\nu\times n_y} & V = [\mathbf{v_1} \dots \mathbf{v}_\nu] \in \mathbb{C}^{\nu\times n_u} \end{array} \tag{5.3}$$

Remark 5.1.2. The tangential directions $\{\mathbf{r}_i\}_{i=1}^{\rho}$ and $\{\mathbf{l}_j\}_{j=1}^{\nu}$ are not relevant in the SISO case and can be fixed to 1. The resolution of the general tangential interpolation problem is exposed here: it will be used in the next Chapter when defining the class of achievable reference models for the proposed method.

A key in the resolution of the generalized realization problem are the Loewner and shifted Loewner matrices, completely defined by the interpolation points and the tangential data, given in (5.4) and (5.5) respectively.

$$\mathbb{L} = \begin{pmatrix} \dfrac{\mathbf{v_1}\mathbf{r_1} - \mathbf{l_1}\mathbf{w_1}}{\mu_1 - \lambda_1} & \cdots & \dfrac{\mathbf{v_1}\mathbf{r}_\rho - \mathbf{l_1}\mathbf{w}_\rho}{\mu_1 - \lambda_\rho} \\ \vdots & \ddots & \vdots \\ \dfrac{\mathbf{v}_\nu\mathbf{r_1} - \mathbf{l}_\nu\mathbf{w_1}}{\mu_\nu - \lambda_1} & \cdots & \dfrac{\mathbf{v}_\nu\mathbf{r}_\rho - \mathbf{l}_\nu\mathbf{w}_\rho}{\mu_\nu - \lambda_\rho} \end{pmatrix} \in \mathbb{C}^{\nu\times\rho} \tag{5.4}$$

$$\mathbb{L}_s = \begin{pmatrix} \dfrac{\mu_1\mathbf{v}_1\mathbf{r}_1 - \mathbf{l}_1\mathbf{w}_1\lambda_1}{\mu_1 - \lambda_1} & \cdots & \dfrac{\mu_1\mathbf{v}_1\mathbf{r}_\rho - \mathbf{l}_1\mathbf{w}_\rho\lambda_\rho}{\mu_1 - \lambda_\rho} \\ \vdots & \ddots & \vdots \\ \dfrac{\mu_\nu\mathbf{v}_\nu\mathbf{r}_1 - \mathbf{l}_\nu\mathbf{w}_1\lambda_1}{\mu_\nu - \lambda_1} & \cdots & \dfrac{\mu_\nu\mathbf{v}_\nu\mathbf{r}_\rho - \mathbf{l}_\nu\mathbf{w}_\rho\lambda_\rho}{\mu_q - \lambda_\rho} \end{pmatrix} \in \mathbb{C}^{\nu\times\rho} \tag{5.5}$$

Assuming that the data comes from a rational matrix function $\mathbf{G}(s)$, the shifted-Loewner matrix $\mathbb{L}_s$ is the Loewner matrix generated by $s\mathbf{G}(s)$.

Considering that the system $\mathbf{G}$ is equipped with a descriptor state-space model $(E, A, B, C, 0)$ of order n, the generalized tangential observability and controllability matrices, $\mathcal{O}_\nu$ and $\mathcal{C}_\rho$, are introduced in (5.6) and (5.7) respectively. The main difference with the generalized observability and controllability matrices introduced in Chapter 2, see (2.15) and (2.14), is the introduction of the tangential directions, which changes the

dimension of these matrices, and of the shift points $\{\mu_j\}_{j=1}^{\nu}$ and $\{\lambda\}_{i=1}^{\rho}$.

$$\mathcal{O}_\nu = \begin{pmatrix} \mathbf{l}_1 C(\mu_1 E - A)^{-1} \\ \vdots \\ \mathbf{l}_\nu C(\mu_\nu E - A)^{-1} \end{pmatrix} \in \mathbb{R}^{n_y \nu \times n} \tag{5.6}$$

$$\mathcal{C}_\rho = \begin{pmatrix} (\lambda_1 E - A)^{-1} B\mathbf{r}_1 & \dots & (\lambda_\rho E - A)^{-1} B\mathbf{r}_\rho \end{pmatrix} \in \mathbb{R}^{n \times n\rho} \tag{5.7}$$

Following these matrices, the Loewner matrices, $\mathbb{L}$ and $\mathbb{L}_s$, can be factored as follows:

$$\mathbb{L} = -\mathcal{O}_\nu E \mathcal{C}_\rho \quad \text{and} \quad \mathbb{L}_s = -\mathcal{O}_\nu A \mathcal{C}_\rho \tag{5.8}$$

Therefore, if $(E, A, B, C, 0)$ is a minimal realization of the plant $\mathbf{G}$, $\mathcal{O}_\nu$ and $\mathcal{C}_\rho$ have full rank. Consequently, according to (5.8), the rank of the Loewner matrix $\mathbb{L}$ is the McMillan degree k of the plant $\mathbf{G}$. Obtaining the McMillan degree of the considered system is one of the main advantages of the Loewner framework. In practice, the McMillan degree is obtained by applying a rank revealing decomposition, such as a Singular Value Decomposition (SVD), on the Loewner matrix $\mathbb{L}$.

The order n of a minimal realization of the system $\mathbf{H}$, given interpolatory conditions as in (5.2), is determined by the rank of the Loewner pencil as follows:

$$n = \operatorname{rank}[\mathbb{L}, \mathbb{L}_s] = \operatorname{rank} \begin{bmatrix} \mathbb{L} \\ \mathbb{L}_s \end{bmatrix}. \tag{5.9}$$

As for the McMillan order, the order n of the minimal realisation of $\mathbf{G}$ is obtained by applying a SVD to the Loewner pencil, see (5.10).

$$[\mathbb{L}, \mathbb{L}_s] = Y \Sigma_l \tilde{X}^*, \qquad \begin{bmatrix} \mathbb{L} \\ \mathbb{L}_s \end{bmatrix} = \tilde{Y} \Sigma_r X^* \ , \tag{5.10}$$

where $\Sigma_l, \Sigma_r \in \mathbb{R}^{n \times n}$ are diagonal matrices containing the non-zero singular values only, $Y \in \mathbb{C}^{\nu \times n}$ and $X \in \mathbb{C}^{\rho \times n}$. This decomposition allows to deal with the cases were redundant data are given in the interpolatory conditions.

A minimal generalized state-space model as in (5.1) can be deduced from this factorization. The matrices of the model are then computed as in (5.11).

$$\begin{aligned} E &= -Y^* \mathbb{L} X \\ A &= -Y^* \mathbb{L}_s X \\ B &= Y^* V \\ C &= W X \end{aligned} \tag{5.11}$$

In addition to determining the smallest exact interpolating model, the Loewner framework allows to control the complexity of the identified model. If one wants to reduce the order of the obtained model to an order $r < n$, only the r biggest singular values are kept in (5.10). The rest of the SVD is truncated. The reduced-order representation is obtained as in (5.11).

Remark 5.1.3. Adding a D-term As said earlier in Remark 5.1.1, a D-term, which corresponds to a singular value at infinity, can be added if the McMillan degree is not equal to the order of the minimal realization, see [Antoulas et al., 2015] for more information.

Remark 5.1.4. This algorithm is implemented in the MOR Toolbox, see [MOR Toolbox, 2018]. It is a Matlab based toolbox created for the reduction of large-scale models or the approximation of FRF data.

A variant of the Loewner algorithm has been proposed in [Ionita and Antoulas, 2014] and [Rapisarda and Antoulas, 2016] in order to identify pLTI models as defined in Section 2.1.3. It should be noted that the Loewner framework also allows to take into account derivative constraints as $\dot{\mathbf{H}}(z) = \dot{\mathbf{G}}(z)$ with $z \in \mathbb{C}$, as detailed in [Mayo and Antoulas, 2007]. This will be of particular interest when determining an achievable reference model in the next Chapter.

5.1.3 Subspace-based identification

The subspace approach is a singular value decomposition based identification algorithm. In this work, we used the algorithm proposed in [McKelvey et al., 1996] where a state space model $\mathbf{H} = [A, B, C, D]$ in discrete form is built directly from the frequency-domain data of the plant $\mathbf{G}$ to be identified:

$$\mathbf{H} : \begin{cases} \mathbf{x}_{k+1} = A\mathbf{x}_k + B\mathbf{u}_k \\ \mathbf{y}_k = C\mathbf{x}_k + D\mathbf{u}_k \end{cases}, \tag{5.12}$$

with $\mathbf{x}(t) \in \mathbb{R}^n$, $\mathbf{y}(t) \in \mathbb{R}^{n_y}$ the state vector and $\mathbf{u}(t) \in \mathbb{R}^{n_u}$ the input vector.

The subspace approach requires samples of the frequency response:

$$G_k = \mathbf{G}(\imath\omega_k) \in \mathbb{C}^{p\times m},\ k = 1 \dots N.$$

Remark 5.1.5. Here, only the algorithm for arbitrarily spaced data from [McKelvey et al., 1996] is presented. For the special case of uniformly spaced data, a dedicated algorithm is proposed in this same paper, allowing to get rid of the influence of noise when the number of data points tends to infinity. To obtain the same consistency result for arbitrarily spaced noisy data, a weighting matrix is introduced, assuming that the covariance of the noise is known.

Considering the discrete Fourier transform of (5.12), we have:

$$\begin{aligned} e^{\imath\omega}\mathbf{X}(\omega) &= A\mathbf{X}(\omega) + B\mathbf{U}(\omega) \\ \mathbf{Y}(\omega) &= C\mathbf{X}(\omega) + D\mathbf{U}(\omega) \end{aligned} \tag{5.13}$$

where $\mathbf{X}(\omega)$, $\mathbf{U}(\omega)$ and $\mathbf{Y}(\omega)$ denotes the Fourier transform of the time-domain signals $\mathbf{x}(t)$, $\mathbf{u}(t)$ and $\mathbf{y}(t)$ respectively. Using (5.13) recursively and considering input vectors such that $\mathbf{U}(\omega) = \mathbf{e}_i$, with $\mathbf{e}_i$ the unit vector with one at the ith position, the following equation is obtained, see [McKelvey, 1995]:

$$G = \mathcal{O}_q X + \Gamma W, \tag{5.14}$$

where G and W are matrices constructed exclusively from the data as follows:

$$G = \frac{1}{\sqrt{N}} \begin{bmatrix} G_1 & G_2 & \dots & G_N \\ e^{j\omega_1} G_1 & e^{j\omega_2} G_2 & \dots & e^{j\omega_N} G_N \\ \vdots & \vdots & \ddots & \vdots \\ e^{j(q-1)\omega_1} G_1 & e^{j(q-1)\omega_2} G_2 & \dots & e^{j(q-1)\omega_n} G_N \end{bmatrix} \in \mathbb{C}^{qn_y \times n_u N}, \tag{5.15}$$

$$W = \frac{1}{\sqrt{N}} \begin{bmatrix} I_{n_u} & I_{n_u} & \dots & I_{n_u} \\ e^{j\omega_1} I_{n_u} & e^{j\omega_2} I_{n_u} & \dots & e^{j\omega_M} I_{n_u} \\ \vdots & \vdots & \ddots & \vdots \\ e^{j(q-1)\omega_1} I_{n_u} & e^{j(q-1)\omega_2} I_{n_u} & \dots & e^{j(q-1)\omega_N} I_{n_u} \end{bmatrix} \in \mathbb{C}^{qn_u \times n_u N}. \tag{5.16}$$

In (5.14), $\mathcal{O}_q$ is the extended observability matrix, defined in (5.17), according to the matrices of the state-space model to be identified:

$$\mathcal{O}_q = \begin{pmatrix} C \\ CA \\ \vdots \\ CA^{q-1} \end{pmatrix}. \tag{5.17}$$

Its dimension is fixed by the user through the parameter $q \in \mathbb{N}$. Finally, the Γ matrix used in (5.14) is given by:

$$\Gamma = \begin{bmatrix} D & 0 & \dots & 0 \\ CB & D & \dots & 0 \\ \vdots & & \vdots & \vdots \\ CA^{q-2}B & CA^{q-3} & \dots & D \end{bmatrix}$$

while the X matrix is given by:

$$X = \frac{1}{\sqrt{N}} \left[X^c(\omega_1) \dots X^c(\omega_N) \right]$$

with $X^c(\omega) = \left[\mathbf{X}^1(\omega) \dots X^{n_u}(\omega) \right]$ where $\mathbf{X}^i(\omega)$ is the transform state obtained for an input $\mathbf{U}(\omega) = \mathbf{e}_i$.

The basic idea of [McKelvey et al., 1996] is that the range space of the extended observability matrix (5.17) can be estimated from the input-output frequency-domain data. Indeed, (5.14) gives:

$$GW^{\perp} = \mathcal{O}_q X W^{\perp},$$

wit $^{\perp}$ denoting the orthogonal of a matrix. As proved in [McKelvey et al., 1996], if $N \geq q+n$ and if the considered frequencies $\{\omega_i\}_{i=1}^{N}$ are distinct and satisfy $e^{\imath\omega_i} \notin \lambda(A)$, then the range space of $GW^{\perp}$ is equal to the range space of $\mathcal{O}_q$. Therefore, the identification boils down to the obtention of the range space of $GW^{\perp}$.

To that extent, the following QR decomposition is performed on the data matrices:

$$\begin{bmatrix} Re(W) & Im(W) \\ Re(G) & Im(G) \end{bmatrix} = \begin{bmatrix} R_{11} & 0 \\ R_{21} & R_{22} \end{bmatrix} \begin{bmatrix} Q_1^T \\ Q_2^T \end{bmatrix}. \tag{5.18}$$

Then, the singular value decomposition of the R_{22} matrix gives:

$$R_{22} = \begin{bmatrix} \hat{U}_s & \hat{U}_o \end{bmatrix} \begin{bmatrix} \hat{\Sigma}_s & 0 \\ 0 & \hat{\Sigma}_o \end{bmatrix} \begin{bmatrix} \hat{V}_s \\ \hat{V}_o \end{bmatrix} \tag{5.19}$$

with $\hat{\Sigma}_s \in \mathbb{R}^{n \times n}$ containing the n largest singular values and being an estimate of $\mathcal{O}_q$. Then, n is the order of the estimated model and is fixed by the user. n can also be

selected automatically as the number of non-zero singular values, as in the Loewner framework.

Then, the matrices A and C can be computed from the observability matrix, see (5.17). Finally, B and D are chosen so that the frequency response of the model is as close as possible to the experimental one. Matrices A and C are given by:

$$\begin{aligned} A &= (J_1\hat{U}_s)^\dagger J_2\hat{U}_s \\ C &= J_3\hat{U}_s \end{aligned} \tag{5.20}$$

with:

$$\begin{aligned} J_1 &= \begin{bmatrix} I_{(q-1)p} & 0_{(q-1)p\times p} \end{bmatrix} \\ J_2 &= \begin{bmatrix} 0_{(q-1)p\times p} & I_{(q-1)p} \end{bmatrix} \\ J_3 &= \begin{bmatrix} I_p & 0_{p\times(q-1)p} \end{bmatrix}. \end{aligned}$$

Remark 5.1.6. If one wants to limit the influence of the noise on the identified model, it is possible to introduce a weighting matrix R. The SVD of Equation (5.19) is then performed on RR_{22} instead of R_{22} only. The A and C matrices are then obtained through the following equation, which differs from (5.20) through the introduction of the weighting matrix R:

$$\begin{aligned} A &= (J_1R\hat{U}_s)^\dagger J_2R\hat{U}_s \\ C &= J_3R\hat{U}_s \end{aligned}.$$

In [McKelvey et al., 1996], R is built on the basis of the noise covariance function while it is proposed in [Liu et al., 1996] to build R on the basis of the available plant's data.

Matrices B and D are solutions of the following least squares problem:

$$\{B, D\} = \arg\min \sum_{k=0}^{M} ||G_k - D - C(e^{j\omega_k}I - A)^{-1}B||_F^2 \tag{5.21}$$

Use of LMIs for eigenvalue control

One of the main strengths of the subspace algorithm is that it is possible to constraint the position of the poles of the identified model in LMI regions. This extension of the original subspace algorithm was proposed in [Miller and De Callafon, 2013] and [Demourant and Poussot-Vassal, 2017]. As explained in [Chilali et al., 1999], a LMI region $\mathcal{D}$ is characterized by two matrices $P = P^T \in \mathbb{R}^{r\times r}$ and $Q \in \mathbb{R}^{r\times r}$:

$$\mathcal{D} = \{z \in \mathbb{C} \mid P + Qz + Q^T\bar{z}\}. \tag{5.22}$$

The eigenvalues of a matrix $A = \varphi^\dagger b$, with $\varphi = J_1\hat{U}_s$ and $b = J_2\hat{U}_s$, see (5.20), lies in $\mathcal{D}$ if and only if the following problem has a solution:

$$\min_{\tilde{A},\Psi,\beta} \beta \tag{5.23}$$

subject to:

$$P \otimes \Psi + Q \otimes \tilde{A} + Q^T \otimes \tilde{A}^T < 0 \tag{5.24}$$

$$\begin{pmatrix} I & (\varphi\tilde{A} - b\Psi) \\ (\varphi\tilde{A} - b\Psi)^T & \beta \end{pmatrix} > 0 \tag{5.25}$$

$$\Psi > 0 \tag{5.26}$$

where $\tilde{A} = A\Psi$. The decision variables are β, Ψ and $\tilde{A}$. Then, φ and b are given by the standard subspace approach (5.20): the LMI (5.25) corresponds to the fitting objective of the data.

In our case, we require that the dynamical process (i.e. the controller) be stable, so the poles of A must lie in the unit circle which corresponding LMI region $\mathcal{D}$ is defined by (5.22) with:

$$P = \begin{pmatrix} -1 & 0 \\ 0 & -1 \end{pmatrix}$$

$$Q = \begin{pmatrix} 0 & 0 \\ 1 & 0 \end{pmatrix}.$$

The matrix A of the model is given by $\tilde{A} = A\Psi$. The matrices C, B and D are obtained as in the classic method: C is deduced from the same singular value decomposition and B and D are the solutions of the same least squares problem.

Remark 5.1.7. It should be noted that the consistency of the problem is not affected by the use of LMIs if the constraints are relevant with the controller to identify. Therefore, in this work, the subspace approach will always be used with LMI constraints to identify a stable controller.

Comparison of these two methods

The Loewner framework and the subspace approach both allow to identify a reduced-order model on the basis of frequency-domain measurements. The subspace approach also requires to fix the size of the extended observability matrix to be estimated. Both techniques are based on a SVD which is a rank revealing decomposition. Therefore, these two methods allow to fix the model order automatically by eliminating all the singular values equal to zero.

The Loewner framework can address tangential interpolation problems. It also may include derivative constraints. These two aspects will be of particular interest when choosing a reference model in the next Chapter. The main weakness of this method is to be extremely sensitive to noisy data. This issue will be tackled in the next section.

The subspace approach is more robust to noisy data and frequency weightings have been proposed in [McKelvey et al., 1996] to improve the results of the method to noise. In addition, the possibility to use LMI constraints to control the location of the poles of the identified model constitutes a major advantage.

5.2 Identification of the controller

In this Section, the Loewner framework and the subspace algorithm, recalled in Section 5.1.2 and 5.1.3 respectively, are now used to identify a controller for the problem exposed in Chapter 4. These two methods are applied on the frequency response samples of the ideal controller $\mathbf{K}^\star$, which define the interpolation problem given in (4.4).

The resulting controllers, obtained through the Loewner framework and the subspace algorithm, are denoted $\mathbf{K}_l = (E_l, A_l, B_l, C_l, 0)$ and $\mathbf{K}_s = (A_s, B_s, C_s, D_s)$ respectively. In the first time, it is assumed that they are minimal realizations of the ideal controller $\mathbf{K}^\star$. It means that all the non-zero singular values are kept to build a model, considering (5.10) for the Loewner framework and (5.19) for the subspace approach.

5.2.1 Enforcing the stability of the identified controller

In many industrial applications, it is preferable to have a stable controller. This the case when the plant to be controlled presents an input saturation for example. Enforcing the stability of the controller will also be important to evaluate the choice of a reference model in Chapter 6. Having a stable controller is also one of the necessary conditions to apply the internal stability test proposed in Chapter 7.

To guarantee the stability of the controller, the subspace approach can be used under LMI constraints, as explained in Section 5.1.3. For the Loewner framework, no technique has been proposed to ensure the stability of the obtained realization. To that extent, in [Kergus et al., 2018b], a projection on the $\mathcal{RH}_\infty$ space, proposed in [Köhler, 2014], is used as a post-processing technique to obtain a stable controller model. The objective of this paragraph is to recall this technique. It should be noted that this algorithm has already been combined with the Loewner framework in [Gosea and Antoulas, 2016] in the area of model reduction.

Given an unstable continuous LTI descriptor system, the method proposed in [Köhler, 2014] allows to find a stable one of the same order which is an optimal approximation of the original system in the space $\mathcal{RH}_\infty$. In our case, this algorithm will be applied to the the interpolating descriptor model $\mathbf{K}_l$ of order n. The goal is to obtain a n^{th} order stable controller $\mathbf{K}_l^s$ that is an optimal $\mathcal{RH}_\infty$-approximation of $\mathbf{K}_l$, meaning that $\mathbf{K}_l^s$ solves:

$$\mathbf{K}_l^s = \underset{\mathbf{K}\in\mathbb{S}^+_{r,n_u,n_y}}{\arg\min} \left\|\mathbf{K}_l - \mathbf{K}\right\|_\infty . \tag{5.27}$$

Let us introduce the following notations:

$$\begin{aligned}
\mathbb{S}_{r,n_u,n_y} &= \quad \mathbb{R}^{r\times r} \times \mathbb{R}^{r\times r} \times \mathbb{R}^{r\times n_u} \times \mathbb{R}^{n_y\times r} \times \mathbb{R}^{n_y\times n_u}, \\
\mathbb{S}^+_{r,n_u,n_y} &= \left\{(E,A,B,C,D) \in \mathbb{S}_{r,n_u,n_y}; \mathbb{C}_{\geq 0} \subset \rho(E,A)\right\}, \\
\mathbb{S}^-_{r,n_u,n_y} &= \left\{(E,A,B,C,D) \in \mathbb{S}_{r,n_u,n_y}; \mathbb{C}_{\leq 0} \subset \rho(E,A)\right\},
\end{aligned} \tag{5.28}$$

where $\sigma(E,A)$ is the set of eigenvalues of (E,A) and $\rho(E,A)$ is the resolvent set: $\rho(E,A) = \mathbb{C} \setminus \sigma(E,A)$.

The first step is to decompose $\mathbf{K}_l$ into $\mathbf{K}_+ \in \mathbb{S}^+_{r,n_u,n_y}$ and $\mathbf{K}_- \in \mathbb{S}^-_{r,n_u,n_y}$. The existence of such a decomposition is proved in [Köhler, 2014] and a method is proposed

to compute it. Note that $\mathbf{K}_+$ is the $\mathcal{RH}_2$-problem optimal approximation of $\mathbf{K}_l$:

$$\mathbf{K}_+ = \underset{\mathbf{K}\in\mathbb{S}^+_{r,n_u,n_y}}{\arg\min} \|\mathbf{K}_l - \mathbf{K}\|_2 .$$

The unstable part $\mathbf{K}_- = (E^-, A^-, B^-, C^-, D^-)$ is then used to compute $\mathbf{K}^s_r$. The controllability and observability gramians of $\mathbf{K}_-$, denoted $\mathcal{W}_c$ and $\mathcal{W}_o$ respectively, are computed by solving the following generalized Lyapunov equations:

$$\begin{cases} A^-\mathcal{W}_c{E^-}^T + E^-\mathcal{W}_c{A^-}^T + B^-{B^-}^T = 0 \\ {A^-}^T\mathcal{W}_oE^- + {E^-}^T\mathcal{W}_oA^- + C^-{C^-}^T = 0 \end{cases} \tag{5.29}$$

Let us introduce $\sigma_1 = \sqrt{\max(\sigma(\mathcal{W}_o^T\mathcal{W}_c))}$ and the matrix $R = \mathcal{W}_oE^-\mathcal{W}_c{E^-}^T - \sigma_1^2 I$, where I is the identity matrix. The optimal $\mathcal{RH}_\infty$-approximation is then given by:

$$\mathbf{K}^s_l = \mathbf{K}_+ + (E^s, A^s, B^s, C^s, D^s), \tag{5.30}$$

where the matrices $(E^s, A^s, B^s, C^s, D^s)$ are computed as in (5.31) (readers can refer to [Köhler, 2014] for further details).

$$\begin{aligned} E^s &= {E^-}^T R \\ B^s &= {E^-}^T\mathcal{W}_oB^- \\ C^s &= C^-\mathcal{W}_c{E^-}^T \\ A^s &= -{A^-}^T R - {C^-}^T C \\ D^s &= D^-. \end{aligned} \tag{5.31}$$

5.2.2 Dealing with noisy data

Due to the definition of the ideal controller $\mathbf{K}^\star$, see (4.2), the quality of the FRF measurements of the plant directly impact the computed FRF of $\mathbf{K}^\star$. Therefore, as explained in Section 4.1.2, the plant's data should reflect the dynamics to be controlled and be not too biased. Different references to experiment design techniques and FRF processing procedures have been given in this paragraph. However, this study would be incomplete if the noisy case was not considered.

Concerning the subspace approach, a weighting filter is used in the original version of the algorithm presented in [McKelvey et al., 1996]. However, the design of this filter requires to know the covariance function.

The Loewner framework can identify a system from given noise-free measurements in the frequency-domain (see [Antoulas et al., 2015]). An analysis of the effects of noise on the performances of the Loewner approach is provided in [Lefteriu et al., 2010]: it exhibits poor performances for high noise levels. Noise affects the recovered poles: the largest singular values of the Loewner pencil does not necessarily reflect the physical poles of the system and often include noise-related dynamics. In this case, overmodeling is the only way, in the Loewner context, to capture the physical poles of the original system.

In the classical Loewner framework, the poles of the system are determined through a rank revealing factorization. In order to make the selection of the poles robust to noise, the SVD step is replaced by ordering the poles of the high-order system according to the norm of the associated residues, as explained in [Lefteriu et al., 2010]. This approach was used in [Kergus et al., 2018b] in the proposed data-driven control technique and is recalled hereafter.

The reduction is applied to the stable n^{th}-order controller model $\mathbf{K}_l^s = (E_l^s, A_l^s, B_l^s, C_l^s, D_l^s)$ obtained in the previous paragraph as the optimal approximation of the interpolating controller in $\mathcal{RH}_\infty$. The objective is to obtain a stable n^{th}-order controller $\mathbf{K}_r$ by selecting the poles in a noise-proof way. Instead of using the SVD approach, the importance of a pole λ_i of $\mathbf{K}_l^s$ is measured by the norm of the corresponding residue r_i. This strategy is based on the pole-residue expansion of the transfer function, see Section 2.1: a pole with a larger residue norm contributes more to the response of the system, while the rest do not influence it that much.

As explained in [Lefteriu et al., 2010], using this technique to select the poles instead of the classical SVD approach, the approximated poles are within appropriate pseudospectra bounds corresponding to the noise level in comparison with the physical poles of the controller.

Finally, the r poles of the reduced-order controller are the ones corresponding to the r^{th} largest residue norms. The poles are then ordered downward, so that λ_1 is the pole with the highest dominance measure and λ_r has the smallest one. The poles of the reduced stable model are $[\lambda_1 \dots \lambda_n]$. After that, it is possible to adjust the residues and the D-term to fit the data by solving the following least squares problem:

$$\underset{r_i, D}{min} \sum_{j=1}^{N} \left|\left| \sum_{i=1}^{r} \frac{r_i}{\imath\omega_j - \lambda_i} + D - \mathbf{K}(\imath\omega_j) \right|\right|_F^2 . \tag{5.32}$$

Finally, the r^{th} order controller $\mathbf{K}_r$ is given by:

$$\mathbf{K}_r(s) = D + \sum_{i=1}^{n} \frac{r_i}{s - \lambda_i} \tag{5.33}$$

Since the poles of the reduced-order controller come from the stable model $\mathbf{K}_l^s$, the obtained r^{th}-order controller $\mathbf{K}_r$ remains stable.

5.2.3 The parametric case

For some applications, it might be useful to identify parametric controllers which can be tuned as a function of the working point for example. This will be the case in Chapter 8 for example, when applying the proposed method to the hydrogeneration control problem.

As mentioned earlier, the Loewner framework has been extended in [Ionita and Antoulas, 2014] and [Rapisarda and Antoulas, 2016] to the identification of p-LTI models.

The subspace-based methods are well-established for LTI systems. However, the obtained models are valid for a single operating point only. Extension to LPV modelling and identification have been proposed, as detailed in [Tóth, 2010]. As explained in Section 2.1.3, frequency-domain data are not relevant in the LPV framework. For this reason, in [Kergus et al., 2018a], a subspace-based algorithm to identify p-LTI models on the basis of frequency-domain data has been proposed. It is still possible to impose the location of its poles through LMI constraints. This extension of the classic subspace-based algorithm is recalled here.

Considering local FRF measurements $\{\omega_i, \mathbf{H}(\mathbf{p}^{(j)}, \imath\omega_i)\}_{i=1}^{N}$, obtained at the operating points $\{\mathbf{p}^{(j)}\}_{j=1}^{N_p}$ from a plant $\mathbf{G}(\mathbf{p})$, the objective is to find a p-LTI model $\mathbf{H}$ as defined in Section 2.1.3, see (2.19) and recalled hereafter:

$$\mathbf{H}(\mathbf{p}) : \left\{ \begin{array}{rcl} \mathbf{x}_{k+1} & = & A(\mathbf{p})\mathbf{x}_k + B(\mathbf{p})\mathbf{u}_k \\ \mathbf{y}_k & = & C(\mathbf{p})\mathbf{x}_k + D(\mathbf{p})\mathbf{u}_k \end{array} \right. . \tag{5.34}$$

In the present case, the matrices have an affine parameter-dependancy:

$$M(\mathbf{p}) = M_0 + \sum_{k=1}^{n_p} \mathbf{p}_k M_k, \tag{5.35}$$

where $\mathbf{p}_k$ is the k^{th} component of the parameter vector $\mathbf{p}$. Considering the structure of the matrices of the desired state-space representation (see (5.34) and (5.35)), it is possible to concatenate all the LTI problems to solve the parametric problem directly instead of interpolating N_p local models as it is traditionally done.

All the local observability matrices $\hat{\mathcal{O}}_q^{(j)}$, estimated at every operating point $\mathbf{p}^{(j)}$, are considered. They are obtained using the classic LTI subspace algorithm recalled in Section 5.1.3, see (5.19), at every operating point where data is available. It allows to derive all the local equations (5.20) for $j = 1 \dots N_p$. Those are then expressed in a same basis, which is not guaranteed by the classical subspace-based algorithm of [McKelvey et al., 1996].

In [Kergus et al., 2018a], the observability canonical form is considered. It has been extended for multivariable system in [Luenberger, 1967]. In the MIMO case, assuming that the state-space representation is state-observable, the computation of the transformation matrix T_j consists in choosing n independent rows of the full column rank observability matrix $\hat{\mathcal{O}}_n^{(j)} \in \mathbb{R}^{n_y n \times n}$. The choice of this equivalent tranformation is detailed in [Tóth, 2010].

Finally, the equivalence transformation T_j is available for all $j = 1 \dots N_p$. The $A(\mathbf{p})$ and $C(\mathbf{p})$ matrices of the parametric model then satisfy:

$$\left\{ \begin{array}{rcl} A(\mathbf{p}^{(j)}) & = & T_j A^{(j)} T_j^{-1} \\ C(\mathbf{p}^{(j)}) & = & C^{(j)} T_j^{-1} \end{array} \right. , \tag{5.36}$$

where $A^{(j)}$ and $C^{(j)}$ are the solution of equation (5.20) of the LTI identification problem at the operating point $\mathbf{p}^{(j)}$. Considering equations (2.19) and (5.20), and the transformation into the observable canonical form (5.36), finding the $A(\mathbf{p})$ and $C(\mathbf{p})$ matrices of the parametric model consists in solving the following set of equations $\forall j = 1 \dots N_p$:

$$J_1 \hat{\mathcal{O}}_n^{(j)} T_j A(\mathbf{p}^{(j)}) T_j^{-1} = J_2 \hat{\mathcal{O}}_n^{(j)}, \tag{5.37}$$

$$C(\mathbf{p}^{(j)})T_j^{-1} = J_3\hat{\mathcal{O}}_n^{(j)}, \tag{5.38}$$

where the matrices J_1, J_2 and J_3 are the same ones as in the LTI case, see (5.20). The matrices $A(\mathbf{p})$ and $C(\mathbf{p})$ are obtained by concatenating all these local problems in one single large one (see [Kergus et al., 2018a] more details). The matrices $B(\mathbf{p})$ and $D(\mathbf{p})$ are obtained by solving a least squares problem similar to the one of the LTI case, see (5.21).

LMI regions constraints in the parametric case

This parametric model computation can be performed under LMI constraints to impose the poles location, as explained in [Kergus et al., 2018a]. By extension of what has been done in [Miller and De Callafon, 2013] and [Demourant and Poussot-Vassal, 2017] in the LTI case, the eigenvalues of the matrix $A(\mathbf{p})$ lie in $\mathcal{D}$ if and only if $X = X^T > 0 \in \mathbb{R}^{n\times n}$ exists such that the following LMI is verified:

$$\forall \mathbf{p} \in \Delta, P \otimes X + Q \otimes (A(\mathbf{p})X) + Q^T \otimes (A(\mathbf{p})X)^T < 0, \tag{5.39}$$

where $\Delta = \{\mathbf{p} \mid \forall k = 1 \dots n_p, \mathbf{p}_k \in [0,1]\}$ is a convex set (we assume that the parameters are normalized). Its convex hull is defined by:

$$\Delta_0 = \{\mathbf{p} \mid \forall k = 1 \dots n_p, \mathbf{p}_k \in \{0,1\}\}. \tag{5.40}$$

To ensure that the eigenvalues of $A(\mathbf{p})$ lies in $\mathcal{D}$ for an affine parameter-dependency, one just needs to check the LMI given in equation (5.39) for $\mathbf{p} \in \Delta_0$, which contains a finite number of elements. Therefore, the matrices A_k forming $A(\mathbf{p})$ ensuring that the poles of the system lie in $\mathcal{D}$ are found by solving a problem containing a finite number of LMIs. It is the pLTI equivalent of problem (5.23), see [Kergus et al., 2018a] for more information.

5.3 Application to numerical examples

The objective of this section is to apply the proposed method on the same examples than in Section 4.2: the DC motor and the flexible transmission. This time, noise will be introduced in the measurements. As in [Lefteriu et al., 2010], the noise is directly introduced on the FRF of the considered plants. For a plant $\mathbf{P}$, the considered noisy data $\{\Phi_i\}_{i=1}^N$ is obtained as follows:

$$\begin{aligned} &\forall i = 1 \dots N,\ \Phi_i = \mathbf{P}(\imath\omega_i) + \mathbf{N}(\imath\omega_i) \\ &\mathbf{N}(\imath\omega_i) = \mathbf{P}(\imath\omega_i) \cdot 10^{-\frac{SNR}{10}} R \end{aligned} \tag{5.41}$$

where $\mathbf{N}$ is the noise, defined through R, a $n_y \times n_u$ complex matrix. The real and imaginary parts of its elements are normally distributed random numbers. SNR denotes the Signal to Noise Ratio. The $\cdot$ symbol stands for the entry-by-entry multiplication.

In order to highlight the influence of noisy data on the control design process, the following measures are introduced:

- the $\mathcal{H}_2$-error between the resulting closed-loop $\mathbf{H}$ and the reference model $\mathbf{M}$:

$$\mathcal{H}_2 \text{ error} = \sqrt{\frac{\sum_{i=1}^{N} \|\mathbf{H}(\imath\omega_i) - \mathbf{M}(\imath\omega_i)\|_2^2}{\sum_{i=1}^{N} \|\mathbf{M}(\imath\omega_i)\|_2^2}}. \tag{5.42}$$

- the $\mathcal{H}_\infty$-error between the resulting closed-loop $\mathbf{H}$ and the reference model $\mathbf{M}$:

$$\mathcal{H}_\infty \text{ error} = \frac{\max\limits_{i=1\ldots N} \overline{\sigma}\left(\mathbf{H}(\imath\omega_i) - \mathbf{M}(\imath\omega_i)\right)}{\max\limits_{i=1\ldots N} \overline{\sigma}(\mathbf{M}(\imath\omega_i))}. \tag{5.43}$$

- the $\mathcal{H}_2$- norm of the noise: $\sqrt{\sum_{i=1}^{N} \|\mathbf{N}(\imath\omega_i)\|_2^2}$.
- the $\mathcal{H}_\infty$- norm of the noise: $\max\limits_{i=1\ldots N} \overline{\sigma}(\mathbf{N}(\imath\omega_i))$.

These measures can be seen as a data-based equivalent of the norms of systems introduced in Chapter 2.

The DC motor

Three noisy data-sets, defined with SNR=50, SNR=20 and SNR=10, are considered, in addition to the noise-free case, already seen in Section 4.2 (the same frequency grid is used). For information, the norms of the two noise signals are given in Table 5.1. The noisy measurements from the plant $\mathbf{P}$ are represented on Figure 5.1a for SNR=10. The associated frequency-response of the ideal controller, biased by the noise, is given on Figure 5.1b. For the sake of clarity, the two others noisy data-sets, SNR=20 and SNR=50, have not been represented.

	SNR=50	SNR=20	SNR=10
$\mathcal{H}_2$-norm	9.0793e-6	0.0090	0.0931
$\mathcal{H}_\infty$-norm	2.6730e-6	0.0032	0.0336

Table 5.1: Norms of the considered noise signals.

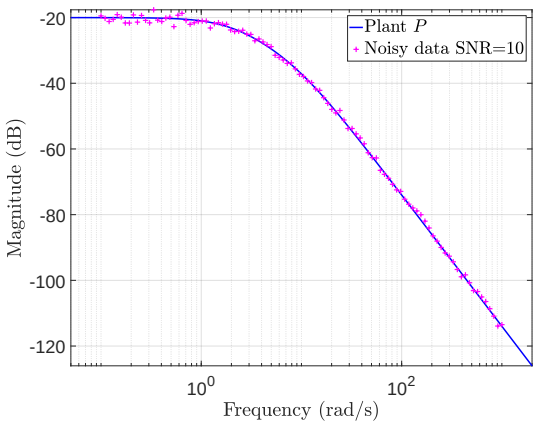

(a) Noisy measurements from the plant $\mathbf{P}$.

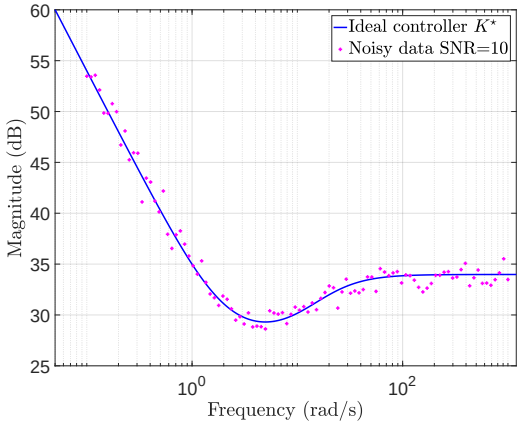

(b) Associated response of the ideal controller $\mathbf{K}^\star$.

Figure 5.1: Use of noisy frequency-domain measurements from the DC motor (SNR=10) and computation of the frequency-response of the associated ideal controller $\mathbf{K}^\star$.

The first impact of the noise on the identification of the controller is to complicate the choice of the order for the controller model. Indeed, both the Loewner framework and the subspace approach rely on a SVD to reveal the rank of the underlying dynamical system. The obtained normalized singular values for the two algorithms and the three data-sets are shown on Figure 5.2. It shows that the noise perturbs the singular values that are equal to zero in the noise-free case. When the SNR increases, it becomes more and more difficult to determine the order of the underlying system: the drop of the singular values turns almost invisible for SNR=80. On this aspect, the impact of the noise appears more important on the Loewner framework than on the subspace approach.

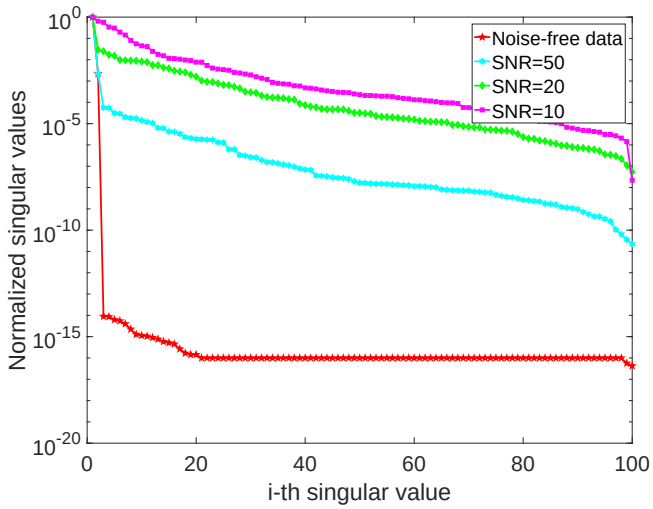

(a) Normalized singular values of the Loewner matrix $\mathbb{L}$

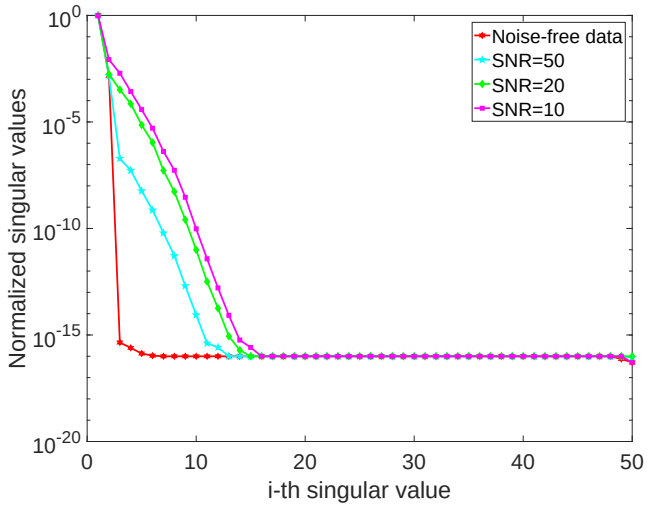

(b) Normalized singular values of the extended observability matrix $\mathcal{O}_q$

Figure 5.2: Singular Value Decomposition in the Loewner framework (left) and in the subspace approach (right) for different levels of noise.

According to Figure 5.2, in the noise-free case, it is clear that the ideal controller $\mathbf{K}^\star$ is a second-order system. The exact expression of $\mathbf{K}^\star$ is given in Section 4.2, see (4.7). Identifying a second-order controller on the basis of the three considered noisy data-sets gives the controllers of Table 5.2.

	Loewner framework	Subspace approach
Noise-free	$\frac{50(s+9.997)(s+2.003)}{s(s+20)}$	$\frac{50(s+9.997)(s+2.003)}{s(s+20)}$
SNR=50	$\frac{-622.86(s+1.965)}{(s-2.069e-5)(s-24.45)}$	$\frac{49.996(s+9.975)(s+2.004)}{(s+2.014e-5)(s+19.97)}$
SNR=20	$\frac{48.792(s-0.05281)}{(s-0.001577)(s-0.0458)}$	$\frac{48.53(s^2+6.983s+12.93)}{(s+0.006399)(s+12.44)}$
SNR=10	$\frac{39.262(s-0.00618)}{(s^2+0.004273s+0.002775)}$	$\frac{45.639(s+0.2565)(s-40.79)}{(s-1.107)(s-26.7)}$

Table 5.2: Identification of the ideal controller for different levels of noise.

The frequency responses of the identified controllers are visible on Figure 5.3 and the associated closed-loop performances are shown on Figure 5.4. The associated closed-loop errors are given in Table 5.3. For a low noise level (SNR=50), the subspace algorithm performs well. In most cases, the identified controllers do not reflect the behaviour of the ideal controller and the corresponding closed-loops present significant overshoots. Using the model of the considered system, the controllers obtained by the subspace approach at SNR=20 and SNR=10 give unstable closed-loops. Concerning the Loewner approach, the three controllers identified for SNR=50, 20 and 10 give unstable closed-loops.

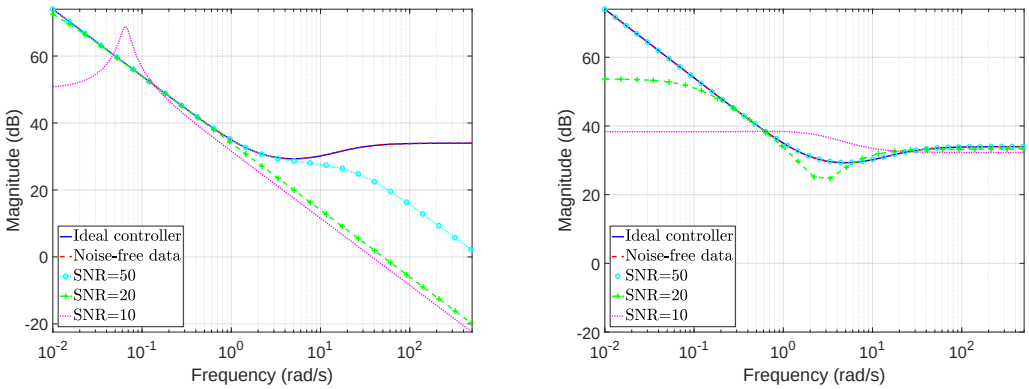

(a) Through the Loewner framework.

(b) Through the subspace approach

Figure 5.3: Approximation of the ideal controller by a second-order model for different levels of noise through the Loewner framework and the subspace approach (as introduced in Section 5.1).

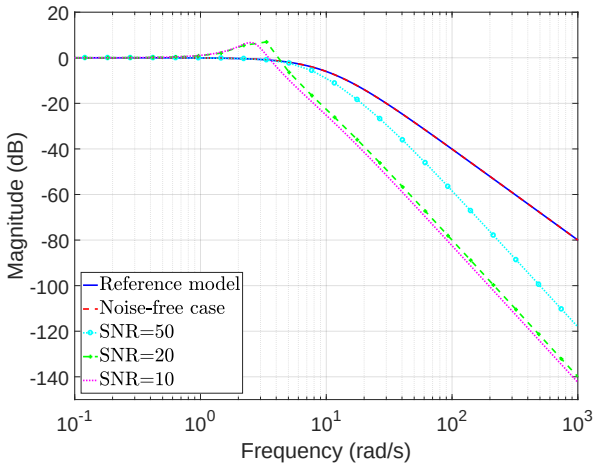

(a) Through the Loewner framework.

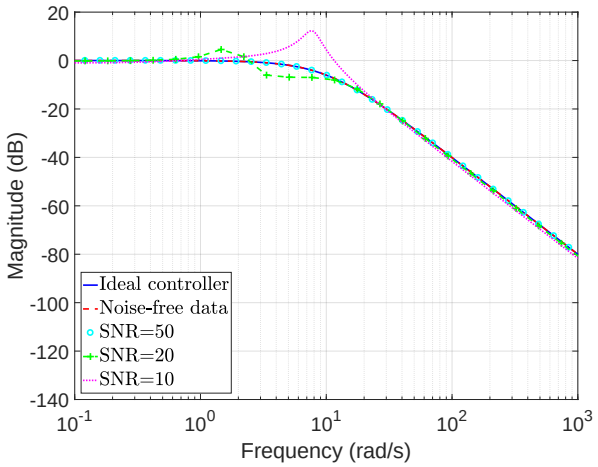

(b) Through the subspace approach

Figure 5.4: Frequency-responses of the resulting closed-loops, obtained with the controllers identified through the Loewner framework (left) and the subspace approach (right).

	Loewner framework		Subspace approach	
	$\mathcal{H}_2$-error	$\mathcal{H}_\infty$-error	$\mathcal{H}_2$-error	$\mathcal{H}_\infty$-error
SNR=50	0.0812	0.1469	**1.6891e-5**	**2.9922e-4**
SNR=20	0.9776	2.8150	**0.6369**	**1.5852**
SNR=10	**0.8578**	**2.0711**	1.1224	3.4032

Table 5.3: Closed-loop performances: error between the reference model and the closed-loop obtained with controllers identified through the Loewner framework and the subspace approach.

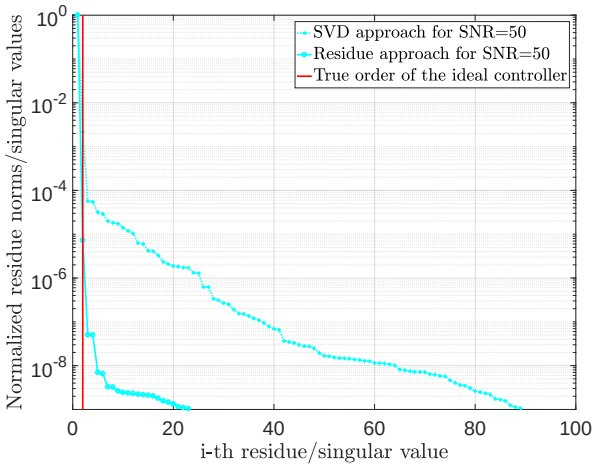

(a) SNR=50.

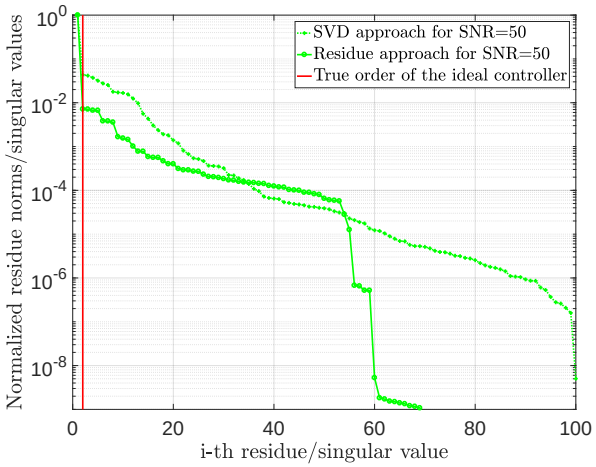

(b) SNR=20.

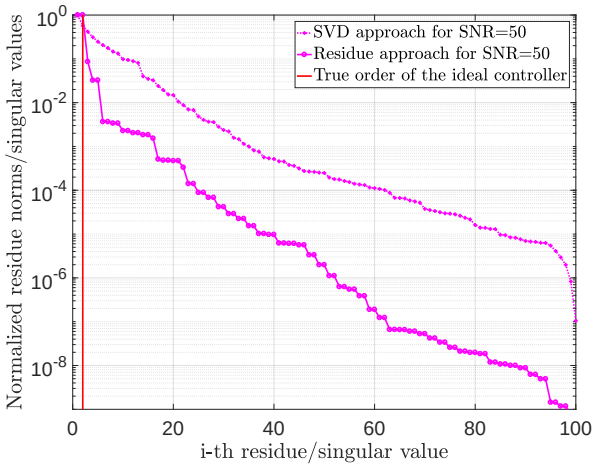

(c) SNR=10.

Figure 5.5: Decrease of the normalized residue norms and singular values to compare the two reduction approaches in the Loewner framework for different noise levels.

In order to identify better controllers on the basis of noisy data, the stability of the controller is enforced, using LMI constraints for the subspace approach or the projection on $\mathcal{RH}_\infty$ for the Loewner framework, see Section 5.2.1. To go further, the noise is handled through a weighting matrix in the subspace approach. For the Loewner framework, the traditionnal SVD implementation is replaced by the residue-based one, as explained in Section 5.2.2. The decrease of the residue norms is shown on Figure 5.5 and compared to the classical SVD approach: the physical poles appear more clearly with the residue approach for the highest noise level SNR=10: it is now visible that a second-order model can describe the ideal controller.

The controllers obtained using this new version of the method, presented in [Kergus et al., 2018b] for the Loewner framework, are shown on Figure 5.6. The closed-loop errors with respect to the reference model are given in Table 5.4. The corresponding closed-loop behaviours are visible on Figures 5.7a and 5.7b. For the Loewner framework, the obtained closed-loop behaviours are much closer to the reference model **M** than the ones on Figure 5.4. The results were also improved using the subspace approach. Furthermore, using the theoretical expression of the DC motor, these closed-loops are all stable. The associated step responses are visible on Figures 5.7c and 5.7d. Concerning the static error visible on Figures 5.7c and 5.7d, the best solution would be to enforce the presence of an integrator in the controller. This will be done in Chapter 7 on this example.

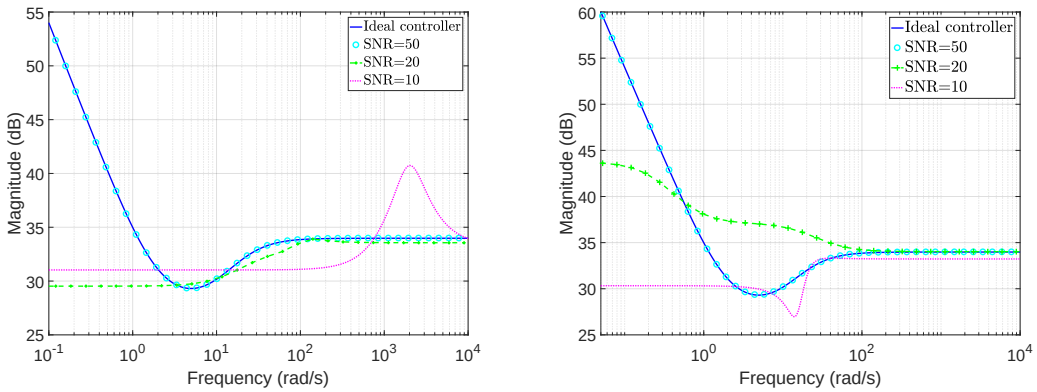

(a) Through the Loewner framework combined with the $\mathcal{RH}_\infty$-projection and the residue-based reduction.

(b) Through the subspace approach under LMI constraints and using a frequency-weighting.

Figure 5.6: Identification of the ideal controller for different levels of noise.

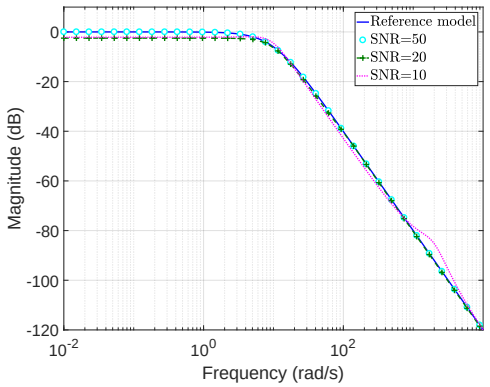

(a) Obtained closed-loops with controllers identified through the enhanced Loewner framework.

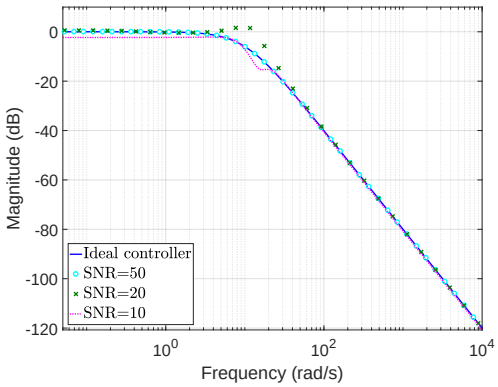

(b) Obtained closed-loops with controllers identified through the subspace approach under LMI constraints and using frequency-weighting.

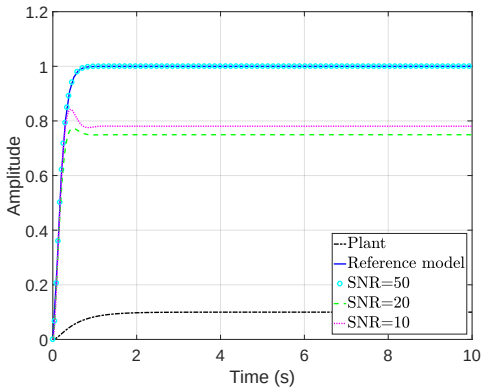

(c) Step responses obtained with controllers identified through the enhanced Loewner framework.

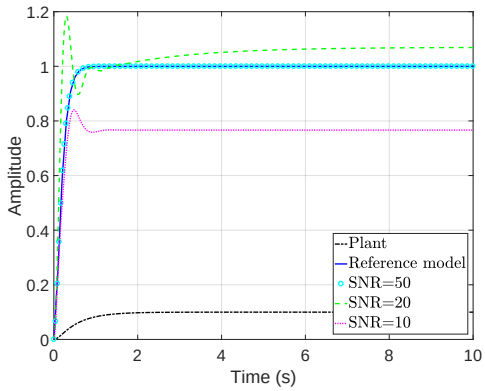

(d) Step responses obtained with controllers identified through the subspace approach under LMI constraints and using a frequency-weighting.

Figure 5.7: Closed-loop performances of the resulting closed-loops, obtained with the controllers identified through the Loewner framework (left) and the subspace approach (right), for different noise levels. The controllers is forced to be stable and noisy data are handled through frequency weigthing for the subspace approach and residue-based reduction in the Loewner framework.

In order to complete this study about noisy data, for each considered SNR, 50, 20 and 10, 50 noisy FRF measurements have been considered. Each time, controllers are identified using the Loewner framework and the subspace approach, with and without stability enforcement and specific noise treatments. The results in terms of closed-loop performances are indicated by the error between the resulting closed-loop and the reference model $\mathbf{M}$, see Figures 5.8 and 5.9. Enforcing the stability of the identified controller and the proposed techniques to handle noise (frequency weigthing for the subspace approach and residue-based reduction in the Loewner framework) allow to improve closed-loop performances when working with noisy FRF measurements.

	Loewner framework		Subspace approach	
	$\mathcal{H}_2$-error	$\mathcal{H}_\infty$-error	$\mathcal{H}_2$-norm	$\mathcal{H}_\infty$-error
SNR=50	**6.3205e-5**	**1.1692e-04**	5.3472e-4	9.3650e-4
SNR=20	**0.2354**	**0.2505**	0.4106	0.8185
SNR=10	**0.2144**	**0.2194**	0.2203	0.2336

Table 5.4: Closed-loop performances: error between the obtained closed-loop and the reference model when enforcing the stability of the controller and using a specific technique to handle noisy data (residue-based reduction for the Loewner framework and frequency weighting for the subspace approach).

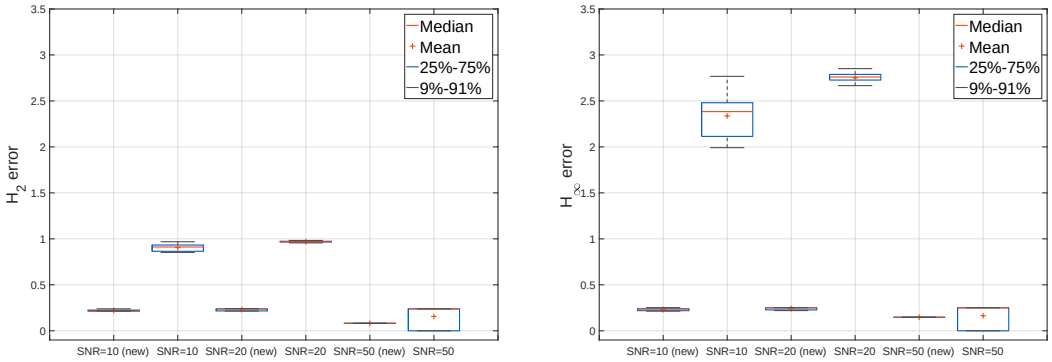

(a) $\mathcal{H}_2$-error (b) $\mathcal{H}_\infty$-error

Figure 5.8: Impact of the noise on the performances obtained with the controllers identified through the Loewner framework.

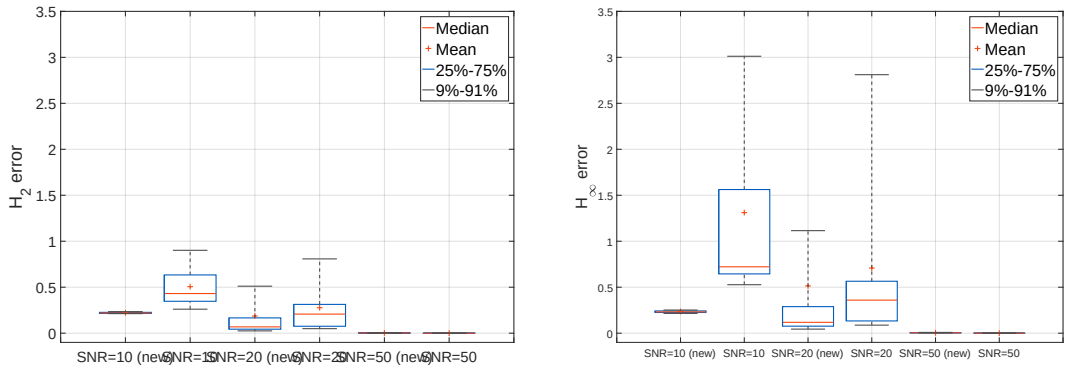

(a) $\mathcal{H}_2$-error (b) $\mathcal{H}_\infty$-error

Figure 5.9: Impact of the noise on the performances obtained with the controllers identified through the subspace approach.

The flexible transmission

On the DC motor example, identifying a stable controller works fine because the ideal controller is stable. On the flexible transmission example, since the system is NMP, the stability of the ideal controller mostly depends on the choice of the reference model $\mathbf{M}$. In Section 4.2, it has been shown that choosing a reference model that does not contain the RHP zeros of the plant leads to an unstable ideal controller. Its instabilities come from the compensation of the plant's RHP zeros. Therefore, the ideal controller destabilizes the plant internally.

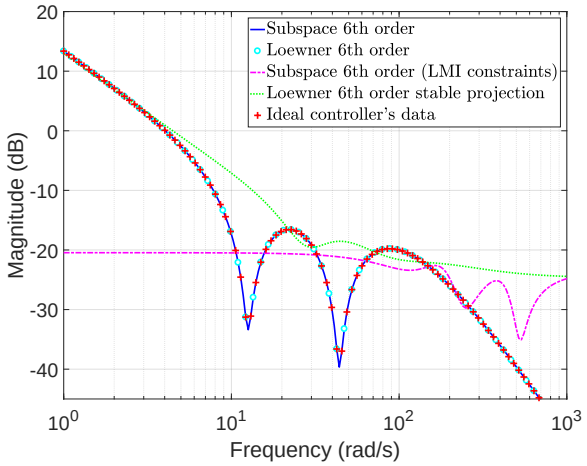

(a) Controller identification.

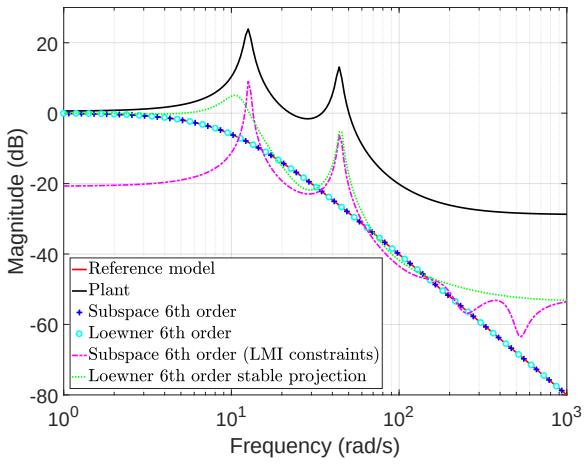

(b) Resulting closed-loops.

Figure 5.10: Identification of a 6th order stable controller and resulting closed-loop frequency-response for the flexible transmission example.

First, the same reference model than in Section 4.2 is considered, the data is noise-free and the same frequency-grid is used. When identifying a stable controller as proposed in this chapter, the closed-loop performances are far from the desired ones, see Figure 5.10b. Indeed, modelling an unstable ideal controller by a stable model intro-

duces a large error, see Figure 5.10a. Furthermore, if enforcing the stability of the controller prevents the compensation of instabilities in the open-loop, it is not sufficient to ensure closed-loop stability. In addition, in terms of overall strategy, trying to get as close as possible to a destabilizing controller is not a wise choice. To sum up, the choice of the reference model is crucial to obtain good results when identifying a controller. This problem is addressed in the following chapter.

Summary

In this chapter, the Loewner framework and the subspace approach were recalled. These are the two techniques considered in this work to obtain a model of the ideal controller. Since they both rely on a rank revealing decomposition, it makes the reduction of the controller an easy task. The main contribution of this Chapter is to enforce the stability of the identified controller and to study the impact of noisy data on the proposed control design.

To that extent, the subspace approach is already equipped with all the necessary tools: LMI constraints allow to monitor the location of the modes of the identified model and the algorithm is strongly consistent when it comes to noisy data. This robustness to noise is also one of the reason why this method is so popular in system identification.

On the other side, Loewner interpolation is really sensitive to noisy data. The model reduction has been modified as proposed in [Lefteriu et al., 2010] in order to be more robust. Furthermore, the projection technique introduced in [Köhler, 2014] is used to enforce the stability of the identified controller.

Then, the controller identification step is applied on the DC motor example, on the basis of noisy plant's measurements. It highlights the robustness of the subspace approach to noise. It also shows that the proposed modifications of the Loewner algorithm allow to improve the results when dealing with noisy data. In the end, the flexible transmission benchmark underlines that identifying a stable controller to avoid compensations of instabilities in the open-loop is not a sufficient solution. It is necessary to choose carefully the reference model $\mathbf{M}$, which is the topic of the next Chapter, and to perform a closed-loop stability analysis, see Chapter 7.

Chapter 6

Choice of an achievable reference model

The objective of this chapter is to investigate the influence of the reference model $\mathbf{M}$ in the proposed data-driven method and to propose a method to find an adequate one. In Section 6.1, the influence of the reference model on the performances of the proposed method is studied. It is shown that the reference model should be chosen according to the instabilities of the plant. A data-driven technique to estimate these instabilities is described in Section 6.2. The overall method to choose an adequate reference model is finally exposed in Section 6.3. All along this Chapter, the proposed techniques are applied on the DC motor example and the flexible transmission benchmark.

Contents

6.1 Specifications in data driven model-reference techniques

This section aims at showing the importance of the reference model, its influence on the control design and the resulting closed-loop performances. Data-driven model-reference techniques such as the VRFT or CbT, and the one presented in this thesis, can seem really attractive since the only requirement is to furnish the desired closed-loop behaviour. However, the reference model should also take into account the ability of the unknown plant to reproduce its behaviour. This makes the choice of the objective closed-loop a critical step in data-driven techniques using a model-reference paradigm. This problem is highlighted in [Bazanella et al., 2011], [Piga et al., 2018] and [Selvi et al., 2018].

6.1.1 Influence of the specifications on the control design

Compromising between performances and controller's complexity

As highlighted in Section 4.2 by the application of the proposed method on the DC motor example, if the user wants to reduce the complexity of the identified controller, a loss of closed-loop performances is observed. To some extent, when giving a maximal order for the controller, specifying a less performing reference model might be a wise choice. For the DC motor example, if one wants to obtain a first order controller, better results are obtained by decreasing the cutoff frequency of the reference model, which corresponds to a slower feedback system.

This can be explained by the definition of the ideal controller $\mathbf{K}^\star$ given in Chapter 4 and recalled hereafter:

$$\mathbf{K}^\star = \mathbf{P}^{-1}\mathbf{M}(I_{n_y} - \mathbf{M})^{-1}. \tag{6.1}$$

The closer the reference model $\mathbf{M}$ gets to the plant $\mathbf{P}$, the more easily the factor $\mathbf{P}^{-1}\mathbf{M}$ can be reduced without losing too much closed-loop performances.

It is well known in automatic control that the subtlety is to find a good compromise between the controller's complexity and the desired closed-loop performances. The desired performances form itself a compromise, between speed and overshoot in the case of the DC motor for example. If one wants to prioritize the speed over the absence of overshoot, it is possible to increase the cutoff frequency of the reference model but the damping factor must be decreased.

Challenging cases: non-minimum phase and unstable plants

In the example of the flexible transmission, treated in Section 4.2, the ideal controller compensates the right-half plane zeros of the plant, see (4.10). The same occurs when applying the method to unstable plants: the ideal controller will exhibit NMP zeros compensating the unstable poles of the plant. Therefore, the closed-loop with the ideal controller is internally unstable, see Chapter 2.

In Chapter 5, it has been proposed to identify stable controllers. If avoiding compensations of instabilities in the open-loop when dealing with NMP plants, enforcing the stability of the controller when the ideal controller is unstable clearly deteriorates the performances of the obtained controller. As a matter of fact, trying to approximate an unstable frequency-response by a stable model results in controllers that will be really different from the ideal controller. Consequently, the associated closed-loops will not present the expected dynamical behaviour, see Figure 5.10.

To sum up, the reference model should be chosen so that the corresponding ideal controller stabilizes the plant internally.

6.1.2 Finding an achievable model reference

As explained before, the choice of the reference model affects the design process in two ways:

1. If the reference model does not take into account the plant instabilities, it is not achievable by the system: the ideal controller destabilizes the system internally.

2. The closed-loop performances will impact the reduction of the controller (as in the DC motor example): the more performances the user asks, the less likely a low-order controller is to achieve them.

The first item is the one treated in this Chapter. The complexity-performance compromise can be dealt with later on, by iterating on the desired performances. Before that, given some performance specifications, a technique to build an achievable reference model is proposed. The second item will be treated in the end of Chapter 7, after the internal stability analysis.

The compensation of instabilities in the open-loop $\mathbf{PK}^\star$ can be easily understood by looking at the formula of the ideal controller, see (6.1). Regarding non-minimum phase systems, as said in [Bazanella et al., 2011], this problem can be avoided by including the right-half-plane zeros of the plant in the reference model. When it comes to unstable systems, it is also necessary to consider the unstable poles of the plant in the construction of the reference model to preserve internal stability.

To sum up, the choice of a reference model relies on the well known fact that the plant's instabilities are the main limitations of the possible control performances, see [Havre and Skogestad, 1996]. If not taken into account, the ideal controller destabilizes the plant internally and represents a bad behaviour that should not be identified. For this reason, the choice of an appropriate model reference is a critical step for all data-driven techniques.

According to Theorem 2.2.1, the ideal closed-loop, represented on Figure 6.1, is internally stable if and only if $I - \mathbf{M}$ is stable and there is no instability compensation between the plant $\mathbf{P}$ and the ideal controller $\mathbf{K}^\star$.

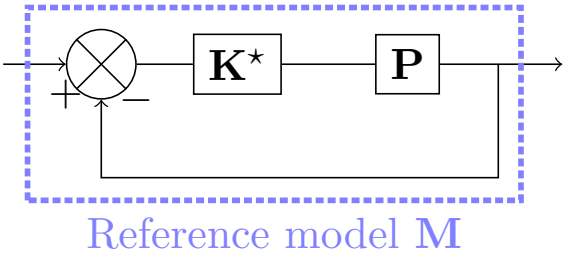

Figure 6.1: The ideal case: feedback interconnection obtained with the ideal controller.

As recalled in Chapter 2, these conditions can be expressed as an interpolation problem on the sensitivity function $I_{n_y} - \mathbf{M}$. In the SISO case, the closed-loop obtained with the ideal controller is internally stable if and only if the model reference satisfy:

$$\begin{cases} \mathbf{M}(z_i) = 0 \\ \mathbf{M}(p_j) = 1 \end{cases} \tag{6.2}$$

where $\{z_i\}_{i=1\ldots n_z}$ and $\{p_j\}_{j=1\ldots n_p}$ are respectively the unstable zeros and poles of the plant $\mathbf{P}$. When the plant has multiple RHP poles or zeros, derivative constraints must

be added in the SISO case as follows:

$$\begin{cases} \mathbf{M}(z_i) = \mathbf{M}^{(1)}(z_i) = \cdots = \mathbf{M}^{(m_{z_i}-1)}(z_i) = 0 \\ \mathbf{M}(p_j) = \mathbf{M}^{(1)}(p_j) = \cdots = \mathbf{M}^{(m_{p_j}-1)}(p_j) = 1 \end{cases}, \tag{6.3}$$

where m_{z_i} and m_{p_j} are the multiplicity of the RHP zeros z_i and poles p_j respectively. $\mathbf{M}^{(m)}$ denotes the m-th derivative of the transfer function $\mathbf{M}(s)$.

For MIMO systems, these conditions are generalized in a tangential interpolation problem, see [Havre and Skogestad, 2001], involving the output directions $\mathbf{y}_{p_j} \in \mathbb{C}^{n_y}$ and $\mathbf{y}_{z_i} \in \mathbb{C}^{n_y}$, associated to the unstable poles p_j and zeros z_i respectively:

$$\begin{cases} \mathbf{y}_{z_i}^T \mathbf{M}(z_i) = 0 \\ \mathbf{M}(p_j)\mathbf{y}_{p_j} = \mathbf{y}_{p_j} \end{cases}. \tag{6.4}$$

Remark 6.1.1. As explained in Section 5.1.2, the tangential directions make sense only if their dimension is strictly superior to 1. Since, in the proposed problem formulation (Chapter 4), the reference model $\mathbf{M}$ is square of size $n_y \times n_y$, the MIMO definition of an achievable closed-loop given in (6.4) should only be used if $n_y > 1$. Otherwise, for SISO or MISO plants, derivative constraints should be used as in (6.3) to treat multiple RHP poles or zeros.

In conclusion, a reference model must satisfy equation (6.3) if $n_y = 1$ or (6.4) if $n_y > 1$ in order to be achievable by the plant $\mathbf{P}$. In [Bazanella et al., 2011] and [Selvi et al., 2018], it is proposed to design the model reference $\mathbf{M}$ along with the controller in the VRFT procedure by parametrizing it. In the SISO case, in [Van Heusden et al., 2009], it is proposed to define an achievable reference model $\mathbf{M}$ for data-driven controller validation purposes: $\mathbf{M}$ is defined according to the nature of the system through a stable filter. This approach will be recalled in the next chapter.

Remark 6.1.2. It should be noted that in [Battistelli et al., 2018], the problem of choosing an achievable reference model is avoided by defining the initial ideal controller as the one giving a certain moderate command objective $\mathbf{W}_u$. Therefore, its expression is:

$$\mathbf{K}_u^\star = (1 - \mathbf{W}_u\mathbf{P})^{-1}\mathbf{W}_u, \tag{6.5}$$

instead of (6.1). For any stable $\mathbf{W}_u$, the corresponding ideal controller $\mathbf{K}_u^\star$ defined by (6.5) stabilizes the plant internally. The method then iterates to compromise between this objective and the classic closed-loop performances specifications given by a reference model $\mathbf{M}$, see Section 3.2.1.

In this work, we propose a technique to define an achievable model reference. First, it is necessary to identify the instabilities of the plant using a data-driven technique thanks to a method proposed in [Cooman et al., 2018b]. This technique is described in Section 6.2. Then, once the instabilities are estimated, the condition given in Equation (6.2) allows to build an achievable reference model. In Section 6.3, a method to define such a model reference is proposed.

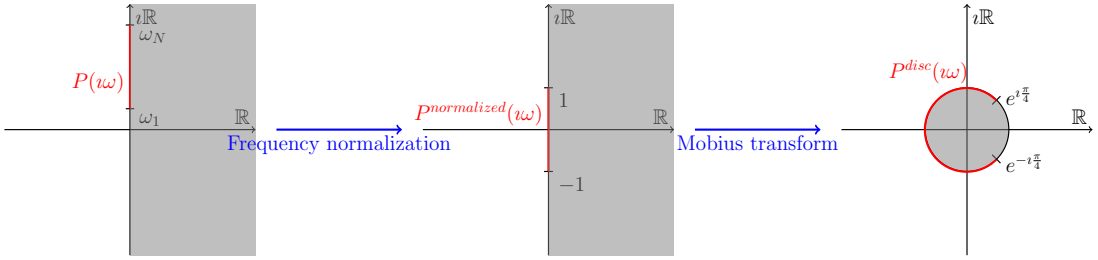

Figure 6.2: Frequency normalization and transformation from the plane to the unit circle.

6.2 Model-free stability analysis and detection of instabilities

The method proposed in [Cooman et al., 2018b] allows to detect and estimate instabilities of a system on the basis of frequency-domain data exclusively. It is then perfectly adapted to find a good reference-model in the proposed data-driven technique. The detection relies on the projection of the frequency-response on a basis of unstable functions. If instabilities are detected, they are estimated through the unstable part obtained during the projection. Originally, this method has been developed for the design of electronic circuits. It is implemented in the PISA toolbox [PISA Toolbox, 2018].

6.2.1 Stable and unstable projection of frequency-domain data

It is assumed that $\mathbf{P}(\imath\omega) \in \mathcal{L}_2$, meaning that it can be written as follows:

$$\mathbf{P}(\imath\omega) = \mathbf{P}^s(\imath\omega) + \mathbf{P}^{as}(\imath\omega), \tag{6.6}$$

where $\mathbf{P}^s$ is its stable projection, belonging to the Hardy space $\mathcal{H}_2$, and $\mathbf{P}^{as} \in \overline{\mathcal{H}}_2$ is its antistable projection.

The frequency response of the plant $\mathbf{P}$ is available on a discrete frequency grid $\{\omega_i, \mathbf{P}(\imath\omega_i)\}_{i=1\ldots N}$ only. First, the frequency grid is normalized and moved to the unit circle as explained on Figure 6.2. The passage to the unit circle is done using the Mobius transform, see Equation (6.7). This transformation sends the right-half plane inside the unit disc.

$$\mathbf{P}^{disc}(z) = \mathbf{P}\left(\alpha\frac{z+1}{z-1}\right) \quad \text{with } \alpha = \frac{1}{1+\sqrt{2}}. \tag{6.7}$$

Since the frequency response is assumed to be zero outside $[\omega_1, \omega_N]$, the data is then filtered to avoid edge effect during the projection: the sudden ending of the data would appear in the antistable part. The applied filter $\mathbf{F}$ is a finite-impulse-response and stable one, see (6.8).

$$\begin{aligned} \mathbf{P}^{filtered}(e^{\imath\theta}) &= \mathbf{F}(e^{\imath\theta})\mathbf{P}^{disc}(e^{\imath\theta}) \\ \mathbf{F}(e^{\imath\theta}) &= \sum_{k=1}^{N_f} a_k e^{\imath k\theta} \end{aligned} \tag{6.8}$$

Due to its stability, the filter $\mathbf{F}$ will mainly affect the stable projection $\mathbf{P}^s$ (it only modifies the residues of the unstable poles). In addition, its zeros are designed to be outside the unit disc to avoid the cancellation of poles of the unstable projection. However, the filter will suppress instabilities close to the boundaries of the set of frequencies. For this reason, it is recommended to choose a wide frequency set around the region of interest.

The data $\mathbf{P}^{filtered}(e^{\imath\theta})$ is then projected on the basis functions $\mathbf{B}_k^{disc}$ corresponding to the powers of z:

$$\mathbf{B}_k^{disc}(z) = z^k = e^{\imath k\theta}.$$

Therefore, the projection of the frequency response $\mathbf{P}^{filtered}(e^{\imath\theta})$ consists in calculating its Fourier coefficients $\{c_k\}$, as follows:

$$\begin{aligned} \forall k,\ c_k &= \frac{1}{2\pi}\int_0^{2\pi} \mathbf{P}^{filtered}(e^{\imath\theta})e^{-\imath k\theta}d\theta \\ \mathbf{P}^s_{disc}(z) &= \sum_{k=0}^{\infty} c_k\mathbf{B}_k^{disc}(z) = \sum_{k=0}^{\infty} c_k z^k \\ \mathbf{P}^{as}_{disc}(z) &= \sum_{k=1}^{\infty} c_{-k}\mathbf{B}_{-k}^{disc}(z) = \sum_{k=1}^{\infty} c_{-k} z^{-k} \end{aligned} \tag{6.9}$$

A numerically efficient way to compute a given number N_F of Fourier coefficients $\{c_k\}$ is the Fast Fourier Transform (FFT):

$$\forall k = -\frac{N_F}{2}\dots\frac{N_F}{2}-1,\ c_k = \sum_{j=0}^{N_F-1} \mathbf{P}^{filtered}(e^{\imath\theta_j})e^{-\imath k\theta_j} \tag{6.10}$$

with $\theta_j = \frac{2\pi j}{N_F}$ linearly spaced on the unit circle between 0 and 2π. According to Equation (6.10), the FFT requires N_F samples of $\mathbf{P}^{filtered}$ in order to compute N_F Fourier coefficients. The $\frac{N_F}{2}$ coefficients with positive index corresponds to the stable projection and the $\frac{N_F}{2}$ with negative index to the unstable one.

To apply (6.10), it is necessary to know $\mathbf{P}^{filtered}(e^{\imath\theta_j})$ for $j = 0\dots N_f - 1$. To this aim, $\mathbf{P}^{filtered}$ is interpolated using a basic linear interpolation technique. The interpolation error is then estimated in order to evaluate the influence of the interpolation on the projection.

After the interpolation, $\mathbf{P}^{filtered}(e^{\imath\theta_j})$ is known on the given linear grid $\{\theta_j\}_{j=1\dots N_F}$. The FFT can be performed as in (6.10) and the resulting coefficients are used to build $\mathbf{P}^s_{disc}$ and $\mathbf{P}^{as}_{disc}$ according to (6.9). Finally, $\mathbf{P}^s$ and $\mathbf{P}^{as}$ are obtained by applying the inverse Mobius transformation, see (6.7).

Remark 6.2.1. Usually, the FFT is performed on time-domain signals to obtain frequency-domain information. In the present case, it is applied on frequency-domain data, projected on the unit disc: it is for this reason that the coefficients $\{c_k\}$ are called Fourier coefficients and not Markov parameters.

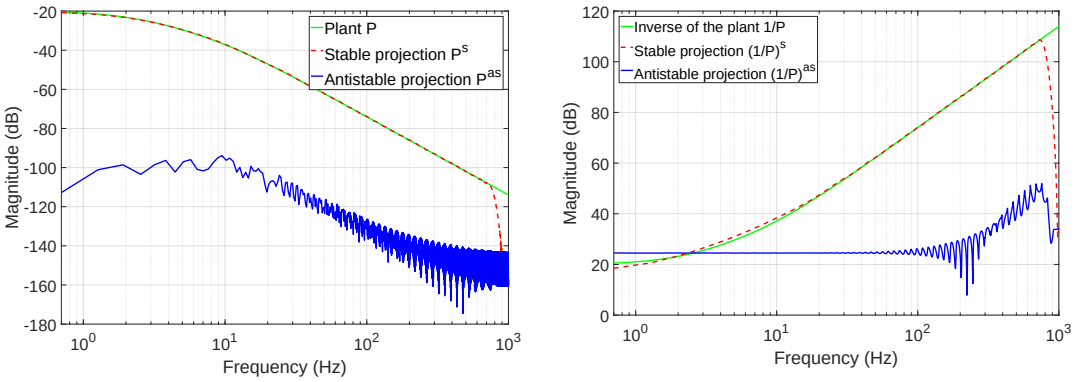

(a) Projection $\{\omega_i, P(\imath\omega_i)\}_{i=1}^N$.

(b) Projection of $\{\omega_i, P^{-1}(\imath\omega_i)\}_{i=1}^N$

Figure 6.3: Projection of the available frequency-domain data to determine the nature of the plant $\mathbf{P}$ in the DC motor example: the plant is stable and minimum phase.

Application on the DC motor example

As in Section 4.2, $N = 100$ samples of the frequency-response of the plant $\mathbf{P}$ are considered. The corresponding frequencies are logarithmically spaced between 0.1 and 10^3 rad.s^{-1}. The considered data is noise-free. The projection of the FRF measurements is shown on Figure 6.3. Since, on Figure 6.3a, the stable projection fits the plant's data, the system is stable. For the same reason, when projecting the inverse of the plant's data, the system is found to be minimum phase, see Figure 6.3b.

Application on the flexible transmission benchmark

As in Section 4.2, $N = 200$ samples of the frequency-response of the plant $\mathbf{P}$ are considered. The corresponding frequencies are logspaced between 1 and 10^3 rad.s^{-1}. In the first time, the considered data is noise-free. The projection of the FRF measurements is shown on Figure 6.4. Since the stable projection fits the plant's data, the system is stable.

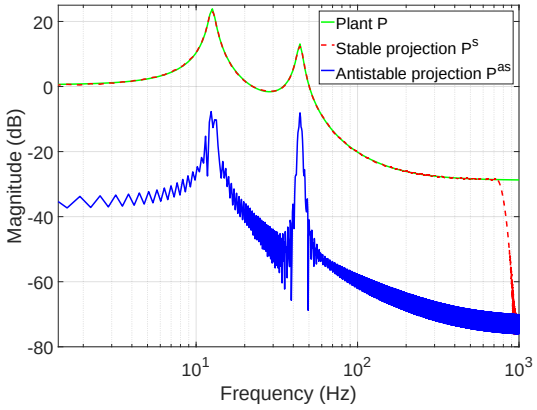

Figure 6.4: Projection of $\{\omega_i, P(\imath\omega_i)\}_{i=1}^N$ to detect the presence of unstable poles.

Applying the projection technique on $\left\{\omega_i, P^{-1}(\imath\omega_i)\right\}_{i=1}^{N}$, the results, visible on Figure 6.5, show that the inverse of the plant is unstable. Therefore, the plant is non-minimum phase.

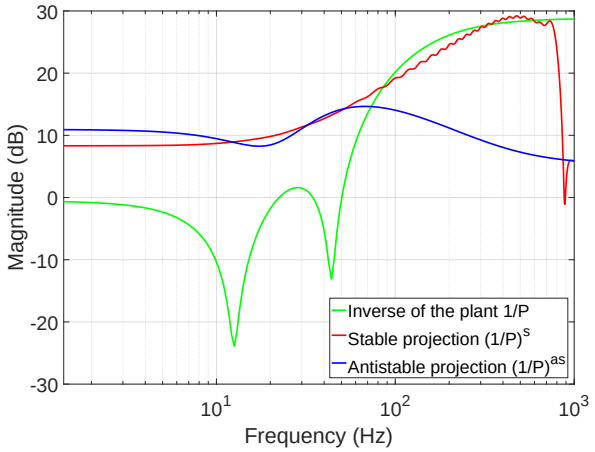

Figure 6.5: Projection of $\left\{\omega_i, P^{-1}(\imath\omega_i)\right\}_{i=1}^{N}$ to detect the presence of RHP zeros.

6.2.2 Estimation of the instabilities

Once the stable and unstable projection are obtained from the frequency response of the plant, if the system is determined to be unstable or NMP, it is possible to estimate its instabilities as it is done in [Cooman et al., 2018a]. It relies on the Hankel matrix containing the Fourier coefficients corresponding to the unstable projection $\mathbf{P}_{disc}^{as}$, see (6.11).

$$\Phi = \begin{pmatrix} c_{-1} & c_{-2} & \dots \\ c_{-2} & \ddots & \\ \vdots & & \end{pmatrix} \tag{6.11}$$

Assuming that a state-space representation $(A^{as}, B^{as}, C^{as}, D^{as})$ of $\mathbf{P}_{disc}^{as}$ is available, the associated observability and controlability matrices, respectively denoted $\mathcal{O}^{as}$ and $\mathcal{C}^{as}$ satisfy:

$$\Phi = \mathcal{O}^{as}\mathcal{C}^{as}. \tag{6.12}$$

In practice, a truncation Φ_{n_F} of sie $n_F \times n_F$ of the infinite dimensionnal matrix Φ is used. For a rational system with n_p poles, the Hankel matrix Φ is of rank n_p. In order to find the number of poles of $\mathbf{P}_{disc}^{as}$, which corresponds to the unstable poles of $P^{filtered}$, a SVD is performed on the truncated Hankel matrix Φ_{n_F}:

$$\Phi_{n_F} = USV^T. \tag{6.13}$$

The number of poles n_p is the number of non-zero singular values in (6.13). Moreover, from (6.13), it is possible to estimate the observability and controlability matrices of

the unstable projection $\mathbf{P}^{as}_{disc}$. The SVD of Φ_{n_F} is partitioned as in (6.14), with $S_P \in \mathbb{R}^{n_P \times n_P}$ containing the n_P largest singular values, $U_P \in \mathbb{R}^{n_F \times n_P}$ and $V_P \in \mathbb{R}^{n_F \times n_P}$:

$$\Phi_{n_F} = \begin{pmatrix} U_P & U_R \end{pmatrix} \begin{pmatrix} S_P & 0 \\ 0 & S_R \end{pmatrix} \begin{pmatrix} V_P^T \\ V_R^T \end{pmatrix}. \tag{6.14}$$

Following (6.12), for a given number n_F of Fourier coefficients, the observability and controlability matrices can be approximated by:

$$\mathcal{O}_{n_F} = U_p \sqrt{S_P} \quad \text{and} \quad \mathcal{C}_{n_F} = \sqrt{S_P} V_P. \tag{6.15}$$

$\mathcal{O}_{n_F}$ is the extended observability matrix of $\mathbf{P}^{as}_{disc}$ and satisfies:

$$\mathcal{O}_{n_F} = \begin{pmatrix} C^{as} \\ C^{as}A^{as} \\ C^{as}(A^{as})^2 \\ \vdots \\ C^{as}(A^{as})^{n_F-1} \end{pmatrix}. \tag{6.16}$$

As in the subspace approach, see Chapter 5, it is possible to estimate the matrix A^{as} from $\mathcal{O}_{n_F}$ as follows:

$$\hat{A}^{as} = (J_1 \mathcal{O}_{n_F})^{\dagger} J_2 \mathcal{O}_{n_F}, \tag{6.17}$$

with $J_1 = \begin{bmatrix} I_{(n_F-1)n_P)} & 0_{(n_F-1)n_P \times n_P} \end{bmatrix}$ and $J_2 = \begin{bmatrix} 0_{(n_F-1)n_P \times n_P} & I_{(n_F-1)n_P)} \end{bmatrix}$. Finally, the poles of $\mathbf{P}^{as}_{disc}$, which are the unstable poles of $P^{filtered}$, are given by the eigenvalues of $\hat{A}^{as}$.

Application on the flexible transmission benchmark

Let us come back to the application of the flexible transmission. The projection of its frequency-response samples indicates that the plant is stable but non-minimum phase. The next step consists in looking for the plant's RHP zeros by estimating the unstable poles of the frequency response $\left\{\omega_i, P^{-1}(\imath\omega_i)\right\}_{i=1}^{N}$ as explained earlier.

The SVD of the Hankel matrix Φ defined in (6.11) is visible on Figure 6.6. There are four singular values before the sharp drop, so it is chosen to estimate four instabilities. The estimated RHP zeros of the plant along with its real RHP zeros are given in Table 6.1. A good estimation of the NMP zeros is obtained even though the plant's NMP zero of multiplicity 3 has been estimated by three distinct zeros. It is interesting to note that the mean of these three estimated zeros is equal to the value of the associated true plant's NMP zero.

Real RHP zeros of the system	140.5	40	40	40
Estimated RHP zeros	140.58	41.3-2$\imath$	41.3+2$\imath$	37.4

Table 6.1: Estimation of the RHP zeros of the flexible transmission system.

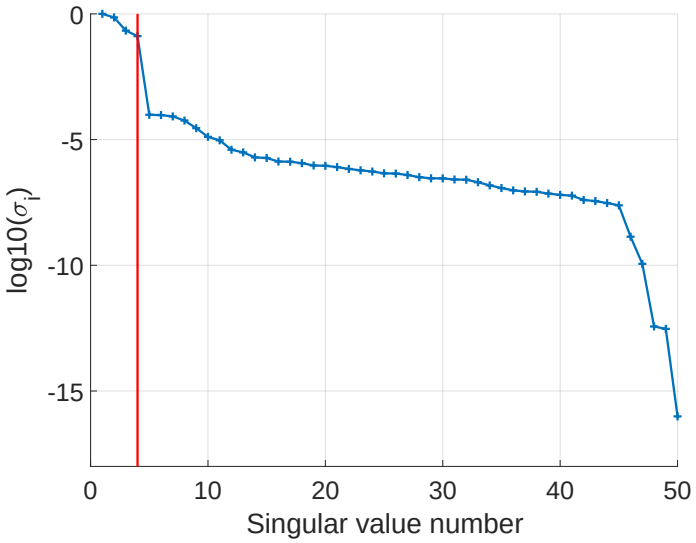

Figure 6.6: Singular Value Decomposition of the Hankel matrix Φ: detection of four RHP zeros.

6.2.3 Advantage of the projection approach

When it comes to analyse a system's stability on the basis of its FRF measurements, two options are available:

(i) obtain a rational fitting of the FRF measurements to determine all the poles and zeros of the system;

(ii) project the FRF.

Considering the numerical applications, the flexible transmission and the DC motor, presented in this manuscript to illustrate the proposed method, one could argue that option (i), i.e. obtaining a model of the plant, would much more straightforward when it comes to the determination of the plant's instabilities. It is true that for simple examples like these, using the Loewner framework, for example, would give a good estimate of the RHP poles and zeros of the plant. However, these two examples do not illustrate the added value of using the second option (ii), the projection approach.

As explained in [Cooman et al., 2018b], the main drawback of (i) is that pole-zero identification through rational fitting faces the same challenges than system identification in the frequency-domain. The order selection, for example, is a critical step. Indeed, the main difficulty will be to distinguish the approximation artefacts from the true instabilities of the system. Knowing that data-driven control is supposed to address the cases where a control-oriented model is difficult to get, (i) does not seem like an appropriate solution in a data-driven control framework.

In order to illustrate the limits of rational interpolation to estimate the RHP poles and zeros, noise has been added to the considered frequency-domain data as in Chapter 5. For the DC motor example, ten different noisy data-sets (SNR=50), still containing $N = 100$ points with frequencies logarithmically spaced between 0.1 and 10^3 rad.s^{-1},

were considered and interpolated through the Loewner framework. All the obtained models are of order $N = 100$ and are unstable. However, for a low noise-level like SNR=50, the approximation artefacts are easy to spot and to eliminate: most of the non-physical poles, including the unstable ones, are almost compensated by non-physical zeros. In four cases, a RHP zero is identified in a high frequency range, suggesting that the system is non-minimum phase while the true plant is not.

When considering ten noisy data-sets with a higher noise level (SNR=20), it becomes more difficult to eliminate the non-physical instabilities identified when interpolating the data. For this noise level, the interpolated models suggest in 3 cases that the system is unstable and in 7 cases that the system is NMP. Considering these same 10 noisy data-sets, the PISA projection allows to conclude that the system is stable and minimum phase in every case.

The same occurs for the flexible transmission benchmark: the higher the noise, the more difficult it gets to spot the non-physical instabilities in the interpolated high-order models. However, it should be noted that the interpolated models contain estimation of the real NMP zeros of the system with a similar error compared to the ones obtained with PISA. Indeed, as shown in [Mårtensson and Hjalmarsson, 2009], the RHP poles and zeros of a plant have a limited variance: therefore, they will appear in a limited error bound around the true values of the RHP poles and zeros of the system. The problem is to distinguish these estimates from the RHP artefacts introduced by the rational approximation when dealing with noisy data or irrational systems as in Chapter 8 for example. Avoiding this problem is the main strength of the PISA algorithm.

For this reason, using PISA is more interesting since it avoids the main problem of poles-zeros identification, which to separate the approximation artefacts from the physical poles and zeros of the system. This task gets more complicated when the noise is more important. Using the same 10 noisy data-sets, the PISA algorithm allows to determine that the system is stable and non-minimum phase with 4 RHP zeros.

6.3 Selection of an achievable model reference

Once the nature of the plant and its instabilities are determined from the projection of its frequency-response, it is possible to determine what are its achievable behaviours. This Section aims at finding a model-reference that satisfies the analiticity constraints given (6.2) and imposed by the RHP poles and zeros of the system to be controlled.

6.3.1 The SISO case

Now that the instabilities of the plant are estimated, it is possible to build a stable reference model that gives the desired performances and satisfies (6.2). In order for the proposed method to stay user-friendly, in the SISO case, the achievable reference model $\mathbf{M}_f$ is obtained by filtering the initial one $\mathbf{M}$. As a matter of fact, the easiest way for the user to express closed-loop performance specifications is to define a stable first or second model-reference. It is a similar approach to what have been proposed in [Van Heusden et al., 2009]: the main difference is that the filter is designed to ensure internal stability in the ideal case instead of specifying the desired performances.

The proposed choice of an achievable reeference model relies on the Blaschke products $\mathbf{B}_z$ and $\mathbf{B}_p$, defined respectively by the estimated RHP zeros $\{z_i\}_{i=1}^{n_z}$ and poles $\{p_j\}_{j=1}^{n_p}$ of the plant, and recalled hereafter:

$$\mathbf{B}_z(s) = \prod_{i=1}^{n_z} \frac{s - z_i}{s + z_i} \qquad \mathbf{B}_p(s) = \prod_{j=1}^{n_p} \frac{s - p_j}{s + p_j}. \tag{6.18}$$

$\mathbf{B}_z$ and $\mathbf{B}_p$, are stable. The choice of a stable reference model $\mathbf{M}_f$ that satisfies the interpolatory conditions (6.2) is done as follows:

1. **If the plant is stable and minimum phase**: any stable and minimum-phase $\mathbf{M}$ specified by the user is achievable by the plant.

$$\mathbf{M}_f = M \tag{6.19}$$

2. **If the plant is stable and non-minimum phase**:

$$\mathbf{M}_f = \mathbf{M}\mathbf{B}_z \tag{6.20}$$

3. **If the plant is unstable and minimum phase**:

$$\mathbf{M}_f = 1 - (1 - \mathbf{M})\mathbf{B}_p \tag{6.21}$$

4. **If the plant is unstable and non-minimum phase**:

$$\mathbf{M}_f = \mathbf{M}\mathbf{B}_z\mathbf{F}_\mathbf{M} \tag{6.22}$$

where the filter $\mathbf{F}_\mathbf{M}$ is defined as follows:

$$\mathbf{F}_\mathbf{M}(s) = \frac{\sum_{k=1}^{n_p} \gamma_k l_k(s)}{\prod_{j=1}^{n_p}(s + p_j)}, \tag{6.22}$$

with, for $k = 1 \dots n_p$,

$$\gamma_k = \frac{\prod_{j=1}^{n_p}(p_k + p_j)}{M(p_k)B_z(p_k)} \tag{6.22}$$

and

$$l_k(s) = \prod_{j=1, j\neq k}^{n_p} \frac{s - p_j}{p_k - p_j}. \tag{6.22}$$

Proof: In case 1, for a stable and minimum phase plant $\mathbf{P}$ and a stable model reference $\mathbf{M}$, the functions $(1 - \mathbf{M})$ and $\mathbf{P}(1 - \mathbf{M})$ are also stable. Finally, according to the definition of the ideal controller, $\mathbf{K}^\star(1 - \mathbf{M}) = \mathbf{M}\mathbf{P}^{-1}$ is also stable. Therefore, $\mathbf{K}^\star$ stabilizes the plant internally and $\mathbf{M}$ is achievable by the plant $\mathbf{P}$.

For other cases, $\mathbf{K}^\star$ stabilizes the plant internally if and only if $\mathbf{M}_f$ is stable and satisfies (6.2). In case 2 and 3, this is obviously the case since, by definition, $\mathbf{B}_z$ and $\mathbf{B}_p$ are stable and satisfy

$$\begin{cases} \forall i,\ \mathbf{B}_z(z_i) = 0 \\ \forall j,\ \mathbf{B}_p(p_j) = 0 \end{cases}. \tag{6.23}$$

In case 4, the use of $\mathbf{B}_z$ ensures that, for any RHP zeros z_i, $\mathbf{M}_f(z_i) = 0$. The additional filter $\mathbf{F}$ is stable and is supposed to ensure that, for any RHP poles p_j, $\mathbf{M}_f(p_j) = 1$. It is defined using Lagrange polynomials which satisfies $l_k(p_j) = \delta_{k,j}$. Consequently, $\mathbf{M}_f$ is stable and satisfies (6.2).

Remark 6.3.1. Concerning the application of the proposed method to unstable plants, it should be noted that measurements from such plants are only accessible when performing an experiment with an initial stabilizing controller or if their frequency-response can be accessible through frequency-domain simulations as in the application considered in Chapter 8 or in [Kergus et al., 2019a].

Remark 6.3.2. In case 2 or 3, the multiplicity of the instabilities can be taken into account to satisfy the derivative constraints of (6.3) by taking:

$$\mathbf{B}_z(s) = \prod_{i=1}^{n_z} \left(\frac{s - z_i}{s + z_i}\right)^{m_{z_i}} \text{ and } \mathbf{B}_p(s) = \prod_{j=1}^{n_p} \left(\frac{s - p_j}{s + p_j}\right)^{m_{p_j}} .$$

Solving (6.3) is more complicated in case 4, where the Loewner framework could be used with derivative constraints in order to find an achievable reference model.

6.3.2 The MIMO case

In this paragraph, a more general solution allowing to deal with multivariable systems is proposed. As a matter of fact, the choice of a reference model proposed earlier cannot be easily extended to the MIMO case because of the tangential directions that appear in this case in the definition of an achievable closed-loop, see (6.4).

Instead of filtering an initial reference model, we propose for the MIMO case to identify one using the Loewner framework. As explained in Chapter 5, this technique allows to find a minimal realization that solves a given tangential interpolation problem. Therefore, an achievable reference model $\mathbf{M}_f$ can be obtained by solving (6.24) through the Loewner framework:

$$\left\{ \begin{array}{cc} \mathbf{y}_{z_i}\mathbf{M}_f(z_i) = 0 & \forall i = 1 \dots n_z \\ \mathbf{M}_f(p_j)\mathbf{y}_{p_j} = \mathbf{y}_{p_j} & \forall j = 1 \dots n_p \\ \mathbf{M}_f(\imath\omega_k) = \mathbf{M}(\imath\omega_k) & \forall k = 1 \dots N \end{array} \right. , \tag{6.24}$$

where $\mathbf{M}$ is an initial reference model specifying the desired performances, as in the SISO case. The obtained achievable model $\mathbf{M}_f$ does not necessarily need to be reduced: a minimal realization is sufficient to be used as a reference model.

The tangential directions $\left\{\mathbf{y}_{p_j}\right\}$ associated to the estimated RHP poles $\{p_j\}$ can be computed easily during the estimation of instabilities in the end of Section 6.2. Indeed, the RHP poles are obtained through the matrices A^{as} and C^{as} from the antistable projection. As explained in Chapter 2, considering an unstable pole p_j, these two matrices allow to compute the associated output direction from:

$$\mathbf{y}_{p_j} = C^{as}\mathbf{x}_R, \qquad A^{as}\mathbf{x}_R = p_j\mathbf{x}_R \ . \tag{6.25}$$

6.3.3 Choice of an initial reference model

Whether the considered plant is SISO or MIMO, the proposed method to build an achievable reference mode is based on an initial specification $\mathbf{M}$ furnished by the user. Even though the method proposed in this Chapter allows to turn this initial reference model into an achievable one, the choice of $\mathbf{M}$ is a key aspect of the method for the two reasons already exposed in paragraph 6.1.1. First, the performances specified by the initial reference model $\mathbf{M}$ will impact the controller reduction because of the complexity-performance tradeoff. This was already illustrated on the DC motor example in Chapter 4 and will be discussed also in the next Chapter.

In addition, the choice of the specifications is critical due to the performance limitations of the plant. Indeed, as recalled in Chapter 2, the analiticity constraints (6.4) imposed by the system's instabilities limit the possible closed-loop performances. Therefore, once the instabilities of the system are estimated, the lower bounds of the sensitivity function and of the closed-loop transfer can be computed. The cutoff frequency of the closed-loop is also limited by eventual NMP zeros. Finally, if the initial reference model $\mathbf{M}$ does not respect these limitations, it is recommended to redefine it once the RHP poles are estimated. This is highlighted in the following paragraph when applying the proposed procedure on the flexible transmission benchmark.

In the end, the method proposed in this Chapter to build an achievable reference model only ensures that the corresponding ideal controller stabilizes the plant internally. It avoids the worst case scenario described in Chapter 4 and recalled in paragraph 6.1.1, when applying the proposed control technique on the flexible transmission benchmark. Therefore, the performance specifications, imposed through the initial reference model $\mathbf{M}$, remain an important tuning parameter. On this topic, good practices for the user involve:

- using the estimation of instabilities to verify that $\mathbf{M}$ does not specify non-feasible performances;
- increasing progressively the desired performances until reaching a desirable trade-off. This iterative aspect will be discussed in the outlooks in Chapter 9.3.

6.3.4 Application on the flexible transmission benchmark

According to the projection of its data in Section 6.2, the flexible transmission is non-minimum phase and stable. Its estimated instabilities are given in Table 6.1. Therefore, according to the proposed selection of a reference model in the SISO case, an achievable reference model is given by:

$$\mathbf{M}_f(s) = \mathbf{M}(s)\mathbf{B}_z(s) \tag{6.26}$$

with $\mathbf{M}$ the initial second-order reference model given by:

$$\mathbf{M}(s) = \frac{1}{\frac{s^2}{\omega_0^2} + \frac{2\xi}{\omega_0}s + 1} \tag{6.26}$$

with $\omega_0 = 10$ rad.s^{-1} and $\xi = 1$. The Blaschke product $\mathbf{B}_p$ is defined as in Equation (6.18) thanks to the estimated NMP zeros of Table 6.1:

$$\mathbf{B}_z(s) = \frac{(s-140.6)(s-37.39)(s^2-82.6s+1710)}{(s+140.6)(s+37.39)(s^2+82.6s+1710)}. \tag{6.27}$$

Interpolating the frequency-response of the corresponding ideal controller $\mathbf{K}^\star$ using the Loewner framework leads to the following 10th order model $\mathbf{K}$:

$$\begin{aligned}\mathbf{K}(s) = & \frac{2765.5(s^2+1.071s+157.9)(s^2+3.172s+1936)}{s(s+148.5)(s^2+19.98s+485.8)(s^2+112.1s+4540)} \\ & \times \frac{(s-140.6)(s-37.39)(s^2-82.6s+1710)}{(s-140.5)(s-39.73)(s^2-80.27s+1611)}.\end{aligned} \tag{6.28}$$

As indicated in red, this minimal realization of the ideal controller compensates the NMP zeros of the system. However, considering the blue part in (6.28), these instabilities are almost compensated thanks to the choice of $\mathbf{M}_f$ (6.26) as reference model. As a matter of fact, when using the projection on $\mathcal{RH}_\infty$ proposed in [Köhler, 2014], the minimal realisation $\mathbf{K}$ of the ideal controller can be assimilated to its stable projection $\mathbf{K}^s$, see Figure 6.7.

$$\mathbf{K}(s) = \frac{-3.7293e-05(s-2.966e06)(s^2+1.067s+157.9)(s^2+3.153s+1935)}{s(s+140.9)(s+25.65)(s+5.03)(s^2+92.98s+2303)} \tag{6.29}$$

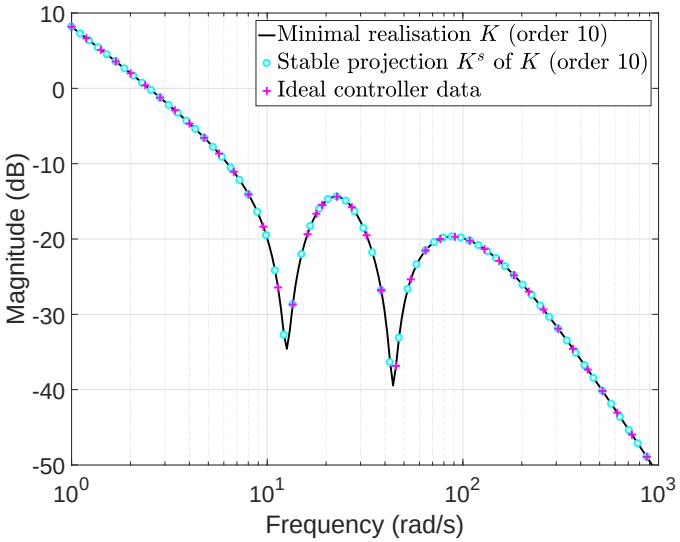

Figure 6.7: Stable projection $\mathbf{K^s}$ of the minimal realisation $\mathbf{K}$ of the ideal controller when using $\mathbf{M_f}$ as a reference model: the ideal controller can be assimilated to $\mathbf{K^s}$.

This example illustrates well the fact that filtering the initial reference model $\mathbf{M}$, not achievable by the plant $\mathbf{P}$, allows to consider the performance limitations induced by the RHP zeros of the system. As shown on Figure 6.8, the filtered reference model $\mathbf{M_f}$ presents an undershoot behaviour as the plant $\mathbf{P}$ due to the estimated RHP zeros. Therefore, it is slower than the initial reference model $\mathbf{M}$: as explained in Chapter 2, the corresponding response time is not realistic since it is over the natural limit fixed by the RHP zeros of the system.

Remark 6.3.3. The estimation of the instabilities obtained at this step of the method should be used to modify the initial reference model if necessary. In the present case,

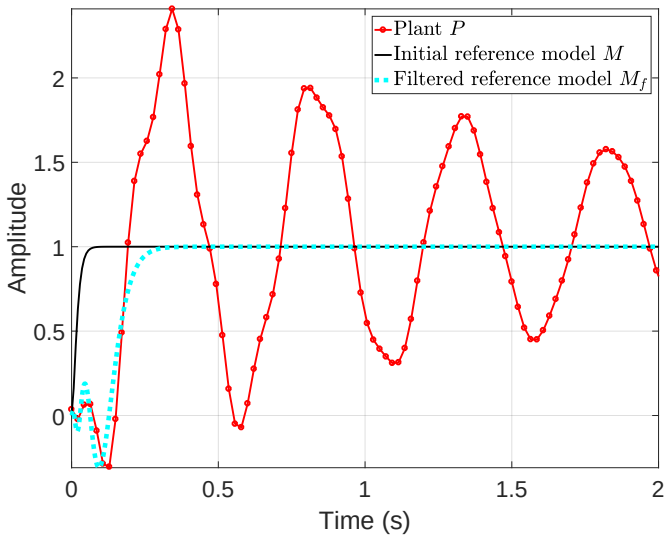

Figure 6.8: Step response of the filtered reference model $\mathbf{M}_f$, the initial one $\mathbf{M}$ and the plant $\mathbf{P}$: the proposed choice of the reference model $\mathbf{M}_f$ allows to introduce the natural limitations of the plant $\mathbf{P}$ in the performance specifications.

the initial reference model is defined by a second-order model with a natural frequency $\omega_0 = 100\text{rad.s}^{-1}$. However, as recalled in Chapter 2, for a plant with RHP zeros, the bandwidth of the closed-loop must be much smaller than the smallest RHP zero frequency (see [Zhou and Doyle, 1998]), which is here 40rad.s^{-1} for the flexible transmission benchmark.

Therefore, choosing a second-order model with a natural frequency $\omega_0 = 10\text{rad.s}^{-1}$ as an initial reference model, denoted $\mathbf{M}_2$, is wiser (the damping factor ξ is kept equal to 1). It is then filtered using $\mathbf{B}_z$:

$$\mathbf{M}_{f_2} = \mathbf{M}_2\mathbf{B}_z.$$

As shown on Figure 6.9, by changing the initial reference model to respect the performance limitations of the system, the filtered reference model $\mathbf{M}_{f_2}$ corresponds to a much more desirable closed-loop behaviour.

In this chapter, only achievable reference models are obtained for the two considered numerical examples. Reduced-order controllers will be identified in the next chapter under internal stability considerations.

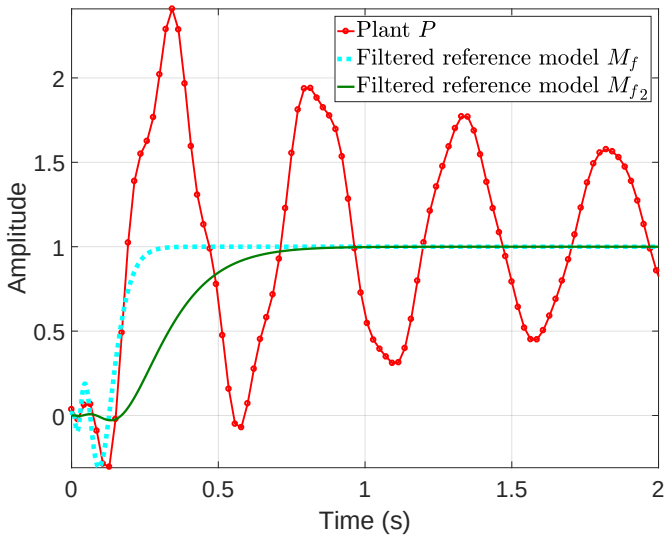

Figure 6.9: Step response of the filtered reference models $\mathbf{M}_f$ and $\mathbf{M}_{f_2}$, and of the plant $\mathbf{P}$: the estimation of the instabilities should be used to modify the performance specifications if necessary.

Summary

In this chapter, it is recalled that the choice of a reference model is critical step for data-driven techniques such as the VRFT, the CbT, the IFT or the one proposed in this work. The main contribution in this Chapter is to propose a method to build an achievable reference model $\mathbf{M}_f$ provided a stable initial one $\mathbf{M}$ specified by the user. It relies on the following three steps:

1. **Determination of the nature of the system** (stable or not, minimum phase or not) thanks to the projection of its frequency-response.

2. **Estimation of the plant's instabilities** through the analysis of the obtained antistable projection.

3. **Construction of an achievable reference model $\mathbf{M}_f$** by filtering the initial one $\mathbf{M}$ in the SISO case or by interpolating a model in the MIMO case given the conditions in (6.24).

The first step allows to conclude that the DC motor is stable. Therefore, any stable reference model $\mathbf{M}$ is achievable. Concerning the flexible transmission benchmark, the projection indicates that the plant is stable but NMP and its NMP zeros are well estimated. The initial reference model $\mathbf{M}$ is then filtered to obtain an achievable one $\mathbf{M}_f$. It should be noted that the performances specified by the initial reference model $\mathbf{M}$ influences a lot the design process.

At this point, the choice of an achievable reference model $\mathbf{M}_f$ ensures that the corresponding ideal controller $\mathbf{K}^\star$ preserves closed-loop internal stability. It is possible to interpolate a minimal realisation of $\mathbf{K}^\star$ through the Loewner framework or to obtain a high-order model through the subspace approach, following what has been done in

Chapter 5. Finally, the only missing piece in the puzzle is the reduction of the controller and an internal stability analysis of the resulting closed-loop: this is the topic of the next chapter.

Chapter 7

Closed-loop stability analysis and enforcement

Analyzing and enforcing closed-loop stability is one of the most important challenges for any data-driven control technique. The objective of this chapter is, in the first place, to recall the different techniques known in data-driven control to analyze and/or ensure stability in Section 7.1. Then, the data-driven stability condition proposed in [Van Heusden et al., 2009] is derived to be applied to the proposed method in Section 7.2: the reduction of the controller is then adjusted in order to preserve internal stability of the closed-loop. The data-driven stability and the reduction step detailed in this chapter are then applied on the numerical examples treated along this manuscript. Finally, some preliminary work on closed-loop robustness analysis is presented in Section 7.3.

Contents

7.1 Preliminary: data-driven closed-loop stability assessment and enforcement

Closed-loop stability is a major challenge for any data-driven control technique. Since this type of techniques do not use any plant model, it is not possible to check the classical stability conditions and the robustness margins. Therefore, the only way to test the stability seems to be to implement the obtained controller in the closed-loop,

which can be risky according to the considered application. Different techniques have been proposed in data-driven control theory to face this problem.

In online data-driven methods, BIBO stability is mostly enforced by introducing some assumptions on the plant. For example, MFAC assumes that the controlled plant satisfy the generalized Lipschitz conditions. Therefore, the Pseudo Partial Derivative (PPD), estimated to construct the control law, is bounded and BIBO stability is ensured. This type of solution is only pertinent when using online data however.

In robust data-driven control, as said in Chapter 3, the Nyquist criteria has been widely used to enforce closed-loop stability. This is made possible by using a stabilizing controller. Stability enforcement is formulated as a constraint in the optimization problem solved by this category of techniques. In the SISO case, it is possible to solve this problem without a stabilizing controller.

When it comes to reference model control techniques, a data-driven test for internal stability is proposed in [Van Heusden et al., 2007], relying on the small-gain theorem. It does not require neither a plant model or to implement the controller in the closed-loop. It showed good performances when applied on the flexible transmission benchmark to check *a posteriori* if controllers obtained by the VRFT technique stabilize the plant internally. In [van Heusden et al., 2008], this stability test is integrated to the non-iterative CbT framework as an LMI constraint. In [Van Heusden et al., 2009], this stability test is detailed and special attention is given to the reliability-conservatism trade-off when only a finite amount of data is available.

As for other reference model methods, this last stability criteria is perfectly suited for the method proposed in this work. In particular, this last technique estimates a maximal admissible error for the controller modelling error thanks to the small-gain theorem. This bound is really helpful in our case to ensure that the reduction of the controller model does not destabilize the plant internally. Therefore, this solution will be recalled hereafter before being used in the proposed method to ensure internal stability during the controller reduction step.

Remark 7.1.1. For the IFT, another stability constraint was proposed in [De Bruyne and Kammer, 1999]. It consists in identifying the sensitivity function and the closed-loop transfer to estimate the stability margins. The destabilizing controllers are then eliminated during the optimization procedure. This solution could be investigated in the proposed method too, but it would require to perform this validation technique for every controller. It seems costly compared to the stability test of [Van Heusden et al., 2007] which can be incorporated into the reduction step, as detailed in the next section.

7.2 Controller reduction under data-driven closed-loop stability condition

In this section, the criteria proposed in [Van Heusden et al., 2009] is derived to include an internal stability condition in the reduction of the controller. As a matter of fact, in the end of Chapter 6, the choice of an achievable reference model $\mathbf{M}_f$ guarantees that the associated controller $\mathbf{K}^\star$ ideal controller stabilizes the plant internally. However,

in general, a minimal realization of $\mathbf{K}^\star$ will exhibit a high order. It is then necessary to obtain a reduced-order model $\mathbf{K}$ for which we do not have anymore information regarding the internal stability of the closed-loop. To tackle this issue, the small-gain theorem is applied on the resulting closed-loop, recalled in Figure 7.1. The computation of the obtained criteria is then detailed.

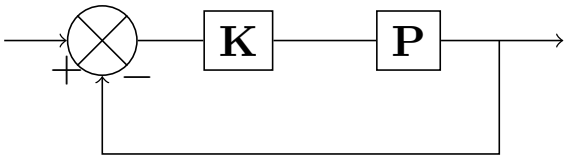

Figure 7.1: The resulting closed-loop: $\mathbf{K}$ is a reduced-order model of the ideal controller $\mathbf{K}^\star$.

7.2.1 Stability condition through the small gain theorem

This criteria relies on the small-gain theorem, recalled in Chapter 2, see Theorem 2.2.2. First, the obtained closed-loop, see Figure 7.1, is written as the interconnection shown on Figure 7.2. As proposed in [Van Heusden et al., 2009], the controller modelling error $\mathbf{\Delta} = \mathbf{K} - \mathbf{K}^\star$ appears as an uncertainty.

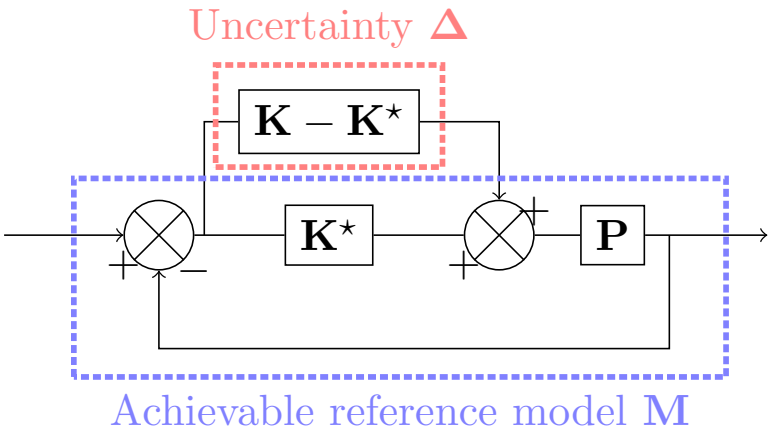

Figure 7.2: Stability analysis scheme: the controller modelling error is written as an uncertainty.

Applying the small-gain theorem on the interconnection shown on Figure 7.2, the following theorem is obtained.

Theorem 7.2.1. Suppose that $\mathbf{G} = \mathbf{P}(1 - \mathbf{M})$ is stable and let $\gamma > 0$. Then the interconnected system shown on Figure 7.2 is well-posed and internally stable for all stable $\mathbf{\Delta} = \mathbf{K} - \mathbf{K}^\star$ with:

(a) $\|\mathbf{\Delta}\|_\infty \leq \frac{1}{\gamma}$ if and only if $\|\mathbf{G}\|_\infty < \gamma$

(b) $\|\mathbf{\Delta}\|_\infty < \frac{1}{\gamma}$ if and only if $\|\mathbf{G}\|_\infty \leq \gamma$

The assumptions are met to apply Theorem 7.2.1. Indeed, the choice of an achievable reference model $\mathbf{M}$ as proposed in Chapter 6 ensures that the associated ideal controller $\mathbf{K}^\star$ is stable and stabilizes the plant $\mathbf{P}$ internally. Therefore, $\mathbf{G} = \mathbf{P}(1 - \mathbf{M})$ is stable. Furthermore, ensuring the stability of the identified controllers $\mathbf{K}$ and $\mathbf{K}^\star$ ensures that $\mathbf{\Delta}$ is also stable.

7.2.2 Stability-preserving reduction of the controller model

The problem is now to reduce the controller model while preserving the internal stability of the closed-loop. To that extent, Theorem 7.2.1 can be seen as a limit for the controller error that should not be crossed to preserve internal stability. The reduction of the controller is then done in two steps:

a. Compute an estimate $\tilde{\gamma}$ of $\gamma_0 = \|\mathbf{G}\|_\infty$;

b. Find $n \in \mathbb{N}$ such that the reduced-order controller $\mathbf{K}$ of order n satisfies:

$$\|\mathbf{K} - \mathbf{K}^\star\|_\infty \leq \frac{1}{\tilde{\gamma}} - \varepsilon, \tag{7.1}$$

where $\epsilon > 0$ is chosen by the user to avoid being too close to the stability limit. Equation (7.1) ensures that the reduced-order controller $\mathbf{K}$ preserves closed-loop internal stability.

a. Data-driven estimation of the $\mathcal{H}_\infty$-norm of the dynamical system G

Since we only have access to samples of the frequency-response of the plant $\mathbf{P}$, the function $\mathbf{G}(s)$ is only known on a discrete grid of frequencies. Therefore, the most simple way to estimate $\gamma_0 = \|\mathbf{G}\|_\infty$ is to take:

$$\tilde{\gamma} = \max_{i=1\ldots N} |\mathbf{G}(\imath\omega_i)| \,. \tag{7.2}$$

However, this estimation deeply depends on the quality of the plant's data. Whenever the data misses a peak of the frequency-response of the plant, it is likely that $\tilde{\gamma}$ underestimates γ_0. According to (7.1), it would lead to an overestimation of the maximal controller modelling error, and might result in the choice of a controller that do not stabilize the plant internally.

Remark 7.2.1. In [Van Heusden et al., 2007], a technique based on the correlation approach is proposed to estimate the $\mathcal{H}_\infty$-norm of a dynamical system on the basis of time-domain measurements.

b. Evolution of the controller modelling error according to the order

The controller modelling error is defined by the difference between the ideal controller $\mathbf{K}^\star$ and reduced order controllers. This error vary according to the selected order n for the controller $\mathbf{K}$.

Using the Loewner framework, recalled in Chapter 5, it is possible to obtain a minimal representation of the ideal controller $\mathbf{K}^\star$. The choice of an achievable reference model $\mathbf{M}$ in Chapter 6 ensures that this representation is either stable or might be assimilated to its stable projection on $\mathcal{RH}_\infty$ whenever the plant's instabilities are not

perfectly estimated (see the case of flexible transmission benchmark in the previous Chapter).

Reduced-order controllers can then be obtained using the Loewner framework and/or the subspace approach. Therefore, the modelling error $\mathbf{\Delta} = \mathbf{K} - \mathbf{K}^\star$ is accessible for every controller order n. It is then possible to determine which orders preserve the internal stability of the closed-loop.

Remark 7.2.2. Complexity-performance trade-off
When reducing the controller's order, the performances are expected to "decrease": the more the controller model is reduced, the less it will capture the dynamics of the ideal controller $\mathbf{K}^\star$. However, the order is not the only important aspect here. Indeed, the trade-off between controller complexity and closed-loop performances also depends on the choice of the specifications. This has already been highlighted on the DC motor example in Chapter 4 and during the choice of an achievable reference model in Chapter 6.

Remark 7.2.3. Comparison with the stability test in [Van Heusden et al., 2007]
The stability test proposed in this Section is inspired from the one detailed in [Van Heusden et al., 2007]. It shares the same base, which is the formulation of the resulting closed-loop as the interconnection of Figure 7.2 and the application of the small-gain theorem. In that sense, the same stability criteria is obtained. The major difference between the work of [Van Heusden et al., 2007] and the present one is the computation of the $\mathcal{H}_\infty$-norm of $\mathbf{G}$. Moreover, it is not used in the exact same way: in [Van Heusden et al., 2007] and [Van Heusden et al., 2009], it used as an a-posteriori stability verification while in [van Heusden et al., 2008], it is incorporated as an LMI constraint to the CbT approach. Here, the internal stability criteria stands as a limitation during the controller reduction.

7.2.3 Application to numerical examples

In this paragraph, the DC motor example and the flexible transmission benchmark are used to illustrate the stability analysis and the controller reduction introduced in this Section.

The DC motor

As in Chapter 4, two reference-models are considered, $\mathbf{M}_1$ and $\mathbf{M}_2$. Both are defined as second order transfer function as in (7.3), with a static gain $k = 1$, a damping factor $\xi = 1$ and natural frequencies ω_0 equal to $\omega_{01} = 10\text{rad.s}^{-1}$ and $\omega_{02} = 1\text{rad.s}^{-1}$ respectively. Then $\mathbf{M}$ reads:

$$\mathbf{M}(s) = \frac{k}{\frac{s^2}{\omega_0^2} + \frac{2\xi}{\omega_0}s + 1}. \tag{7.3}$$

In the noise-free case, the available data from the plant allow to obtain a good estimate of the $\mathcal{H}_\infty$-norm of the transfer $\mathbf{G}_1 = \mathbf{P}(1 - \mathbf{M}_1)$. We obtain $\tilde{\gamma}_1 = \|\mathbf{G}_1\|_\infty = 0.0297$, see Figure 7.3. When using $\mathbf{M}_2$ as reference model, the estimation of $\|\mathbf{G}_2\|_\infty$, with $\mathbf{G}_2 = \mathbf{P}(1 - \mathbf{M}_2)$, is also perfect: $\tilde{\gamma}_2 = \|\mathbf{G}_2\|_\infty = 0.0994$

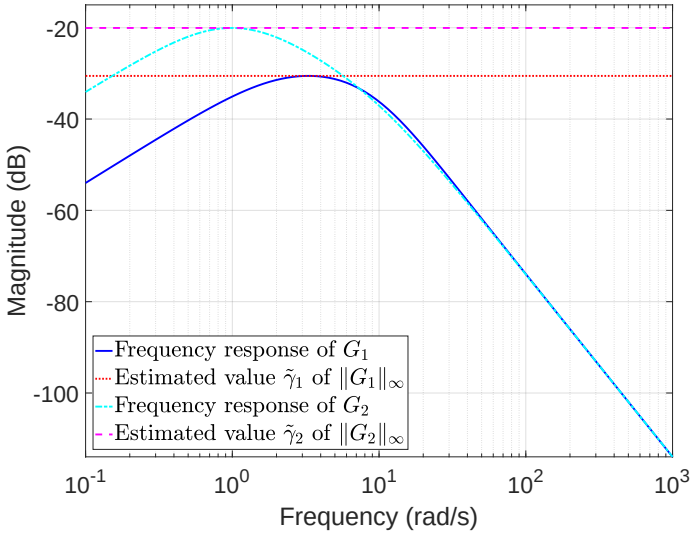

Figure 7.3: Data-driven estimation of $\|\mathbf{G}\|_\infty$ in the noise-free case for the DC motor example, using two different reference models $\mathbf{M}_1$ and $\mathbf{M}_2$.

Controllers of order $n = 1$ and $n = 2$ are identified through the Loewner framework and the subspace approach, as explained in Chapter 5. The corresponding modelling errors are given in Table 7.1. When using $\mathbf{M}_1$ as reference model, the subspace approach does not allow to reduce the controller to an order $n = 1$. When moving to $\mathbf{M}_2$ as reference model, both identification techniques, the Loewner framework and the subspace approach, obtain a stabilizing first order controller.

	Using $\mathbf{M}_1$ $\tilde{\gamma}_1^{-1} = 33.7053$		Using $\mathbf{M}_2$ $\tilde{\gamma}_2^{-1} = 10.0624$	
	Loewner	Subspace	Loewner	Subspace
$n = 2$	$\mathbf{7.4617 \times 10^{-6}}$	**8.3306e − 06**	**0.0020**	**3.6444e − 08**
$n = 1$	**12.9358**	68.4331	**0.0021**	**0.0113**

Table 7.1: Evolution of the controller modelling error $\|\Delta\|_\infty$ for controllers of order $n = 2$ and $n = 1$, using two different reference models $\mathbf{M}_1$ and $\mathbf{M2}$. $\tilde{\gamma}_1^{-1}$ and $\tilde{\gamma}_2^{-1}$ represent the maximal admissible controller modelling error in these two cases. Bold values correspond to cases where the stability test (7.1) is verified.

The flexible transmission benchmark

The proposed stability analysis is now applied on the flexible transmission benchmark. The considered reference model is the achievable one $\mathbf{M}_f$ obtained in the end of Chapter 6:

$$\mathbf{M}_f = \mathbf{M}\mathbf{B}_z$$

where $\mathbf{M}$ is a second-order transfer determining the performance specifications, defined as in (7.3) with $\{k, \xi, \omega_0\} = \{1, 1, 10\text{rad.s}^{-1}\}$, and where $\mathbf{B}_z$ is the Blaschke product associated with the estimated RHP zeros of the plant, see Chapter 6.

As for the previous example, the $\mathcal{H}_\infty$-norm of the dynamical system $\mathbf{G} = \mathbf{P}(1-\mathbf{M}_f)$ is estimated through the available data: we have $\tilde{\gamma} = 20.7152$, which underestimates the true value $\gamma_0 = 20.8505$.

Controllers are then identified through the Loewner framework as explained in Chapter 5 and reduced to orders comprised between 1 and $n_{max} = 10$, which corresponds to the order of the minimal representation of the ideal controller interpolated through the Loewner framework. The evolution of the controller modelling error when using the Loewner framework for the order reduction step is given on Figure 7.4: it shows that the controller can be reduced up to an order $n = 5$. Reducing it to a lower order would lead to destabilize the plant internally.

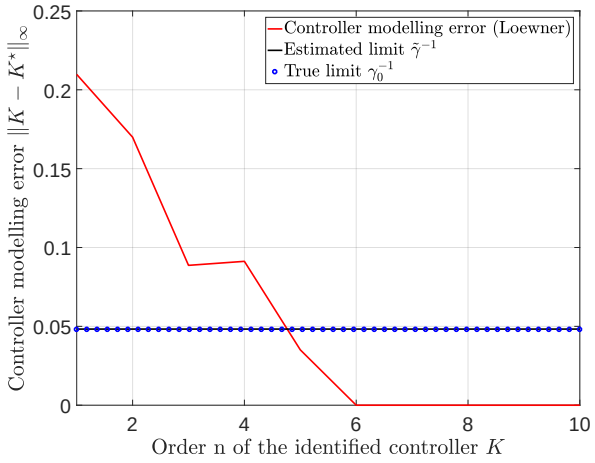

Figure 7.4: Controller reduction for the flexible transmission benchmark: the Loewner framework is used to reduce the minimal realization of the ideal controller to an order n. The reduction of the controller is limited by the internal stability condition.

Since the plant is of order 4, it is necessary to find a way to reduce the controller more than that. As for the DC motor example, changing the specifications for weaker ones allow to reduce the controller to a lower order. In the present case, let us consider an achievable reference model $\mathbf{M}_{f_2} = \mathbf{M}_2\mathbf{B}_z$, where $\mathbf{M}_2$ is a second-order model with $\{k, \xi, \omega_0\} = \{1, 1, 2\text{rad.s}^{-1}\}$, see (7.3). The specifications then correspond to a slower closed-loop behaviour in comparison with $\mathbf{M}_f$. When using $\mathbf{M}_{f_2}$ as reference model, we obtain $\tilde{\gamma}^{-1} = 0.0641$ while the true value for the maximal controller modelling error

is $\gamma_0^{-1} = 0.0638$. In this case, it is possible to reduce the controller up to an order $n = 2$ while preserving the internal stability of the resulting closed-loop.

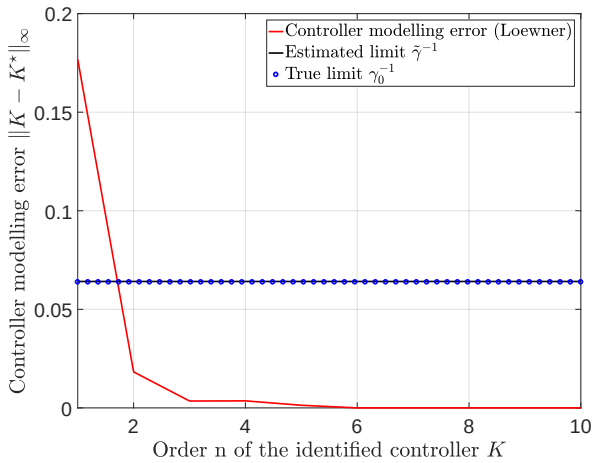

Figure 7.5: Controller reduction for the flexible transmission benchmark using $\mathbf{M}_{f_2}$ as a reference model: giving weaker specifications allows to reduce the controller to a lower order.

Remark 7.2.4. The evolution of the maximal controller modelling error γ^{-1} according to the the natural frequency ω_0 of the initial reference model is represented on Figure 7.6. To a certain extent, specifying a less performing initial reference model allow to reduce the controller more.

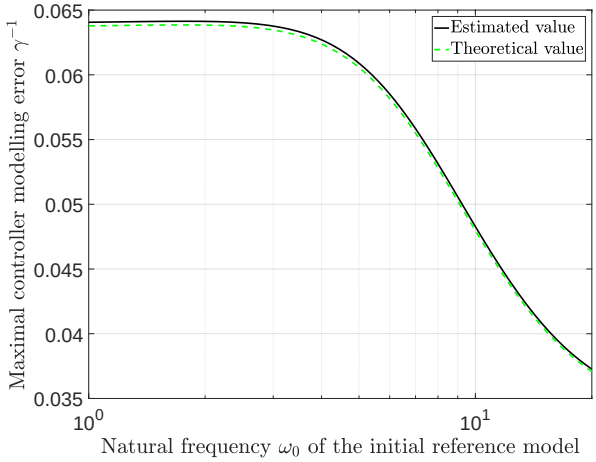

Figure 7.6: Influence of the performance specifications on the reduction of the controller.

The performances in time-domain are visible on Figure7.7. When choosing carefully the performance specifications and ensuring that the reference model is achievable, a 2nd order controller allows to match the desired behaviour.

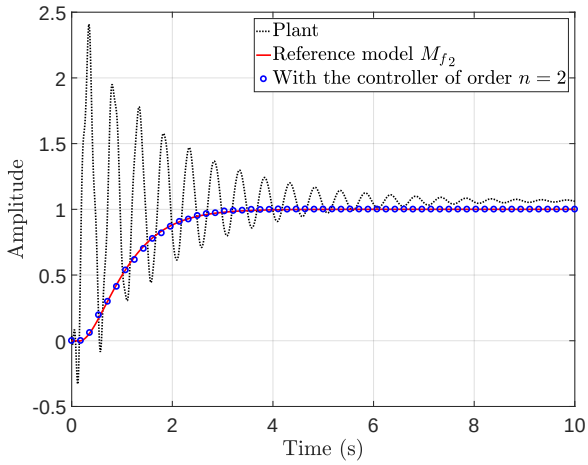

Figure 7.7: Step response of the plant $\mathbf{P}$, the reference model $\mathbf{M}_{f_2}$ and of the closed-loop obtained with the 2nd order controller identified through the Loewner framework.

Remark 7.2.5. Figures 7.4 and 7.5 also highlight that knowing the frequency-response of the plant on a given discrete frequency grid can lead to the underestimation of the $\mathcal{H}_\infty$-norm of the dynamical system $\mathbf{G}$. In the present case, it does not lead to the selection of a destabilizing controller. However, it underlines that the parameter ε in (7.1) can be particularly important to avoid this potential problem.

Application of the subspace approach: conservatism of the proposed stability test and the special case of the integrator

Keeping $\mathbf{M}_{f_2}$ as a reference model, we now use the subspace approach under LMI constraints to identify stable reduced-order controller models. The controller modelling error is then superior to 0.6808, which is bigger than the estimated admissible error $\tilde{\gamma}^{-1} = 0.0665$, for every order between 1 and 10. However, since we know the plant model for this example, it is possible to know that all the controllers identified through the subspace approach, with an order $1 \leq n \leq 10$, stabilize the plant internally.

Remark 7.2.6. It should be noted that the controllers identified through the Loewner framework may contain an integrator. This is why there is no problem when applying this stability test, see Figures 7.4 and 7.5. This is made possible by the $\mathcal{RH}_\infty$-projection of the ideal controller, see Chapter 5.

Remark 7.2.7. In Theorem 7.2.1, it is supposed that the controller modelling error $\mathbf{\Delta}$ is stable. More precisely, according to the small-gain theorem (recalled in Chapter 2), $\mathbf{\Delta}$ should belong to the Hardy space $\mathcal{H}_\infty$ to apply the proposed stability test. Therefore, when the ideal controller contain an integrator, the stability test is supposed to be not applicable. Since we are working in a limited frequency range, defined by the available plant's data, the integrator can be replaced by a stable and very slow pole ($\omega \ll \omega_1$). This is also done in robust control: the frequency weighting functions never contain a pure integrator even if they exhibit a similar behaviour thanks to stable and real slow modes. This is why it is possible to use Theorem 7.2.1 even when the ideal controller contain an integrator.

This case illustrates the conservatism of the proposed stability test. Indeed, Theorem 7.2.1 only ensures that all stable controllers with a modelling error $\|\mathbf{\Delta}\|_\infty < \gamma_0$ stabilize the plant internally. It says nothing about controllers failing the test given in (7.1). However, in order to be less conservative, the small gain theorem could be applied using any other stable and stabilizing controller $\mathbf{K}_0$, if available. The main advantage of relying on the ideal controller $\mathbf{K}^\star$ is that it is known to be stable and stabilizing, but also because it corresponds to a known closed-loop behaviour: the achievable reference model as designed in Chapter 6.

These two aspects are explored in [Van Heusden et al., 2009] to obtain a less conservative stability test: for a given reduced-order controller $\mathbf{K}$, if it is possible to find an achievable reference model $\mathbf{M}$, corresponding to a stabilizing ideal controller $\mathbf{K}^\star$ such that the stability test (7.1) is satisfied, then $\mathbf{K}$ stabilizes the plant internally. The reference model $\mathbf{M}$ is the varying parameter instead of the controller order. However, this less conservative procedure would take much more time in the present case since the test should be run for every reduced-order controller instead of computing once the maximal controller modelling error.

Remark 7.2.8. Using other data-driven stability analysis tools
Whenever the proposed stability test is too conservative, other ways to assess if the resulting closed-loop is stable should be employed. As for the less conservative test of [Van Heusden et al., 2009], it requires however to test the identified controllers one by one. Ab idea could be to use the same stability constraint than [De Bruyne and Kammer, 1999] used in the VRFT approach, see Remark 7.1.1.

Another way to check if a given controller stabilizes the plant internally would be to use the data-driven stability analysis performed by the PISA toolbox and exposed in Chapter 6. Indeed, the choice of a reference model in Chapter 6 ensures that the ideal controller does not cancel any plant's instabilities. The estimation of the plant's instabilities allows to verify easily it is not the case for the considered reduced-order controller $\mathbf{K}$ either. Therefore, as explained in Chapter 2, a stable closed-loop transfer is enough to know that the controller stabilizes the plant internally. First, the frequency-response of the closed-loop $\mathbf{M_K}$ with $\mathbf{K}$ as controller is reconstructed as follows:

$$\forall i = 1 \dots N,\ \mathbf{M_K}(\imath\omega_i) = (I + \Phi_i \mathbf{K}(\imath\omega_i))^{-1} \Phi_i \mathbf{K}(\imath\omega_i).$$

Projecting it on $\mathcal{H}_2$ and $\overline{\mathcal{H}}_2$ is sufficient to determine if the obtained closed-loop is internally stable or not. For example, considering the second-order controller identified though the subspace approach under LMI constraints, the results of the projection are given on Figure 7.8 and shows that the closed-loop-transfer $\mathbf{M_K}$ is stable. Since the controller is stable, it does not compensate the NMP zeros of the plant. Therefore, this controller stabilizes the plant internally.

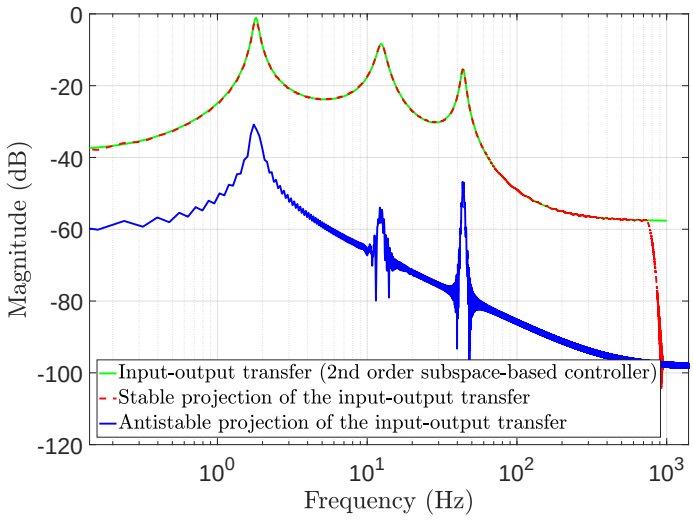

Figure 7.8: Data-driven stability analysis of the closed-loop transfer obtained with the 2nd order controller identified through the subspace approach: the input-output transfer is stable.

Nevertheless, the absence of integrator in the identified controller leads to poor performances. Using the second-order stable controller obtained using the subspace approach under strict LMI constraints, with $\mathbf{M}_{f_2}$ as reference model, gives the step response visible on Figure 7.9: the corresponding static error is equal to 99.7%, which a terrible result. At the same time, the second-order controller obtained through the Loewner framework contains an integrator: there is no tracking error, no overshoot, and the rising time is equal to 2.3s.

In addition, the subspace-based controllers fail the proposed stability test because the ideal controller $\mathbf{K}^\star$ contains an integrator that cannot appear in the subspace-identified controllers because of the LMI constraints. The modelling error is then very important. When relaxing the LMI constraints in the subspace approach, the identified controllers may contain an integrator: the modelling error in this case is given on Figure 7.10. When reducing the controller's model order to $n < 6$, the integrator disappear and the modelling error exceeds the maximal error fixed by the stability test.

A solution consists in enforcing the presence of an integrator in the controller, as it is done in the VRFT approach for this example in [Campi et al., 2002], and also for the original version of the stability test in [Van Heusden et al., 2007]. The ideal closed-loop is then represented on Figure 7.11. The ideal controller is then defined as:

$$\mathbf{K}^\star = \frac{1}{s}\mathbf{K}_2^\star(s). \tag{7.4}$$

The controller identification is then performed on $\mathbf{K}_2^\star$, which frequency-response samples are easily computed from the ones of the ideal controller $\mathbf{K}^\star$. The subspace approach is used to obtain controllers of order $2 \leq n \leq 10$. Once again, they are all rejected by the

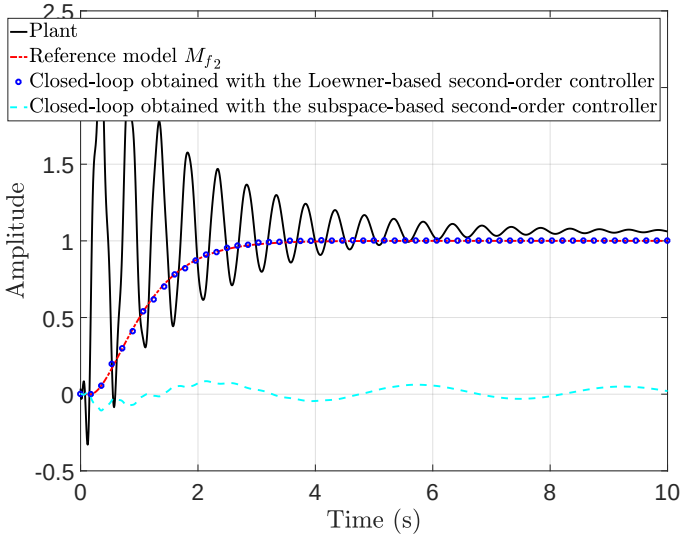

Figure 7.9: Step-response of the closed-loop obtained using the second-order controllers identified through the Loewner framework combined with the $\mathcal{RH}_\infty$-projection and through the subspace approach under LMI constraints. The subspace-based controller does not contain an integrator and leads to poor performances.

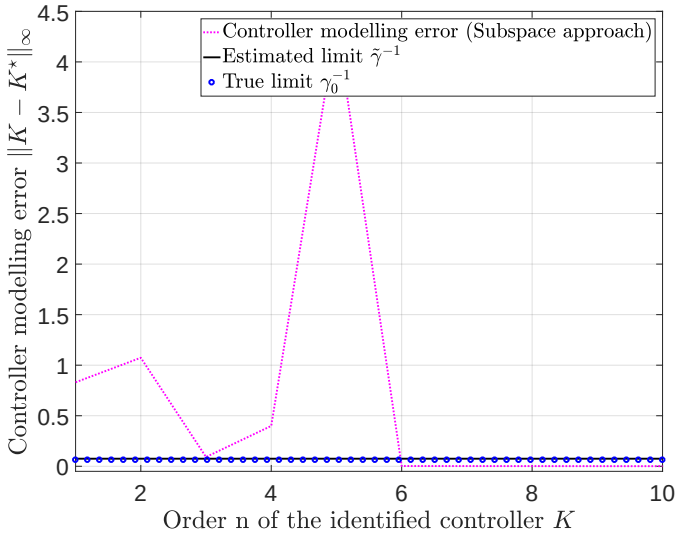

Figure 7.10: Controller reduction using the subspace approach for the flexible transmission benchmark using $\mathbf{M}_{f_2}$ as a reference model.

proposed stability test even though they all stabilize the plant internally. The second-order controller obtained through the subspace approach with an imposed integrator gives the performances visible on Figure 7.12: there is no tracking error, an overshoot of 5.3% and a 5% rising time of 3.8s.

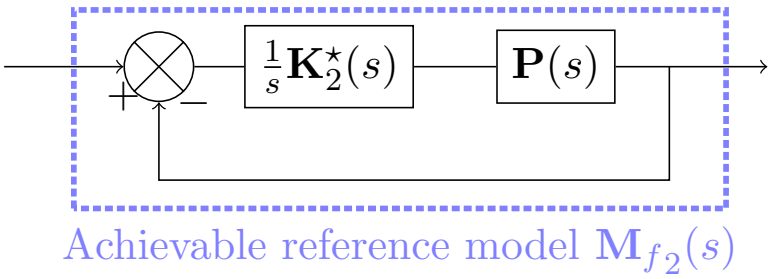

Figure 7.11: Enforcing the presence of an integrator in the controller through the proposed method in the DC motor example.

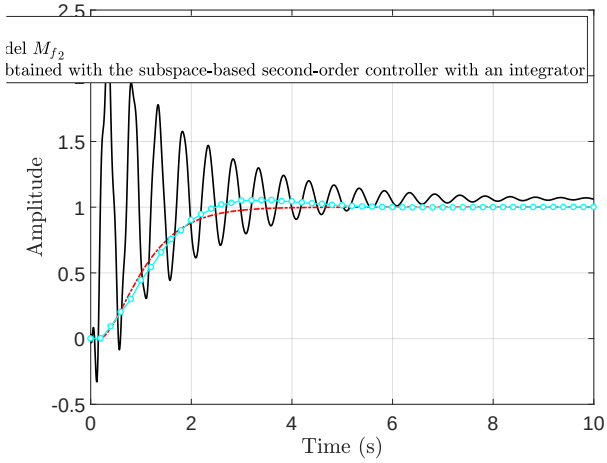

Figure 7.12: Step-response of the closed-loop obtained using the second-order controller with an imposed integrator identified through the subspace.

7.3 Towards data-driven robustness analysis

In the end of Section 7.2, a reduced-order controller $\mathbf{K}$ that stabilizes the plant internally is obtained. Considering the use of the small-gain theorem for data-driven stability enforcement, it is possible to apply the same methodology to determine which system's set is stabilized by the plant internally. To that extent, the work presented in this Section can be seen as a data-driven robustness analysis. However, it should be noted that the word "robustness" is not exact since there is no nominal model available around which a model set is defined. The proposed data-driven robustness analysis is detailed in the following paragraph before being applied to numerical examples.

7.3.1 Data-driven robust stability criteria

As for the analysis of internal stability in Section 7.2, the proposed approach for stability robustness is based on the small-gain theorem. From now on, the plant $\mathbf{P}$ is considered to be subject to uncertainties. The behaviour $\tilde{\mathbf{P}}$ of the system is then given by:

$$\tilde{\mathbf{P}} = \mathbf{P} + \mathbf{\Delta_P}, \tag{7.5}$$

where $\mathbf{\Delta_P}$ represents the plant's uncertainty. The final closed-loop, with a stabilizing reduced-order controller $\mathbf{K}$ obtained in the end of Section 7.2, is written as on Figure

7.13.

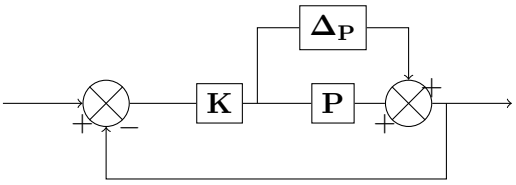

Figure 7.13: Stability robustness analysis scheme.

The small-gain theorem is then applied on this interconnection, giving the following theorem.

Theorem 7.3.1. Suppose that $\mathbf{H} = \mathbf{K}(I + \mathbf{KP})^{-1}$ is stable and let $\beta > 0$. Then the interconnected system shown on Figure 7.13 is well-posed and internally stable for all stable $\mathbf{\Delta_P}$ with:

(a) $\|\mathbf{\Delta_P}\|_\infty \leq \frac{1}{\beta}$ if and only if $\|\mathbf{H}\|_\infty < \beta$

(b) $\|\mathbf{\Delta_P}\|_\infty < \frac{1}{\beta}$ if and only if $\|\mathbf{H}\|_\infty \leq \beta$

Since the reduced-order controller $\mathbf{K}$ stabilizes the plant internally, it is possible to use Theorem 7.3.1 to determine in which bounds the controller stabilizes the plant internally.

As in Section 7.2, since no parametric model of the plant $\mathbf{P}$ is available, the $\mathcal{H}_\infty$-norm of the dynamical system $\mathbf{H}$ should be estimated on the basis of the available samples of its frequency-response:

$$\forall i = 1 \dots N,\ \mathbf{H}(\imath\omega_i) = \mathbf{K}(\imath\omega_i)(I + \mathbf{K}(\imath\omega_i)\mathbf{P}(\imath\omega_i))^{-1}. \tag{7.6}$$

As in Section 7.2, an estimation of $\beta_0 = \|\mathbf{H}\|_\infty$ is obtained through (7.7):

$$\tilde{\beta} = \max_{i=1\dots N} |\mathbf{H}(\imath\omega_i)|\,. \tag{7.7}$$

Then, according to Theorem 7.3.1, the controller $\mathbf{K}$ stabilizes the plant set defined by (7.5) with $\mathbf{\Delta_P} \in \mathcal{H}_\infty$ satisfying the proposed robust stability test:

$$\|\mathbf{\Delta_P}\|_\infty < \tilde{\beta}^{-1} - \varepsilon, \tag{7.8}$$

where ε is a parameter fixed by the user to introduce some conservatism. As in the previous Section, it is used to avoid overestimating the admissible uncertainties when $\tilde{\beta}$ underestimates the $\mathcal{H}_\infty$-norm of $\mathbf{H}$.

7.3.2 Description of the plant's uncertainties

Contrary to the stability criteria exposed in Section 7.2 where the controller modelling error is known to be stable, when analyzing robust stability, there is no guarantee at all that the plant's uncertainty $\mathbf{\Delta_P}$ is stable. Therefore, once the robust stability test given in (7.8) is defined, it is still not possible to represent the set of dynamics stabilized by the controller since $\mathbf{\Delta_P}$ should not only satisfy (7.8) but also be stable.

In traditional robust model-based control, the plant's uncertainties are usually fully described through the uncertain parameters of the system: $\mathbf{\Delta_P}$ is then known to be stable. In this case, the only question left, answered through the application of the small-gain theorem, is to determine in which bounds the uncertain parameters may vary without destabilizing the closed-loop. In the present case, since no plant model is available, no uncertain parameters can be used to build the $\mathbf{\Delta_P}$-block. Therefore, in a data-driven framework, the proposed robust stability test only constitutes an indicator of the robustness of the obtained controller.

In some cases, the proposed robust stability test may be too conservative. This is partly due to the choice of the type of uncertainty. Since the considered uncertainty is additive, see (7.5), (7.8) confines the plant's behaviour $\tilde{\mathbf{P}}$ to a disk centered at $\mathbf{P}(\imath\omega_i)$ and of radius $\tilde{\beta} - \varepsilon$. In practice, the uncertainty is more important in a high-frequency range. To that extent, it may be interesting to use weighting functions to characterize the frequency-domain behaviour of the uncertainty, see (7.9).

$$\tilde{\mathbf{P}} = \mathbf{P} + \mathbf{W}_1\mathbf{\Delta}\mathbf{W}_2,\ \mathbf{\Delta} \in \mathcal{H}_\infty,\ \|\mathbf{\Delta}\|_\infty < 1, \tag{7.9}$$

where $\mathbf{W}_1$ and $\mathbf{W}_2$ determines the neighborhood of the nominal model $\mathbf{P}$ which contains $\tilde{\mathbf{P}}$. As said earlier, in the proposed method, the notion of nominal model is replaced by a nominal frequency-response of the plant, which is the available data from the system.

When using (7.9) as model set, the application of the small-gain theorem gives us that the closed-loop is well-posed and internally stable for all $\mathbf{\Delta} \in \mathcal{RH}_\infty$ such that $\|\mathbf{\Delta}\|_\infty < 1$ if and only if $\|\mathbf{W}_2\mathbf{H}\mathbf{W}_1\|_\infty \leq 1$

Remark 7.3.1. It should be noted that other descriptions of the plant's uncertainties may be used, such as the multiplicative form for example:

$$\tilde{\mathbf{P}} = (I + \mathbf{W}_1\mathbf{\Delta}\mathbf{W}_2)\,\mathbf{P}. \tag{7.10}$$

Many possible definitions of plant's uncertainties are proposed in [Zhou and Doyle, 1998] and the associated robust stability tests are exposed.

7.3.3 Application to numerical examples

DC motor example

In this example, considering the first order controller identified through the Loewner framework when using $\mathbf{M}_2$ as reference model, (7.7) gives $\tilde{\beta} = 9.9236$ while the true value is $\beta_0 = 10.0099$. The corresponding set of models is represented on the complex plane on Figure 7.14. This representation do not imply that all the plant's behaviour in this set are stabilized by the controller since the stability of $\mathbf{\Delta}$ is not ensured.

The main interest of the proposed robustness analysis is, in the present case, to better understand the performance-robustness tradeoff, well known in robust control. To that extent, the estimated uncertainty bound is computed for the first-order controllers identified through the Loewner framework for different reference models. The natural frequency ω_0 of the reference model varies (the damping factor is still $\xi = 1$ and the static gain $k = 1$). As shown on Figure 7.15, specifying a slower dynamics by decreasing

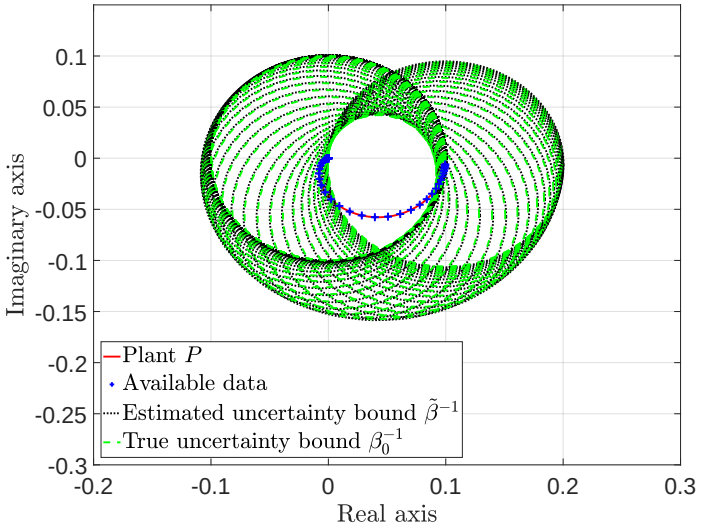

Figure 7.14: Robust stability analysis on the DC motor example: the circles represent the plant's behaviours $\tilde{\mathbf{P}}$ such that the plant's uncertainty $\mathbf{\Delta}$ satisfy (7.8).

the natural frequency ω_0 of the reference model allows to obtain a more robust closed-loop.

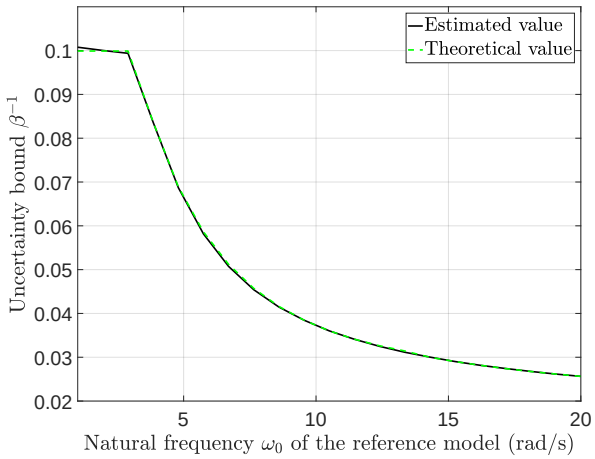

Figure 7.15: Illustration of the performance-robustness compromise: the faster the specifications are, the lower the uncertainty bound gets. The bound is computed using the first-order controller identified through the Loewner framework for every considered reference model.

Flexible transmission benchmark

Considering the second-order controller identified through the Loewner framework when using $\mathbf{M}_{f_2}$ as reference model, (7.7) gives $\tilde{\beta} = 0.7338$, which underestimates the true value $\beta_0 = 0.9400$ occurring at $1.5484 \times 10^{-7}\text{rad.s}^{-1}$. As for the DC motor example, the model set corresponding to uncertainties such that (7.8) is satisfied is represented on Figure 7.16.

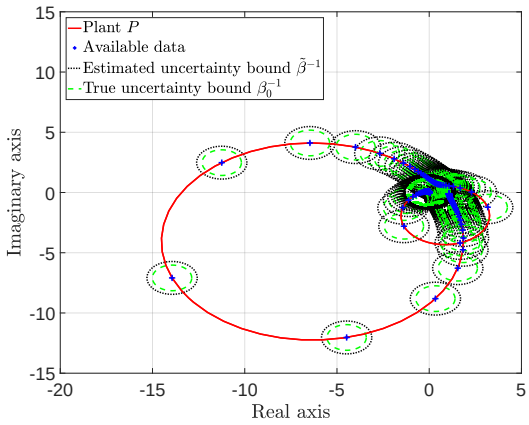

Figure 7.16: Robust stability analysis on the flexible transmission benchmark: the circles represent the plant's behaviours $\tilde{\mathbf{P}}$ such that the plant's uncertainty $\mathbf{\Delta}$ satisfy (7.8).

As for the DC motor example, specifying a slower closed-loop behaviour in the initial reference model allow to improve the robustness of the resulting closed-loop, see Figure 7.17. However, in the present example, the robustness is highly overestimated for low values of ω_0.

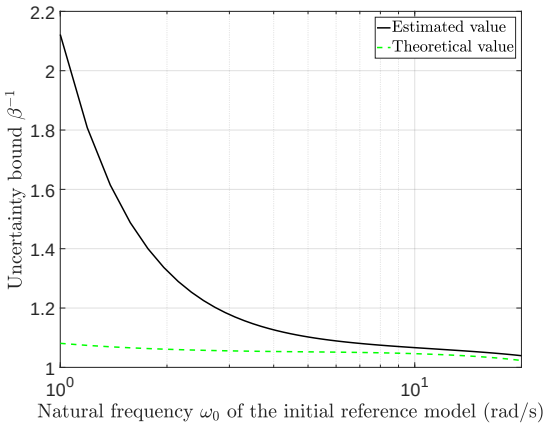

Figure 7.17: Illustration of the performance-robustness compromise: the faster the specifications are, the lower the uncertainty bound gets. The bound is computed using the first-order controller identified through the Loewner framework for every considered reference model.

Summary

In this Chapter, the data-driven stability test introduced in [Van Heusden et al., 2007] for controller validation is recalled. A similar test is proposed, based on the small-gain theorem, and used to limit the controller reduction step: as long as the stability test is verified, the reduced-order controller will preserve internal stability. The main drawback of the approach proposed in this Chapter is that the quality of the data influences a lot the stability criteria and it may lead to the selection of destabilizing controllers.

The application of this stability test on the DC motor example and the flexible transmission benchmark show good results when identifying and reducing controllers through the Loewner framework. However, the application of the subspace approach on the flexible transmission benchmark highlights the conservatism of this test. In the proposed numerical example, since the plant model is known, it is possible to check that the controllers rejected by the proposed stability test stabilizes the plant internally. It is also possible to get this result using the projection technique described in Chapter 6. The flexible transmission example also shows that the closed-loop performances may be improved significantly by enforcing the presence of an integrator in the controller.

In the end, some preliminary work extends the proposed stability considerations with a data-driven robustness analysis. It is deri ved from the small-gain theorem. This step only aims at furnishing a robustness indicator. When applied on the proposed numerical examples, it highlights the performance-robustness trade-off: specifying a less performing reference model may lead to a more robust closed-loop.

Chapter 8

Application to irrational systems

The objective of this Chapter is to illustrate the complete proposed method (Chapters 4 to 7) on industrial examples. Indeed, considering the simple numerical examples developed earlier in this work, for which using a model-based control technique is actually more indicated because of the simplicity of the considered models. On the contrary, the two applications presented in this chapter are representative of the category of systems for which using a data-driven control technique. The first one is a continuous crystallizer, see Section 8.1, and the second one is an open-channel for hydroelectricity generation, see Section 8.2. Both systems are described by Partial Differential Equations (PDE), resulting in irrational transfer functionss.

Contents

8.1 Application to a continuous crystallizer

8.1.1 Presentation of the system

The first considered application is the control of a continuous cooling crystallizer. This process is widely used in the chemical industry. It is a separation process which goal is to produce high-purity solids from liquids. The system is SISO: its input is the solute feed concentration $c_f(t)$ and its output is the solute concentration in the crystallizer $c(t)$. The state of the system is $\mathbf{x}(t) = [n(L,t)\ c(t)]^T$, where $n(L,t)$ denotes the crystal size distribution. Physically, this system is described by population and mass balance

equations. A complete mathematical model of this system is derived in [Rachah et al., 2016].

The objective is to stabilize the plant around a desired steady-state $c(t) = c_{ss} = 4.09mol/L$, which is just above the saturation concentration $c_s = 4.038mol/L$, required for the crystals to be produced. For this steady state, as said in [Vollmer and Raisch, 2001], the system is unstable and presents sustained oscillations which may degrade the crystals quality. Feedback control is therefore needed. This control problem has been treated in [Vollmer and Raisch, 2001] through infinite-dimensional $\mathcal{H}_\infty$ synthesis, which is model-based, and in [Apkarian and Noll, 2018] thanks to a data-driven $\mathcal{H}_\infty$ synthesis.

When linearizing the system's partial differential equations around the desired steady state, the crystallizer is characterized by an irrational transfer with an infinite number of poles, see [Vollmer and Raisch, 2001], [Rachah et al., 2016] or [Apkarian and Noll, 2018] for its expression. It is possible to evaluate numerically the frequency response of the linearized plant $\mathbf{P}$ on a discrete frequency grid, see Figure 8.1. In [Apkarian and Noll, 2018], a rational model $\mathbf{P}_{502}$ of order 502 is obtained through a finite-difference method (see Figure 8.1) to obtain an initial stabilizing controller. The poles and zeros of $\mathbf{P}_{502}$ are given on Figure 8.2: the rational model is minimum phase and two unstable poles of value $3.83 \times 10^{-5} \pm 0.848 \times 10^{-2}\imath$ are visible. In the present work, the model $\mathbf{P}_{502}$ will only be used as a comparison for the data-driven estimation of tha system's instabilities and to simulate the closed-loop dynamics with the different controllers identified along this section.

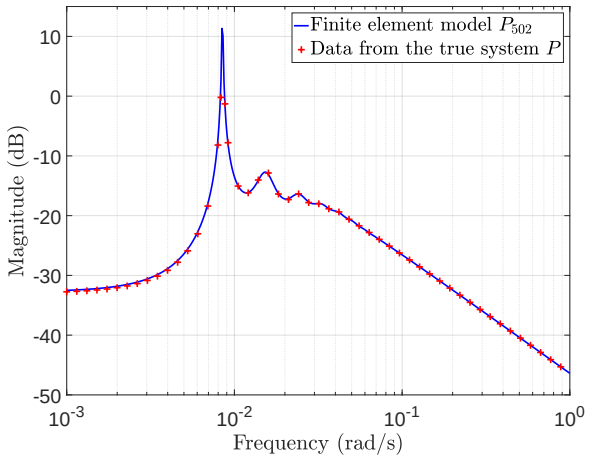

Figure 8.1: Evaluation of the frequency-response of the linearized plant $\mathbf{P}$ on a discrete frequency grid (500 linspaced frequencies between 0.001 and 1 rad.s^{-1}) and frequency response of the finite difference rational model $\mathbf{P}_{502}$.

8.1.2 Selection of an achievable reference model

In order to use the proposed method to select an achievable reference model as proposed in Chapter 6, the considered frequency grid is much smaller: $N = 500$ frequencies are considered, logarithmically spaced between 10^{-3} and 1 rad.s^{-1}. The corresponding sam-

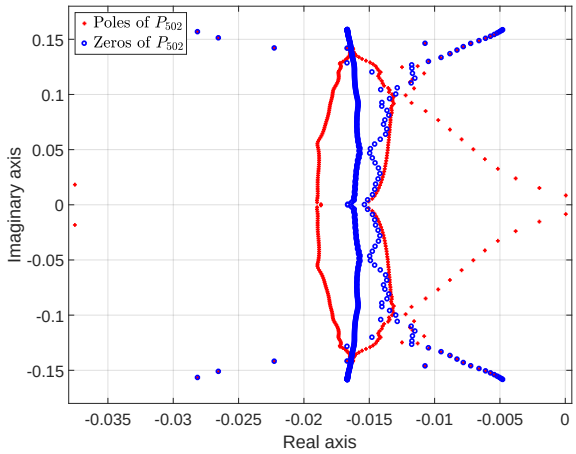

Figure 8.2: Poles and zeros of the rational model $\mathbf{P}_{502}$

ples of the frequency response of the plant are estimated directly through the irrational transfer.

The first step in choosing an achievable reference model consists in the projection of the FRF on the spaces $\mathcal{H}_2$ and $\overline{\mathcal{H}}_2$. The projection is given on Figure 8.3: the antistable projection fits the resonance while the stable part fits the rest of the frequency-response of the plant. Therefore the plant is unstable, as expected considering $\mathbf{P}_{502}$ but also the previous studies of this system given in [Vollmer and Raisch, 2001], [Rachah et al., 2016] and [Apkarian and Noll, 2018].

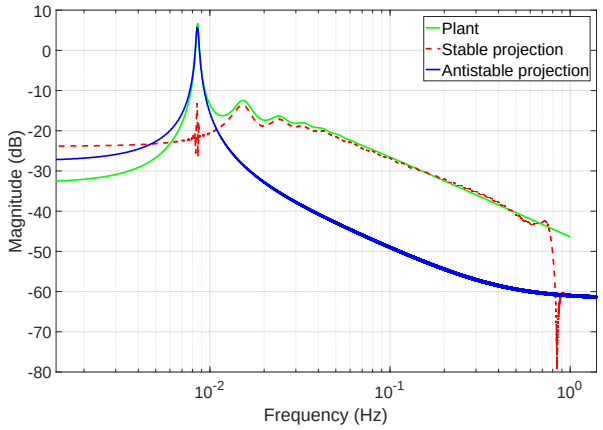

Figure 8.3: Projection of the frequency-response samples from the plant $\mathbf{P}$ on the Hardy spaces $\mathcal{H}_2$ and $\overline{\mathcal{H}}_2$: the system is unstable.

As detailed in [Cooman et al., 2018a], the Hankel matrix of the antistable projection of the plant's data is computed and a singular value decomposition is performed. The rank of this matrix gives us the order of the antistable projection, and consequently

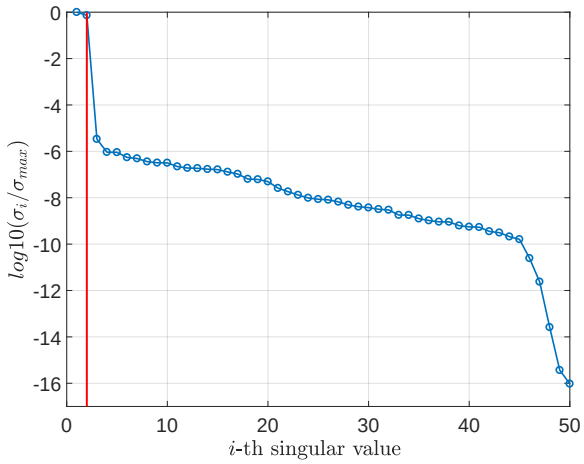

Figure 8.4: Singular Value Decomposition of the Hankel matrix corresponding to the antistable projection of the plant's data: the system exhibits two RHP poles.

the number of RHP poles of the system $\mathbf{P}$. The decomposition is visible on Figure 8.4: according to the drop after the second singular value, the system exhibits two unstable poles. These two RHP poles are then estimated. Their value is given in Table 8.1. The obtained values are coherent with the ones found in [Vollmer and Raisch, 2001] and with the RHP poles of the rational model $\mathbf{P}_{502}$.

RHP poles of $\mathbf{P}_{502}$	$3.83 \times 10^{-5} \pm 0.848 \times 10^{-2}\imath$
Estimated RHP poles	$1.07 \times 10^{-4} \pm 0.852 \times 10^{-2}\imath$
Estimated RHP poles in [Vollmer and Raisch, 2001]	$0.99 \times 10^{-4} \pm 0.89 \times 10^{-2}\imath$

Table 8.1: Estimation of the RHP poles of the plant.

Remark 8.1.1. In [Vollmer and Raisch, 2001], the RHP poles are estimated through a direct search method. This estimation is then used to factorize the plant's expression to solve the mixed-sensitivity problem in the infinite-dimensional case.

Then, the inverse plant's data is analyzed in order to determine whether the plant is minimum phase or not. The projection is then performed on the samples $\left\{\omega_i, \mathbf{P}(\imath\omega_i)^{-1}\right\}$. The result is visible on Figure 8.5: the stable projection of the plant's inverse fits the inverse of the plant's frequency-response samples. Consequently, the plant is minimum phase.

Finally, an achievable reference model is selected as in Chapter 6. The initial stable reference model $\mathbf{M}$ is a first order transfer function:

$$\mathbf{M}(s) = \frac{1}{1+\tau s}, \ \tau = 1s.$$

Since the plant is unstable and minimum-phase, the achievable reference model is chosen as $\mathbf{M}_f = 1 - (1 - \mathbf{M})\mathbf{B}_p$, with $\mathbf{B}_p$ defined according to the estimated RHP poles of the plant, see Table 8.1.

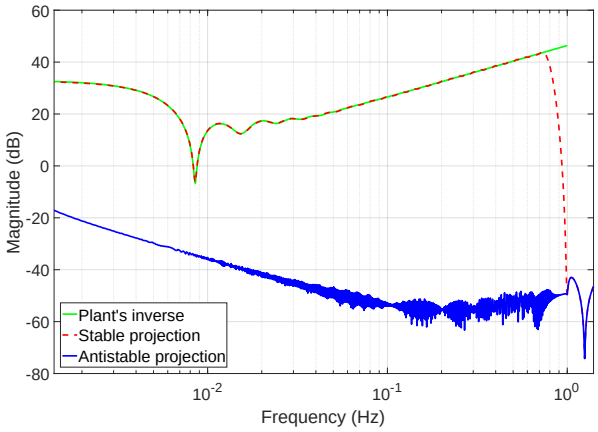

Figure 8.5: Projection of the inverse of the frequency-response samples from the plant $\mathbf{P}$ on the Hardy spaces $\mathcal{H}_2$ and $\overline{\mathcal{H}}_2$: the system is minimum phase.

8.1.3 Control design

Controller identification

In the first place, the achievable reference model designed in the previous paragraph is used to compute the frequency-response of the ideal controller, visible on Figure 8.6. The resulting ideal controller is then interpolated using the Loewner framework: a minimal realisation of order $n = 177$ is obtained. The controller is then reduced to a second-order model $\mathbf{K}_2$:

$$\mathbf{K}_2(s) = \frac{39.084(s^2 + 0.04163s + 0.003132)}{s(s + 0.002751)}. \tag{8.1}$$

The reduced order $r = 2$ is selected in order order to compare the controller obtained with the proposed method with the one obtained in [Apkarian and Noll, 2018], denoted $\mathbf{K}$:

$$\mathbf{K}(s) = \frac{54.47s^2 + 2.317s + 0.02446}{s^2 + 0.002033s + 4.374e - 6}. \tag{8.2}$$

The frequency response of these controllers is visible on Figure 8.6.

Stability analysis

Following the stability test proposed in Chapter 7, the maximal admissible controller error is $\tilde{\gamma}^{-1} = 54.2547$, which largely overestimates $\gamma_0^{-1} = 18.8520$, obtained using the finite-difference model $\mathbf{P}_{502}$. On the other side, the evolution of the controller modelling error is visible on Figure 8.7. The controller modelling error for $\mathbf{K}_2$ is $\|\mathbf{\Delta}\|_\infty = \|\mathbf{K}_2 - \mathbf{K}^\star\|_\infty \simeq 2.1219e+03$. According to Figure 8.7, it is possible to preserve internal stability when reducing the controller up to an order $r = 7$.

The stability test is not verified for $\mathbf{K}_2$ but, as shown in the previous chapter, this test is conservative. In order to check this possibility, the data of the resulting closed-loop $\mathbf{M}_{\mathbf{K}2}$ is projected using the PISA toolbox. The frequency-response samples of the

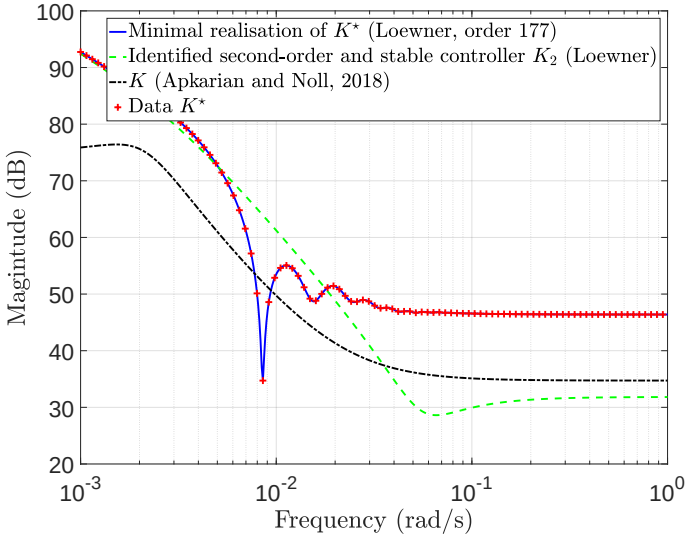

Figure 8.6: Identification of the controller using the Loewner framework: the minimal realization of the ideal controller has 177 states. It is reduced to a second-order controller $\mathbf{K}_2$, see (8.1).

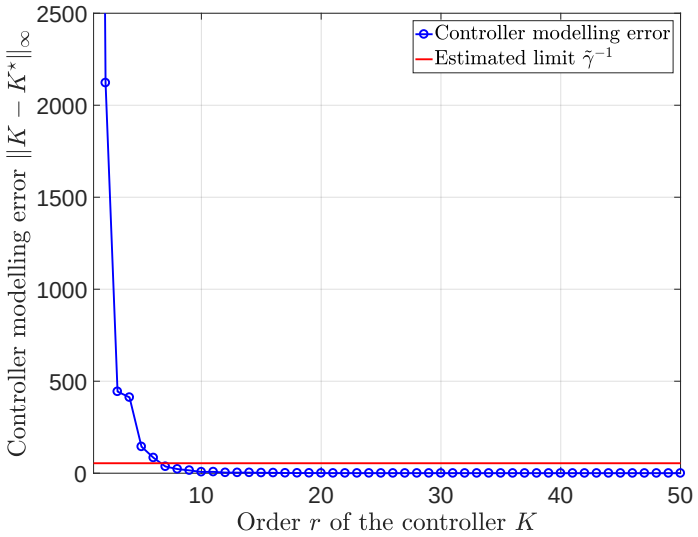

Figure 8.7: Evolution of the controller modelling error when reducing the order of the controller model using the Loewner framework.

resulting closed-loop are computed as follows:

$$\forall i = 1 \dots N,\ \mathbf{M}_{\mathbf{K2}}(\imath\omega_i) = (I + \Phi_i \mathbf{K}_2(\imath\omega_i))^{-1} \Phi_i \mathbf{K}_2(\imath\omega_i).$$

The results of the projection are visible on Figure 8.8: the antistable projection does not contribute to the dynamic of $\mathbf{M}_{K2}$. Therefore, $\mathbf{K}_2$ stabilizes the plant $\mathbf{P}$ internally.

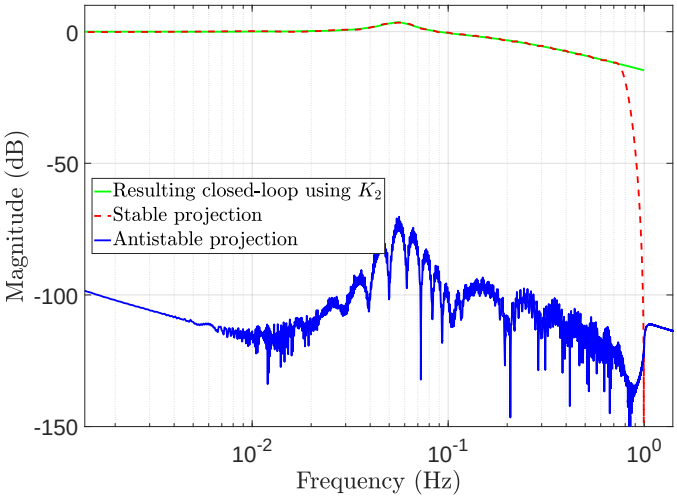

Figure 8.8: Projection of the frequency-response of the resulting closed-loop $\mathbf{M}_{\mathbf{K}2}$: $\mathbf{K}_2$ stabilizes the plant $\mathbf{P}$ internally.

8.1.4 Results

In order to evaluate closed-loop performances, the finite-difference model is then used to simulate the closed-loop behaviour in time-domain. The results are visible on Figure 8.9. The controller obtained in [Apkarian and Noll, 2018] allows to reach the desired steady-state faster with a less important overshoot. These better performances might be explained by two reasons: (i) model-reference control is really limitating when it comes to the expression of the closed-loop specifications and (ii) the reduction of the ideal controller degrades the closed-loop control performances.

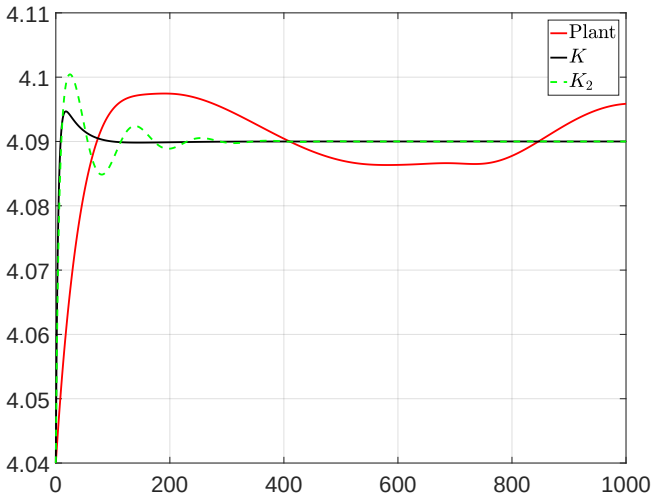

Figure 8.9: Simulation of the passage to a new steady state for the closed-loops built with the second-order controller $\mathbf{K}_2$ obtained by the proposed algorithm and $\mathbf{K}$, the one obtained in [Apkarian and Noll, 2018].

Influence of the controller reduction

First, let us investigate (i) the influence of the reduction of the ideal controller on the closed-loop control performances. To that extant, controllers of order 3 and 5 are obtained through the Loewner framework, respectively denoted $\mathbf{K}_3$ and $\mathbf{K}_5$:

$$\mathbf{K}_3(s)=\frac{92.763(s+0.1574)(s^2+0.0001243s+8.263\times10^{-5})}{s(s^2+0.008329s+2.71\times10^{-5})},$$

$$\mathbf{K}_5(s)=\frac{-7.7499(s-3.444\times10^{5})(s^2+0.001032s+7.226\times10^{-5})(s^2+0.0374s+0.000532)}{s(s+1.328e04)(s+0.004241)(s^2+0.006436s+4.093\times10^{-5})}. \tag{8.3}$$

As shown on Figure 8.10, the more the order of the identified controller is important, the more it will fit the frequency-response of the ideal controller. This is also visible on the time-domain simulations given on Figure 8.11, when simulating the passage to a new steady-state. A high order controller is more likely to give the desired closed-loop behaviour, specified by the reference model $\mathbf{M}_f$.

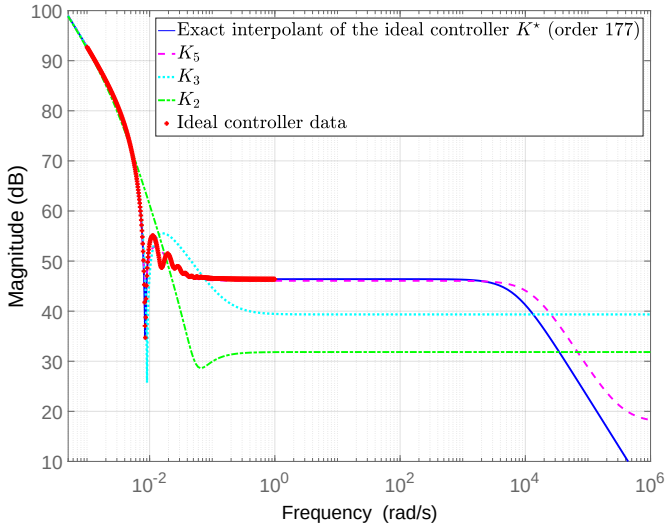

Figure 8.10: Reduction of the ideal controller to different orders (2, 3 and 5). The corresponding controllers are denoted $\mathbf{K}_2$, $\mathbf{K}_3$ and $\mathbf{K}_5$ respectively.

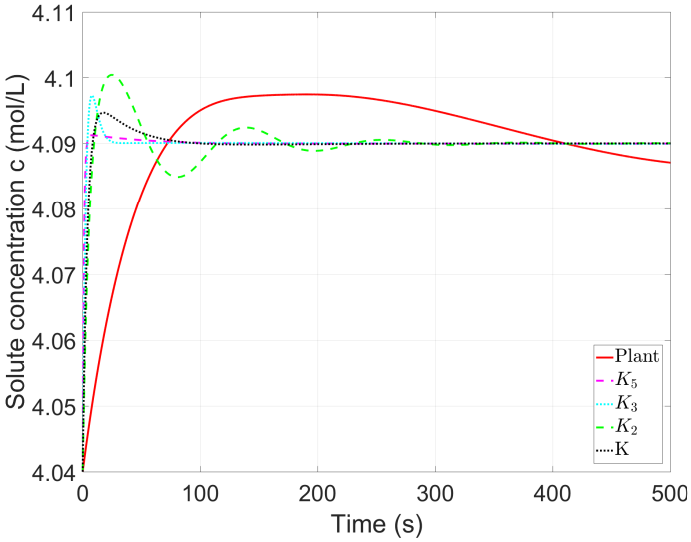

Figure 8.11: Simulation of the passage to a new steady state for the closed-loops built with the controllers $\mathbf{K}_2$, $\mathbf{K}_3$ and $\mathbf{K}_5$, of order to 2, 3 and 5 respectively, identified and reduce through the Loewner framework. They are compared to the controller $\mathbf{K}$ obtained in [Apkarian and Noll, 2018], see (8.2).

Influence of the initial reference model

Finally, let us investigate (ii) the influence of the performance specifications. In [Apkarian and Noll, 2018], the specifications are given as frequency weightings functions, giving more freedom to the desired closed-loop behaviour. To underline this aspect, the closed-loop $\mathbf{M}_2$ reached by the controller $\mathbf{K}$ obtained is [Apkarian and Noll, 2018] is taken as reference model. $\mathbf{M}_2$ has been computed using the finite-difference model $\mathbf{P}_{502}$. It leads to the identification of the second-order controller $\mathbf{K}_{\mathbf{M}_2}$:

$$\mathbf{K}_{\mathbf{M}_2}(s) = \frac{28.282(s+0.08652)(s+0.00982)}{(s^2+0.001967s+4.192e-06)}. \tag{8.4}$$

$\mathbf{K}_{\mathbf{M}_2}$ gives a better response time and a more important overshoot than $\mathbf{K}$. However, the closed-loop performances induced by $\mathbf{K}_{\mathbf{M}_2}$ are much closer to the ones obtained by $\mathbf{K}$ than the ones obtained using $\mathbf{M}_f$ as a reference model.

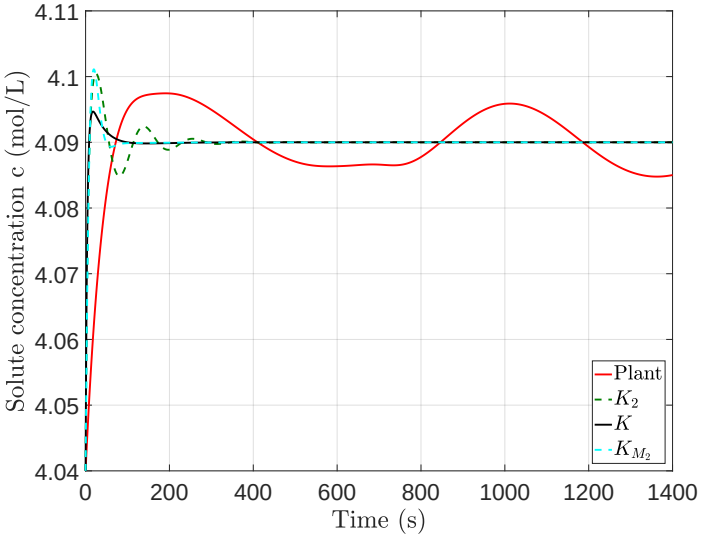

Figure 8.12: Simulation of the passage to a new steady state for the closed-loops built with the controllers $\mathbf{K}_2$ and $\mathbf{K}_{\mathbf{M}2}$ obtained by the proposed method using two different reference models $\mathbf{M}_f$ and $\mathbf{M}_2$, and with the controller $\mathbf{K}$ obtained in [Apkarian and Noll, 2018].

To sum up, the first important aspect in order to obtain good closed-loop performances is the reduction of the ideal controller. The second one is that, for a given controller order, the choice of the reference model remains a critical step: choosing one desired transfer, even achievable, is limiting compared to robust specifications using frequency weightings.

To compare with a model-based method, in [Vollmer and Raisch, 2001], an infinite-dimensional model-based $\mathcal{H}_\infty$ controller synthesis is performed on this very same application. The obtained controller is irrational and a reduction step is needed, which can be quite complicated. On this use-case, a reduced 8th order controller is obtained in [Vollmer and Raisch, 2001]. On the other side, applying a structured model-based technique such as hinfstruct relies on an approximation of the irrational system, here the finite-difference model $\mathbf{P}_{502}$, and is therefore time-consuming due to the complexity of the model.

For these reasons, data-driven control techniques are particularly indicated in this case. In [Apkarian and Noll, 2018], the considerations regarding the limitations due to the RHP poles and zeros of the plant are known through an initial stabilizing controller. Stability is guaranteed by the algorithm thanks to a test on the winding number. However, this method requires to build a fine frequency grid on which samples of the frequency-response of the plant are assumed to be available. Furthermore, the control design relies on iterative non-smooth optimization, which can be time-consuming and is sensitive to the considered initial stabilizing controller.

On the other side, the main strength of the proposed method is its simplicity. It is

a one shot technique, it does not make strong assumptions and does not depend on an initial stabilizing controller.

8.2 Application to an hydroelectricity generation channel

8.2.1 Presentation of the system

The second application is an industrial problem provided by the French power producer EDF (Electricité de France). EDF uses water resources to generate green energy with run-of-the-river power plants. They rely on open-channel hydraulic systems that are non-linear and which dynamic depends on the operating point. Here, for simplicity we will consider one single operating point only.

Their physical model requires partial differential equations (namely Saint-Venant equations). In [Dalmas et al., 2016], a new irrational transfer function is proposed for open channels to represent the level-to-flow variations for any operating point. It is the solution of Saint-Venant equations under many assumptions. The system has two inputs, the entering and the outgoing flows q_e and q_s, and one output, the water depth h. The transfer is given by:

$$\begin{aligned} h(x,s,Q_0) &= G_e(x,s,Q_0)q_e(s) + G_s(x,s,Q_0)q_s(s) \\ &= P(x,s,Q_0)\begin{bmatrix} q_e \\ q_s \end{bmatrix} \end{aligned} , \tag{8.5}$$

where

$$G_e(x,s,Q_0)=\frac{\lambda_1(s)e^{\lambda_2(s)L+\lambda_1(s)x} - \lambda_2(s)e^{\lambda_1(s)L+\lambda_2(s)x}}{B_0 s(e^{\lambda_1(s)L} - e^{\lambda_2(s)L})}$$
$$G_s(x,s,Q_0)=\frac{\lambda_1(s)e^{\lambda_1(s)x} - \lambda_2(s)e^{\lambda_2(s)x}}{B_0 s(e^{\lambda_1(s)L} - e^{\lambda_2(s)L})}$$

where x is the position of the measurement point on the channel, Q_0 the nominal flow, L the length of the open channel. B_0, $\lambda_1(s)$ and $\lambda_2(s)$ depend on the canal configuration and the nominal flow (see [Dalmas et al., 2016]).

The system, which dynamic is visible in Figure 8.13, is extremely slow, has a delay behavior and a pole in limit of stability. Moreover, it has an infinite number of poles since the transfer function is irrational.

The system have been approximated in [Dalmas et al., 2016] by a 8th order rational transfer function depending on the nominal flow with input time delays: $\tau_e \simeq 500s$ and $\tau_s \simeq 1500s$, on q_e and q_s respectively. This approximation is shown in Figure 8.13 (dashed red). This model will be used to evaluate the performances of the identified controller.

The input flow q_e in the open channel is seen as a disturbance (rain for example). The objective is to maintain the water depth to avoid flooding in the area. To this aim, the command signal is the output flow q_s. Therefore, only the transfer G_s between the output flow q_s and the water depth h is considered, see (8.5).

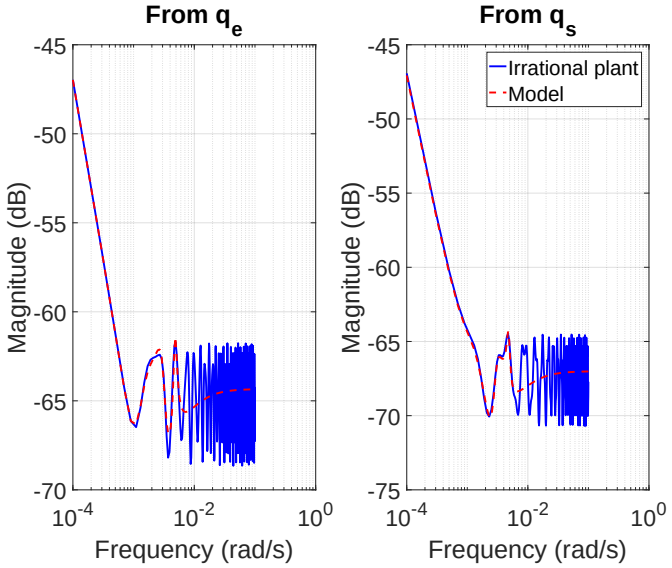

Figure 8.13: System dynamic for nominal flow $Q_0 = 1400\ m^3.s^{-1}$: original plant in solid blue and approximation obtained in [Dalmas et al., 2016] in dashed red.

In this example, the frequency approach is interesting since the system is represented by an irrational transfer function. Therefore, one cannot have a time-domain simulation. However we still can estimate samples of the frequency response of the system $\{\omega_i, \Phi_i\}_{i=1}^N$, from which the ideal controller's frequency response can be deduced. The samples of the frequency response $\Phi_i = G_s(\imath\omega_i),\ i = 1 \dots N$ are extracted from the irrational transfer function G_s, for $N = 500$ linearly spaced frequencies between 10^{-4} and 10^{-1} rad.s^{-1}.

8.2.2 Selection of an achievable reference model

As for the previous application, the first step of the proposed method consist in determining the nature of the system thanks to the projection of its frequency-response measurements. The results of the projection are visible on Figures 8.14 and 8.15 respectively.

Due to the presence of an integrator, the plant's FRF is not in $\mathcal{L}_2$. The data is then filtered by a bandpass filter for the stability analysis, see [Cooman et al., 2018b] for further explanations. Figure 8.14 shows that, except the integrator, the plant has no unstable poles. The mismatch between the projection and the plant's data is due to the use of the bandpass filter. According to Figure 8.15, the plant is minimum phase: the stable projection fits the inverse of the plant's data.

Therefore, the only constraint that the reference model should satisfy is $\mathbf{M}(0) = 1$, which would have been respected anyway to have zero tracking error. The objective is to stabilize the system and to obtain a faster dynamic. The reference closed-loop $\mathbf{M}$ is chosen to be a second order continuous transfer function:

$$\mathbf{M}(s) = \frac{1}{1 + \frac{2\xi}{\omega_0}s + \frac{s^2}{\omega_0^2}}, \tag{8.6}$$

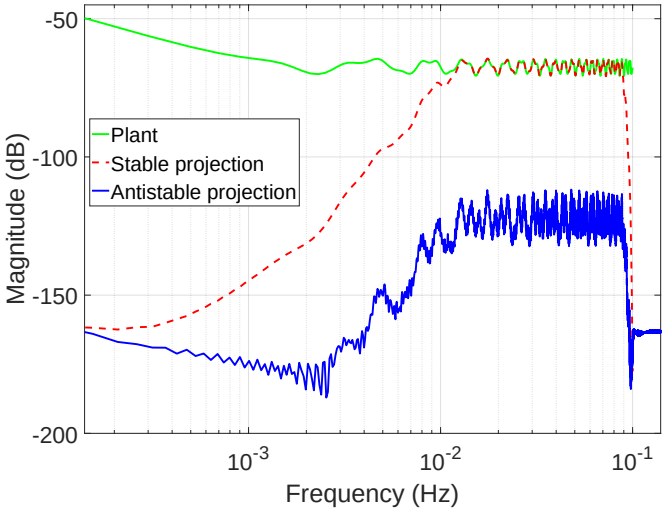

Figure 8.14: Projection of the plant's data: the only instability is the integrator.

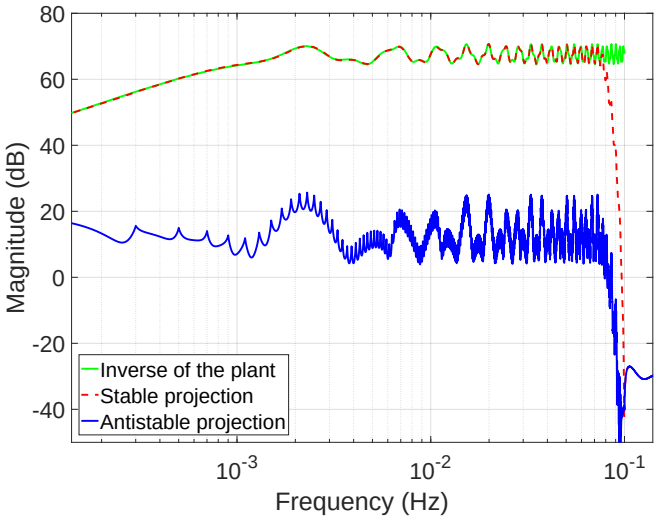

Figure 8.15: Projection of the inverse of the plant's data: the system is minimum phase.

with $\omega_0 = 10^{-4} rad.s^{-1}$ and $\xi = 1$. It satisfies $\mathbf{M}(0) = 1$.

The frequency response of the ideal controller $\mathbf{K}^\star(\imath\omega_i)$, which exactly provides the desired closed-loop behavior dictated by $\mathbf{M}$ when placed in the closed-loop, is obtained as follows:

$$\forall i = 1 \dots N,\ \mathbf{K} \star (\imath\omega_i) = \frac{\mathbf{M}(\imath\omega_i)}{\Phi_i - \mathbf{M}(\imath\omega_i)\Phi_i}. \tag{8.7}$$

8.2.3 Control design

The result of the identification step is given in Figure 8.18. The minimal realisation of the ideal controller is of order 137 and is stable. In the first place, it is necessary to obtain a reduced-order controller that preserves closed-loop internal stability.

Following the stability test proposed in Chapter 7, the maximal admissible controller error is $\tilde{\gamma}^{-1} = 220.9667$, which largely overestimates $\gamma_0^{-1} = 11.3224$, obtained using the rational 8th-order model visible on Figure 8.13. On the other side, the evolution of the controller modelling error is visible on Figure 8.16: it is possible to preserve internal stability when reducing the controller up to an order $r = 1$.

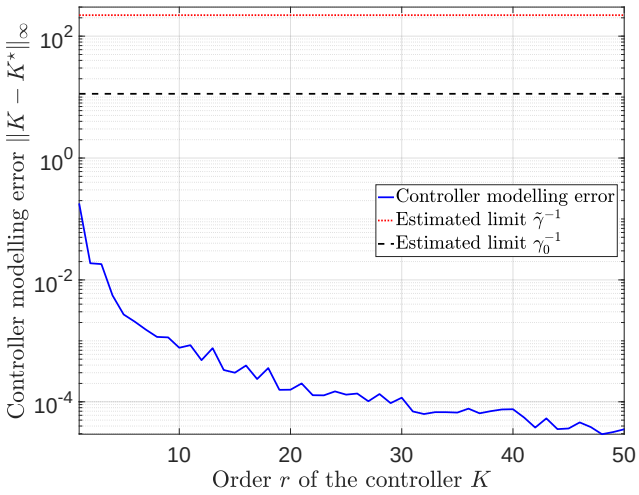

Figure 8.16: Evolution of the controller modelling error when reducing the order of the controller model using the Loewner framework.

The SVD of the Loewner matrix in the present case is given on Figure 8.17: there is only one significant drop around the McMillan order $n = 137$ which gives the minimal realisation of the ideal controller. However, the first singular values decrease fast before reaching. Therefore, a small order controller should be sufficient to reach the desired performances. The minimal representation of the ideal controller is then reduced to a stable second order controller $\mathbf{K}$:

$$\mathbf{K}(s) = \frac{3.3492.10^{-5}(s^2 - 0.0663s + 0.007729)}{(s + 2.001e - 05)(s + 0.001161)}.$$

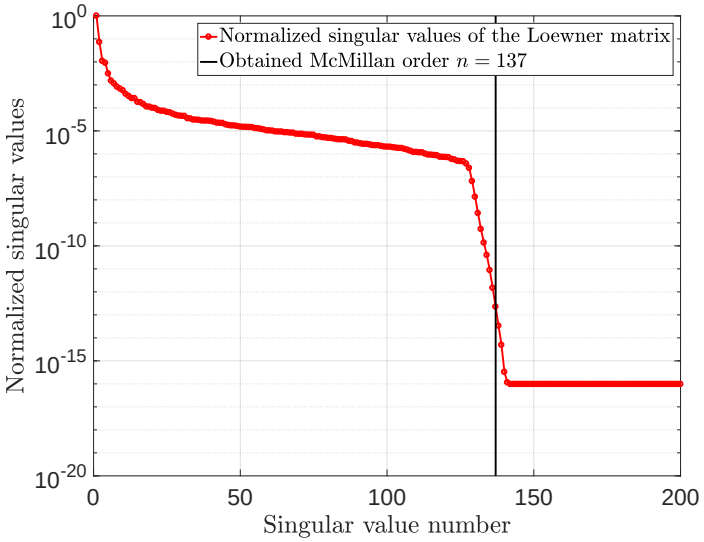

Figure 8.17: Singular value decomposition of the Loewner matrix considering the data of the ideal controller $\mathbf{K}^\star$ given in (8.7).

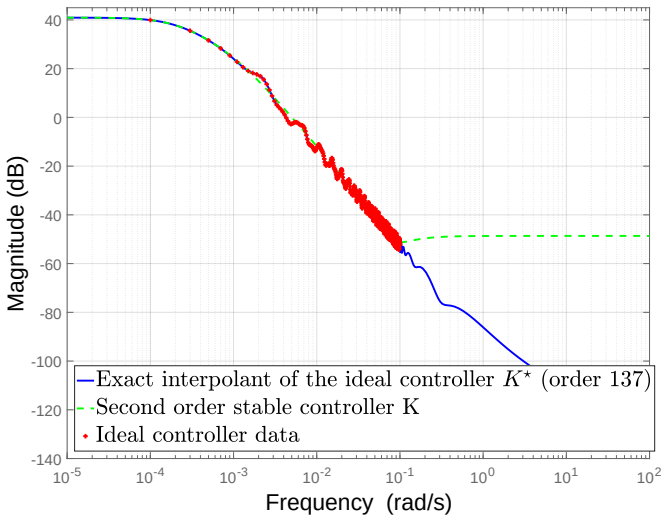

Figure 8.18: Identification of the ideal controller (red dots): minimal realization of order 137 (solid blue) and reduced 2nd order controller $\mathbf{K}$ (dashed blue) obtained through the Loewner framework.

8.2.4 Results

Since we had no access to the EDF simulator, the 8th order rational transfer function of [Dalmas et al., 2016] is used to simulate the closed-loop with the 2nd order controller obtained by applying the method proposed in this work. The results are shown in Figure 8.19: the resulting closed-loop achieve a response time of 4.84×10^5s (134.4 hours) with no overshoot, while the system naturally has a response time of 2.47×10^{13}s. The

closed-loop dynamic is almost the objective one. The command signal is shown on Figure 8.20: it is reasonable, the maximum flow variation is around $8.3m^3.s^{-1}$, which is in the acceptable range for this application with a controller of order 2.

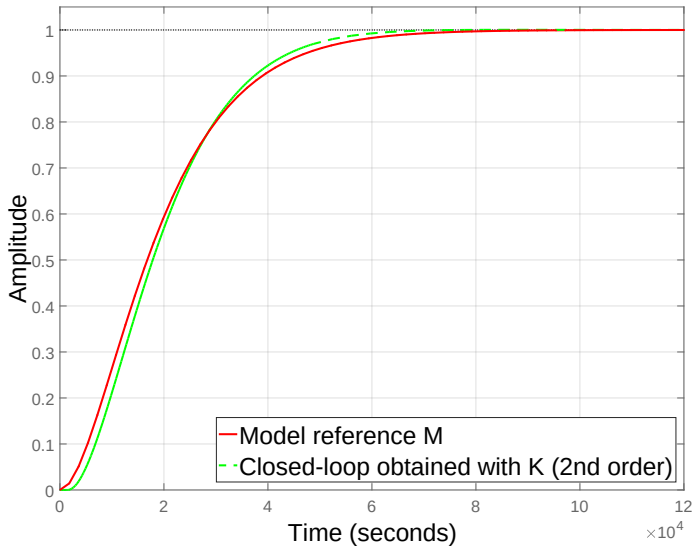

Figure 8.19: Step response of the closed loop obtained with the 2nd order controller identified through the proposed method (dashed green) and of the objective transfer (solid red).

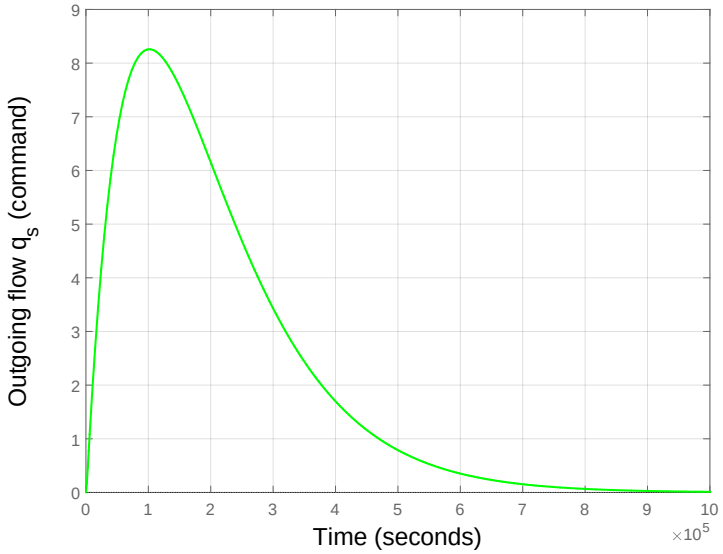

Figure 8.20: Evolution of the outgoing flow q_s when applying a step on the closed-loop obtained with the identified 2nd order controller $\mathbf{K}$.

Finally, the performances in terms of disturbance rejection are shown on Figure 8.21: an input flow of $100m^3/s$ during four hours is considered. This disturbance would increase the water depth of $0.65m$ if not rejected. Figure 8.21 represents the tracking error when this disturbance is applied on the stabilized closed-loop: the water depth increases of $0.54m$ instead of the $0.65m$ without the controller. Finally, the disturbance is completely rejected $0.8 \times 10^5 s$ (2.3 hours) after its application. During the remaining time of the disturbance application, the disturbance does not affect the closed-loop system.

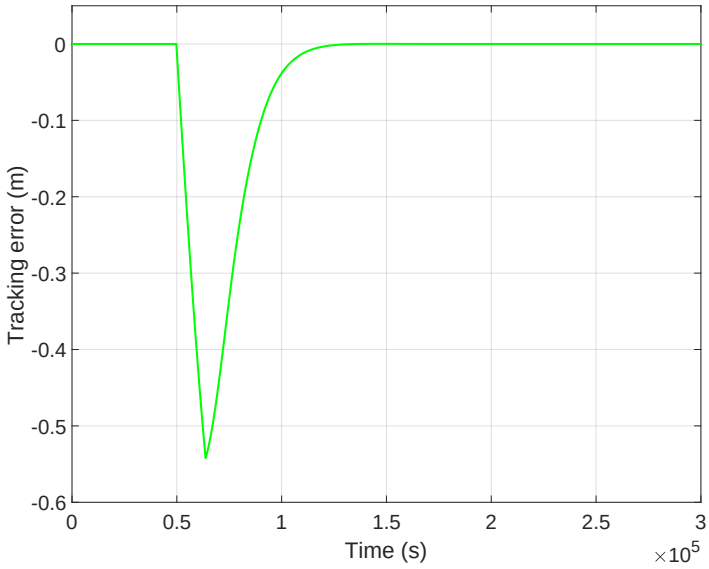

Figure 8.21: Performance of the controlled closed-loop in terms of disturbance rejection.

It should be noted that the closed-loop could be faster by increasing the frequency ω_0 of the reference model $\mathbf{M}$, see (8.6). However, taking $\omega_0 = 10^{-4} rad.s^{-1}$ (instead of $10^{-5} rad.s^{-1}$), leads to the identification of a second-order controller giving an oscillatory behaviour in closed-loop. The consequence is a significant overshoot, which is not acceptable in this application. Furthermore, the command signal q_s rises up to $80m^3/s$ when applying a step on the corresponding closed-loop.

Remark 8.2.1. In this application, it could be interesting to identify a pLTI model of the controller that depends on the sensor position x, see (8.5). It would allow to avoid to design a controller for each open-channel when the only parameter that changes is the sensor's position. To that extent, it would be possible to use the parametric version of the Loewner framework, see [Ionita and Antoulas, 2014], or the extension of the subspace algorithm proposed during this thesis, see [Kergus et al., 2018a].

In this application, the proposed method is appealing since it does not require to simulate the complex system described by an irrational transfer function to obtain time-domain data. Only samples of the frequency response of the plant are needed, which

can be estimated directly from the irrational transfer function. Moreover, one should notice that controlling such an infinite order model is also quite challenging even for model-based methods. A interesting perspective would be to try this controller on the EDF simulator instead of using the approximate model to validate the performances.

Part III

Conclusion

Chapter 9

Discussion

Contents

9.1 Summary of the proposed method

A new data-driven control technique is proposed in this work. The main idea, originally exposed in [Kergus et al., 2017], is exposed in Chapter 4. The specifications are given as a reference model **M**, corresponding to the desired closed-loop transfer. The objective is to design a controller **K** such that the resulting closed-loop is as close as possible to the reference model, see Figure 9.1. The plant's data and the reference model are used to construct the frequency response of the ideal controller, which is then identified. In this work, two identification techniques are considered: the Loewner framework and the subspace approach.

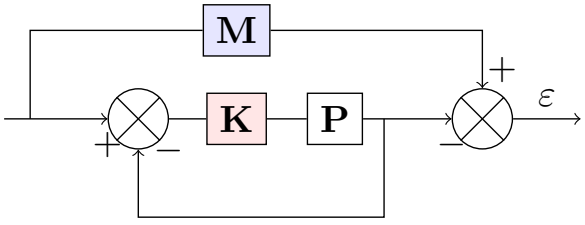

Figure 9.1: Problem formulation: **M** is the desired closed-loop, **P** is the plant and **K** the controller to be designed.

In Chapter 4, the application of this first version of the method, as exposed in [Kergus et al., 2017], on two numerical examples, the DC motor and the flexible transmission benchmark, illustrates the impact of the choice of the reference model on the control design. The flexible transmission example, which is non-minimum phase, shows that it is a particularly challenging step when the plant has RHP poles or zeros. Furthermore, it highlights the necessity to analyze the stability of the obtained closed-loop. Therefore, the initial version of the method is modified to include two additional steps. The final version of the proposed method is recalled hereafter in Algorithm 1 and the different steps are briefly summed up.

Algorithm 1: Data-driven control in the frequency domain: final version of the proposed method

Data:

- Samples of the frequency response of the plant $\{\Phi_i\}_{i=1}^N$ at the frequencies $\{\omega_i\}_{i=1}^N$.
- Stable reference model $\mathbf{M}$ giving the desired closed-loop performances.

Solution:

1. **Construction of an achievable reference model**
   (a) Projection of the available data and determination of the plant's nature and limitations:
      - stable or unstable when projecting $\{\Phi_i\}_{i=1}^N$;
      - minimum phase or not when projecting $\{\Phi_i^{-1}\}_{i=1}^N$.
   (b) If any, estimate the system's RHP poles $\{p_j\}_{j=1}^{n_p}$ and NMP zeros $\{z_i\}_{i=1}^{n_z}$ and their respective output directions $\left\{\mathbf{y}_{p_j}\right\}_{j=1}^{n_p}$ and $\{\mathbf{y}_{z_i}\}_{i=1}^{n_z}$.
   (c) Build an achievable reference model $\mathbf{M}_f$ that satisfy the plant's limitations given by:

$$\begin{cases} \mathbf{y}_{z_i}^T \mathbf{M}_f(z_i) = 0 \\ \mathbf{M}_f(p_j)\mathbf{y}_{p_j} = \mathbf{y}_{p_j} \end{cases} . \tag{9.1}$$

2. **Controller identification**
   (a) Compute the frequency-response samples of the ideal controller $\mathbf{K}^\star$:

$$\forall\ i = 1 \dots N,\ \mathbf{K}^\star(\imath\omega_i) = \Phi_i^{-1}\mathbf{M}_f(\imath\omega_i))(I_{n_y} - \mathbf{M}_f(\imath\omega_i))^{-1}. \tag{9.2}$$

   (b) On the basis of this samples, identify a model $\mathbf{K}$ of $\mathbf{K}^\star$ using the Loewner framework or the subspace approach, of a prescribed order n or a minimal realisation of high-order.

3. **Stability analysis and controller reduction**
   (a) Compute the maximal controller modelling error:

$$\tilde{\gamma} = \max_{i=1\dots N} |\Phi_i(1 - \mathbf{M}_f(\imath\omega_i)(\imath\omega_i)| \,. \tag{9.3}$$

   (b) Reduce the controller order, using the Loewner framework or the subspace approach, and check that the stability test is verified:

$$\|\mathbf{K} - \mathbf{K}^\star\|_\infty \leq \frac{1}{\tilde{\gamma}} - \varepsilon, \tag{9.4}$$

   (c) When the stability test is not verified, two situations may occur:
      - The stability test is too conservative and the projection of step 1a) will determine if the controller stabilizes the plant internally.
      - The considered reduced-order controller does not stabilize the plant internally.

9.1.1 Choice of the reference model

The choice of an achievable reference model, tackled in Chapter 6 and exposed in [Kergus et al., 2019b], is based on a projection of the frequency response of the plant to determine whether the plant has instabilities or not. Indeed, the RHP poles and zeros of a system are the main limitations of the closed-loop performances, expressed as interpolatory constraints on the closed-loop, see step 1c of Algorithm 1. When the plant is unstable and/or NMP, its instabilities are estimated. Then, an achievable reference model $\mathbf{M}_f$ is built from the initial one $\mathbf{M}$ specified by the user to satisfy the analiticity constraints imposed by the RHP poles and zeros of the plant.

Estimating the plant's instabilities may seem like a model-based approach. However, it is necessary to know the plant's performance limitation to avoid the situation where the ideal controller destabilize the plant internally, see Chapter 4. There are two ways to know these limitations: (i) having access to a stabilizing controller or (ii) knowing the system's instabilities. In the present case, no initial stabilizing controller is supposed to be available. Estimating the plant's RHP poles and zeros is then the only available solution. As discussed in Chapter 6, the projection approach allows to avoid identifying a model of the system.

9.1.2 Controller identification

Once an achievable reference model $\mathbf{M}_f$ is obtained, the frequency response of the associated ideal controller is computed following step 2a of Algorithm 1 and identified through the Loewner framework and/or the subspace approach. These two techniques are recalled in Chapter 5 and additional features are considered to use them in a data-driven control framework, as explained in [Kergus et al., 2018b]. First, the stability of the controller is enforced either through a projection on $\mathcal{RH}_\infty$ when using the Loewner framework, or through LMI constraints when using the subspace approach. It avoids to introduce instabilities in the open-loop and to satisfy the conditions of application of the small-gain theorem when it comes to the data-driven stability analysis. Furthermore, noisy data were considered to study how the quality of the data influences the controller identification. It appeared that the Loewner framework is very sensitive to noise and the reduction has consequently been modified to limit its impact on the results.

The Loewner framework and the subspace approach both allow to reduce the controller order up to a prescribed order n in a straightforward way. The reduction of the controller model implies to discard some of the ideal controller dynamics, and consequently it degrades the closed-loop performances in comparison with the expected behaviour specified by $\mathbf{M}$. However, as explained in Chapter 6, the compromise between controller's complexity and closed-loop performances does not only depend on the controller reduction but also on the initial reference model specified by the user. This was already highlighted in Chapter 4 on the DC motor example: for a given controller order, less demanding reference models may lead to better performances. This is also the case for the flexible transmission benchmark, as detailed in Chapter 7.

9.1.3 Data-driven stability analysis

The choice of an achievable reference model $\mathbf{M}_f$ and the stability of the controller model allow us to apply the small-gain theorem as in [Van Heusden et al., 2009] to derive an internal stability condition, given in step 3a of Algorithm 1. As long as the controller modelling error is below a limit determined by the plant $\mathbf{P}$ and the achievable reference model $\mathbf{M}_f$, the identified controller will stabilize the plant internally. The reduction of the controller model is then done while preserving internal closed-loop stability.

The main drawback of this approach is that the proposed stability test is very conservative. As an example, all the controllers identified through the subspace approach for the flexible transmission benchmark are rejected while they all stabilize the plant internally. The projection technique for data-driven stability analysis recalled in Chapter 6 can then be used as a complement to test the stability of the resulting closed-loop.

The second drawback is that the proposed stability test relies on a data-driven estimation of an $\mathcal{H}_\infty$-norm, see step 3b of Algorithm 1. The underestimation of this norm may lead to the selection of destabilizing controllers. Specific tools should be considered to improve the results regarding this aspect, this idea will be further discussed in Section 9.3.

9.2 Conclusion

9.2.1 Results

The proposed method shows good results on the two numerical examples treated along this work (the DC motor and the flexible transmission benchmark). In Chapter 8, two additional and more complex examples illustrate the proposed method: a continuous crystallizer and an open-channel for hydroelectricty generation. These applications are representative of the class of systems for which data-driven control techniques is more appealing than model-based ones. Indeed, their models, which are irrational, are too complex for model-based control.

In both cases, the data-driven stability analysis proposed in [Cooman et al., 2018b] allows to draw the right conclusion concerning the nature of the plant. However, the second example considered in Section 8.2 shows that integral actions are not handled by this technique. In Section 8.1, the continuous crystallizer is shown to be unstable and its unstable poles correspond to the ones previously found in the literature. The technique presented in Chapter 6 is then used to select an achievable reference model. The resulting ideal controllers are stable and, in the case of the continuous crystallizer, do not compensate the plant's instabilities. The associated ideal controllers are then identified and reduced. In each application, the final controller stabilizes the considered system internally and leads to good closed-loop performances.

As shown by the application of the proposed method on the continuous crystallizer, choosing a reference model constitutes a very limited specifications requirement, compared to robust specifications for example. To that extent, it may be interesting to iterate the method proposed in this thesis by changing the initial reference model progressively up to a certain performance level.

9.2.2 Main strengths and limitations

i) Simplicity of the proposed method

The main strength of the proposed method is its simplicity. It only requires frequency-response samples from the plant and a reference model chosen by the user. Contrary to other model reference techniques, there is no need to structure the controller a priori. Furthermore, it does not require an initial stabilizing controller: the system's instabilities are estimated directly from the available data, allowing to know what are the achievable closed-loop dynamics.

The interventions of the user are limited to the following ones:

- Determine the nature of the plant from the projection of the FRF measurements: this step may be touchy if the data are not rich enough, see the following paragraph (ii). Once it is done, the number of instabilities is determined easily by a rank-revealing decomposition. It should be noted that, regarding this aspect, the user may be solicited twice: once to choose a reference model at the beginning, and once in the end if the internal stability test is not verified because of its conservatism.

- Trading between the controller's complexity and closed-loop performances: choosing the order of the controller to fit the ideal controller dynamics is made easy in the two identification techniques used along this work. However, the reduction of the controller, under internal stability considerations, may imply to decrease closed-loop performances for a given reference model. Nevertheless, in the proposed method, the complexity-performance trade-off does not only depend on the controller reduction but also on the choice of the specifications, see (iii).

ii) Impact of the quality of the data

As for system identification, the quality of the available data plays a pivotal role in the success of the proposed method. As a matter of fact, noisy data deteriorate the estimation of the RHP poles and zeros of the system while determining an achievable reference model. In addition, the data should be dense enough to capture the unstable dynamics. However, to determine the nature of the plant (stable or not, minimum-phase or not), the projection of the frequency-response is more robust to noise than the identification of a high-order model of the system.

The noise is obviously passed through the frequency-response of the ideal controller. Its main effect is to increase the order of the minimal realisation obtained through the Loewner framework and the subspace approach. However, when it comes to the identification of the controller, the noise impacts mostly the Loewner interpolation. Additional information concerning the noise covariance function would be needed to improve the results of the subspace identification.

In the end, the most critical step regarding the quality of the data is the internal stability test proposed in Chapter 7. As a matter of fact, it relies on the estimation of the $\mathcal{H}_\infty$-norm of a dynamical system on the basis of samples of its frequency-response. Consequently, the $\mathcal{H}_\infty$-norm is often underestimated, which may lead to the choice of destabilizing reduced-order controller.

Regarding the question of the quality of the data, a pre-filtering step should be considered to limit the impact of noise on the estimation the system's instabilities and on the controller identification. To that extent, other identification techniques, maybe more robust to noisy data like the subspace approach, could be considered.

iii) Formulation of the specifications

The flexible transmission benchmark illustrates that the choice of the specifications has a strong impact on the reduction of the controller. When the initial reference model corresponds to a fast closed closed-loop dynamics, it is not possible to reduce the ideal controller as much as when using slower specifications. In this example, it is explained by the fact that the faster specifications do not respect the performance limitations imposed by the NMP zeros of the plant. Consequently, once the instabilities are estimated, it is suggested to adapt the performance specifications if needed.

Nevertheless, even though the reference model respects the performance limitations, specifying a model reference may be problematic. This is particularly highlighted by the application of the proposed method on the continuous crystallizer application: robust specifications allow a greater flexibility in the specifications than a reference model. Indeed, instead of giving one single desired behaviour, specifications are formulated as frequency-domain weighting functions defining a whole set of expected closed-loop dynamics.

9.3 Outlooks

9.3.1 Extension to other problem formulations

In this work, only the structure presented on Figure 9.1 has been presented. However, as it has been for the VRFT in [Lecchini, 2001] or for unfalsified control in [Battistelli et al., 2018], other objective functions may be considered:

1. The sensitivity function $\mathbf{S}$, see Figure 9.2. A similar formulation has been used as an extension of the VRFT in

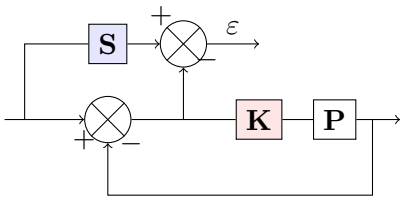

Figure 9.2: Alternative problem formulation: $\mathbf{S}$ is the desired sensitivity function, $\mathbf{P}$ is the plant and $\mathbf{K}$ the controller to be designed.

2. The transfer $\mathbf{T}_{r\to u} = \mathbf{W}_u$ to reach it as a moderate command objective, see Figure 9.3. As said in [Battistelli et al., 2018], the main advantage of this formulation is that the corresponding ideal controller will never compensate the plant's instabilities.

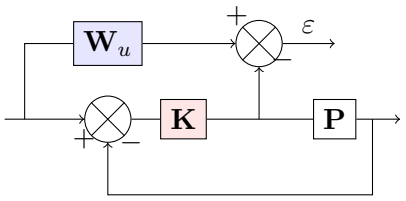

Figure 9.3: Alternative problem formulation: $\mathbf{W}_u$ is the desired transfer in terms of moderate command objectives, $\mathbf{P}$ is the plant and $\mathbf{K}$ the controller to be designed.

3. The disturbance rejection transfer $\mathbf{W}_d$, as specified on Figure 9.4.

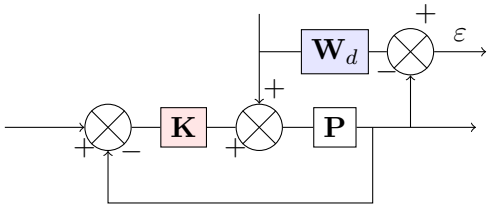

Figure 9.4: Alternative problem formulation: $\mathbf{W}_d$ is the desired disturbance rejection transfer, $\mathbf{P}$ is the plant and $\mathbf{K}$ the controller to be designed.

In each of the mentioned alternative problem formulations, the ideal case allows to compute the frequency-response of the corresponding ideal controller to be identified and reduced. To that extent, it could be interesting to use other identification and reduction techniques. It would also be possible to use time-domain techniques based on virtual signals as in the VRFT framework.

It could also be possible to mix these performance specifications in an iterative way using a similar procedure than the the one proposed in [Battistelli et al., 2018], based on a ponderate objective function.

9.3.2 Overcoming the difficulty of choosing a reference model

As said earlier in Chapter 8, specifying performances as a single desired reference model is much less flexible than robust specifications. The choice of a reference model is then a crucial step for the success of the proposed technique. In order to overcome the difficulty of selecting achievable performance specifications, the following lines of approach may be investigated in future work.

Reference model control and the associated matching problem

In this thesis, the construction of an achievable reference model $\mathbf{M}_f$ is based on the choice of an initial one $\mathbf{M}$. Even if $\mathbf{M}$ is allowed to not respect the analiticity constraints given in (9.1), it might be too demanding in terms of performances considering the impact of (9.1), see Chapter 2.

It is also possible to build an achievable sensitivity function $\mathbf{S}_f$, and therefore an achievable reference model $\mathbf{M}_f = I - \mathbf{S}_f$, without having to specify an initial desired

behaviour. To this end, the problem may be reformulated as a matching one. The specifications for $\mathbf{S}_f$ to be achievable and to impose some closed-loop performances are the following:

1. **Internal stability:** $\mathbf{S}_f$ is stable LTI and satisfies the following interpolatory conditions:
$$\begin{cases} \mathbf{S}_f(z_i)=1 & \forall i = 1 \dots n_z \\ \mathbf{S}_f(p_j)=0 & \forall j = 1 \dots n_p \end{cases}$$
where $\{z_i\}_{i=1\dots n_z}$ and $\{p_j\}_{j=1\dots n_p}$ are the unstable zeros and poles of the plant $\mathbf{P}$.

2. **Limited overshoot:** $\|\mathbf{S}_f\|_\infty \leq \gamma$

3. **Low static error:** $\min\limits_{\mathbf{S}_f} \max\limits_{\theta\in(0,\theta_c)} \left|\mathbf{S}_f(e^{\imath\theta})\right|$, where θ_c is the cutoff frequency.

Consequently, having estimated the instabilities of the plant and given a cutoff frequency, it is possible to shape an achievable sensitivity function $\mathbf{S}_f$ by introducing the following function:

$$f(z) = \frac{1}{\gamma}\mathbf{S}_f\left(\frac{1}{z}\right) \tag{9.5}$$

with γ the lower bound of the sensitivity function, defined according to the plant's instabilities (see [Havre and Skogestad, 1996]). In the SISO case, it is given by:

$$\gamma = \max_{z_i} \prod_{j=1}^{n_p} \frac{|z_i + \overline{p_j}|}{|z_i - p_j|}.$$

If f is a solution of:

$$\text{s.t.} \quad \begin{array}{l} \min\limits_{f \text{ Schur}} \max\limits_{z\in I} |f(z)| \\ \begin{cases} f(z_i^{-1})=\frac{1}{\gamma} & \forall i = 1 \dots n_z \\ f(p_j^{-1})=0 & \forall j = 1 \dots n_p \end{cases} \end{array}, \tag{9.6}$$

then the corresponding sensitivity function $\mathbf{S}_f$, see (9.5), is achievable by the plant. This problem may be solved using the methodology developed in [Martínez et al., 2018], introduced for broadband matching filters synthesis. A similar approach for sensitivity shaping is described in [Karlsson et al., 2010].

Structuring the controller

Another solution to avoid one of the user's interventions is to structure the controller. The choice of this structure $\mathcal{K}$ then becomes an input parameter as well as the reference model $\mathbf{M}$.

The problem would then formulated be formulated as an optimization one, similar to the VRFT, CbT or IFT framework:

$$\min_{\mathbf{K}\in\mathcal{K}} \left\|(I + \mathbf{PK})^{-1}\mathbf{PK} - \mathbf{M}\right\| \tag{9.7}$$

where the distance between the resulting closed-loop and the reference model $\mathbf{M}$ may be the $\mathcal{H}_2$-norm. The main strength of this approach would be to avoid the controller

reduction. Assuming that an initial stabilizing controller is available, it could be possible to include a stability constraint such as the test exposed in Chapter 7.

Th solution avoids the need to build an achievable reference model, and therefore estimating the plant's instabilities would not be required any longer.

Combined use with other control techniques

The basic idea of the data-driven control technique proposed in this thesis is to identify the controller on the basis of some data from the ideal controller $\mathbf{K}^\star$. In this work, this data comes from the choice of a reference model, but it could come from other data-driven control techniques such as ILC for example.

9.3.3 Data-driven stability analysis

Finally, one of the main line of research that should be further developed concerns stability analysis.

Data-driven estimation of the $\mathcal{H}_\infty$-norm of a dynamical system

As said earlier, the proposed stability test relies on the estimation of an $\mathcal{H}_\infty$-norm which should be improved. In the first place, it should be noted that some specific data-driven tools exist to estimate correctly the $\mathcal{H}_\infty$-norm. The technique proposed in [Van Heusden et al., 2007], used for data-driven control design, is based on time-domain data and relies on the discrete Fourier transform. As for the stability test proposed in Chapter 7, it suffers from the finiteness of the available data.

To improve this point, it has been proposed in [Hjalmarsson, 2005] and [Wahlberg et al., 2010] to design the experiment's input in an iterative procedure to overcome the difficulty of dealing with a finite amount of data. Another iterative input design technique is proposed in [Rallo, 2017], relying on expert advice. These type of techniques may be used before the proposed data-driven control techniques to obtain more reliable data.

Towards a less conservative data-driven stability test

Even assuming that the $\mathcal{H}_\infty$-norm may be properly estimated, the considered stability test may be conservative as highlighted by the flexible transmission benchmark, see Chapter 7. Less conservative options should be considered. To that extent, it has been suggested to use the data-driven stability analysis of [Cooman et al., 2018b], recalled in Chapter 6, used to build an achievable reference model. Another interesting and similar technique, suggested in [Poussot-Vassal, 2019], would be to use the Loewner framework coupled with the $\mathcal{RH}_\infty$-projection technique from [Köhler, 2014] as detailed in Chapter 5. Indeed, computing the distance δ:

$$\delta = \|\mathbf{H} - \mathbf{H}^{as}\|_\infty ,$$

where $\mathbf{H}$ is a minimal representation of the closed-loop interpolated through the Loewner framework and $\mathbf{H}^{as} \in \overline{\mathcal{H}}_2$ is its antistable projection, would allow to assess the stability of the resulting closed-loop.

Bibliography

[Ahn et al., 2007] Ahn, H.-S., Chen, Y., and Moore, K. L. (2007). Iterative learning control: Brief survey and categorization. *IEEE Transactions on Systems, Man, and Cybernetics, Part C (Applications and Reviews)*, 37(6):1099–1121.

[Alkhoury et al., 2017] Alkhoury, Z., Petreczky, M., and Mercère, G. (2017). Comparing global input-output behavior of frozen-equivalent LPV state-space models. In *20th IFAC World Congress*.

[Antoulas et al., 2015] Antoulas, A., Lefteriu, S., and Ionita, A. (2015). A tutorial introduction to the Loewner framework for model reduction. *Model Reduction and Approximation for Complex Systems, Birkhäuser, ISNM Series*.

[Apkarian and Noll, 2018] Apkarian, P. and Noll, D. (2018). Structured H_∞ control of infinite dimensional systems. *International Journal of Robust and Nonlinear Control*, 28(9):3212–3238.

[Åström and Hägglund, 1995] Åström, K. and Hägglund, T. (1995). *PID controllers: theory, design, and tuning*, volume 2. Instrument society of America Research Triangle Park, NC.

[Åström et al., 1977] Åström, K. J., Borisson, U., Ljung, L., and Wittenmark, B. (1977). Theory and applications of self-tuning regulators. *Automatica*, 13(5):457–476.

[Battistelli et al., 2018] Battistelli, G., Mari, D., Selvi, D., and Tesi, P. (2018). Direct control design via controller unfalsification. *International Journal of Robust and Nonlinear Control*, 28(12):3694–3712.

[Battistelli et al., 2010] Battistelli, G., Mosca, E., Safonov, M. G., and Tesi, P. (2010). Stability of unfalsified adaptive switching control in noisy environments. *IEEE Transactions on Automatic Control*, 55(10):2424–2429.

[Bazanella et al., 2011] Bazanella, A., Campestrini, L., and Eckhard, D. (2011). *Data-driven controller design: the H2 approach*. Springer Science & Business Media.

[Bontempi et al., 1999] Bontempi, G., Birattari, M., and Bersini, H. (1999). Lazy learning for local modelling and control design. *International Journal of Control*, 72(7-8):643–658.

[Bonvin et al., 2006] Bonvin, D., Srinivasan, B., and Hunkeler, D. (2006). Control and optimization of batch processes. *IEEE Control Systems Magazine*, 26(6):34–45.

[Brozenec et al., 2001] Brozenec, T., Tsao, T., and Safonov, M. (2001). Controller validation. *International Journal of Adaptive Control and Signal Processing*, 15(5):431–444.

[Campestrini et al., 2011] Campestrini, L., Eckhard, D., Gevers, M., and Bazanella, A. S. (2011). Virtual reference feedback tuning for non-minimum phase plants. *Automatica*, 47(8):1778–1784.

[Campi et al., 2002] Campi, M., Lecchini, A., and Savaresi, S. (2002). Virtual reference feedback tuning: a direct method for the design of feedback controllers. *Automatica*, 38(8):1337–1346.

[Campi and Savaresi, 2006] Campi, M. C. and Savaresi, S. M. (2006). Direct nonlinear control design: the virtual reference feedback tuning (vrft) approach. *IEEE Transactions on Automatic Control*, 51(1):14–27.

[Chilali et al., 1999] Chilali, M., Gahinet, P., and Apkarian, P. (1999). Robust pole placement in lmi regions. *IEEE transactions on Automatic Control*, 44(12):2257–2270.

[Cooman et al., 2018a] Cooman, A., Seyfert, F., and Amari, S. (2018a). Estimating unstable poles in simulations of microwave circuits. In *2018 IEEE/MTT-S International Microwave Symposium-IMS*, pages 97–100. IEEE.

[Cooman et al., 2018b] Cooman, A., Seyfert, F., Olivi, M., Chevillard, S., and Baratchart, L. (2018b). Model-free closed-loop stability analysis: A linear functional approach. *IEEE Transactions on Microwave Theory and Techniques*, 66(1):73–80.

[Dalmas et al., 2016] Dalmas, V., Robert, G., Poussot-Vassal, C., Duff, I. P., and Seren, C. (2016). From infinite dimensional modelling to parametric reduced order approximation: Application to open-channel flow for hydroelectricity. In *15th European Control Conference (ECC'16)*.

[De Bruyne and Kammer, 1999] De Bruyne, F. and Kammer, L. C. (1999). Iterative feedback tuning with guaranteed stability. In *Proceedings of the 1999 American Control Conference (Cat. No. 99CH36251)*, volume 5, pages 3317–3321. IEEE.

[Dehghani et al., 2009] Dehghani, A., Lecchini-Visintini, A., Lanzon, A., and Anderson, B. D. (2009). Validating controllers for internal stability utilizing closed-loop data. *IEEE Transactions on Automatic Control*, 54(11):2719–2725.

[Deistler, 2002] Deistler, M. (2002). System identification and time series analysis: Past, present, and future. In *Stochastic Theory and Control*, pages 97–109. Springer.

[Demourant et al., 2002] Demourant, F., Ferreres, G., and Biannic, J.-M. (2002). Falsification of an aircraft autopilot. In *Proceedings of the 2002 American Control Conference (IEEE Cat. No. CH37301)*, volume 1, pages 803–808. IEEE.

[Demourant and Poussot-Vassal, 2017] Demourant, F. and Poussot-Vassal, C. (2017). A new frequency-domain subspace algorithm with restricted poles location through lmi regions and its application to a wind tunnel test. *International Journal of Control*, 90(4):779–799.

[Den Hamer, 2010] Den Hamer, A. (2010). Data-driven optimal controller synthesis: a frequency domain approach. *Eindhoven University of Technology, Eindhoven, the Netherlands*.

[Den Hamer et al., 2009] Den Hamer, A., Weiland, S., and Steinbuch, M. (2009). Model-free norm-based fixed structure controller synthesis. In *Proceedings of the 48h IEEE Conference on Decision and Control (CDC) held jointly with 2009 28th Chinese Control Conference*, pages 4030–4035. IEEE.

[Duan, 2010] Duan, G.-R. (2010). *Analysis and design of descriptor linear systems*, volume 23. Springer Science & Business Media.

[Eckhard et al., 2018] Eckhard, D., Campestrini, L., and Boeira, E. C. (2018). Virtual disturbance feedback tuning. *IFAC Journal of Systems and Control*, 3:23–29.

[Fliess, 2009] Fliess, M. (2009). Model-free control and intelligent pid controllers: towards a possible trivialization of nonlinear control? *IFAC Proceedings Volumes*, 42(10):1531–1550.

[Fliess and Join, 2013] Fliess, M. and Join, C. (2013). Model-free control. *International Journal of Control*, 86(12):2228–2252.

[Formentin et al., 2014a] Formentin, S., Cologni, A. L., Previdi, F., and Savaresi, S. M. (2014a). A data-driven approach to control of batch processes with an application to a gravimetric blender. *IEEE Transactions on Industrial Electronics*, 61(11):6383–6390.

[Formentin et al., 2013] Formentin, S., Panzani, G., and Savaresi, S. M. (2013). Vrft for lpv systems: Theory and braking control application. In *Robust Control and Linear Parameter Varying Approaches*, pages 289–309. Springer.

[Formentin et al., 2015] Formentin, S., Piga, D., Tóth, R., and Savaresi, S. M. (2015). Nonparametric lpv data-driven control. *IFAC-PapersOnLine*, 48(26):146–151.

[Formentin et al., 2012] Formentin, S., Savaresi, S., and Del Re, L. (2012). Non-iterative direct data-driven controller tuning for multivariable systems: theory and application. *IET control theory & applications*, 6(9):1250–1257.

[Formentin and Savaresi, 2011] Formentin, S. and Savaresi, S. M. (2011). Virtual reference feedback tuning for linear parameter-varying systems. *IFAC Proceedings Volumes*, 44(1):10219–10224.

[Formentin et al., 2014b] Formentin, S., Van Heusden, K., and Karimi, A. (2014b). A comparison of model-based and data-driven controller tuning. *International Journal of Adaptive Control and Signal Processing*, 28(10):882–897.

[Gevers, 2005] Gevers, M. (2005). Identification for control: From the early achievements to the revival of experiment design. *European journal of control*, 11(4-5):335–352.

[Gevers, 2006] Gevers, M. (2006). A personal view of the development of system identification: A 30-year journey through an exciting field. *IEEE Control systems magazine*, 26(6):93–105.

[Gevers and Bombois, 2006] Gevers, M. and Bombois, X. (2006). Input design: From open-loop to control-oriented design. *IFAC Proceedings Volumes*, 39(1):1329–1334.

[Goodwin and Payne, 1977] Goodwin, G. C. and Payne, R. L. (1977). *Dynamic system identification: experiment design and data analysis*, volume 136. Academic press New York.

[Gosea and Antoulas, 2016] Gosea, I. and Antoulas, A. (2016). Stability preserving post-processing methods applied in the loewner framework. In *20th Workshop on Signal and Power Integrity*.

[Havre and Skogestad, 1996] Havre, K. and Skogestad, S. (1996). Effect of rhp zeros and poles on performance in multivariable systems. In *UKACC International Conference on Control*, volume 2, pages 930–935. IET.

[Havre and Skogestad, 2001] Havre, K. and Skogestad, S. (2001). Achievable performance of multivariable systems with unstable zeros and poles. *International Journal of Control*, 74(11):1131–1139.

[Hildebrand et al., 2005] Hildebrand, R., Lecchini, A., Solari, G., and Gevers, M. (2005). Optimal prefiltering in iterative feedback tuning. *IEEE Transactions on Automatic Control*, 50(8):1196–1200.

[Hjalmarsson, 1998] Hjalmarsson, H. (1998). Control of nonlinear systems using iterative feedback tuning. In *Proceedings of the 1998 American Control Conference. ACC (IEEE Cat. No. 98CH36207)*, volume 4, pages 2083–2087. IEEE.

[Hjalmarsson, 1999] Hjalmarsson, H. (1999). Efficient tuning of linear multivariable controllers using iterative feedback tuning. *International journal of adaptive control and signal processing*, 13(7):553–572.

[Hjalmarsson, 2002] Hjalmarsson, H. (2002). Iterative feedback tuning—an overview. *International journal of adaptive control and signal processing*, 16(5):373–395.

[Hjalmarsson, 2005] Hjalmarsson, H. (2005). From experiment design to closed-loop control. *Automatica*, 41(3):393–438.

[Hjalmarsson et al., 1998] Hjalmarsson, H., Gevers, M., Gunnarsson, S., and Lequin, O. (1998). Iterative feedback tuning: theory and applications. *IEEE control systems magazine*, 18(4):26–41.

[Hjalmarsson et al., 1994] Hjalmarsson, H., Gunnarsson, S., and Gevers, M. (1994). A convergent iterative restricted complexity control design scheme. In *33rd IEEE Conference on Decision and Control*, volume 2, pages 1735–1740. IEEE.

[Hjalmarsson et al., 1995] Hjalmarsson, H., Gunnarsson, S., and Gevers, M. (1995). Model-free tuning of a robust regulator for a flexible transmission system. *European Journal of Control*, 1(2):148–156.

[Hori et al., 2016] Hori, T., Yubai, K., Yashiro, D., and Komada, S. (2016). Data-driven controller tuning for sensitivity minimization. In *International Conference on Advanced Mechatronic Systems*.

[Horowitz, 1982] Horowitz, I. (1982). Quantitative feedback theory. In *IEE Proceedings D (Control Theory and Applications)*, volume 129, pages 215–226. IET.

[Hou, 1999] Hou, Z. (1999). Nonparametric models and its adaptive control theory. *Science Press*.

[Hou et al., 2017] Hou, Z., Chi, R., and Gao, H. (2017). An overview of dynamic-linearization-based data-driven control and applications. *IEEE Transactions on Industrial Electronics*, 64(5):4076–4090.

[Hou and Wang, 2013] Hou, Z.-S. and Wang, Z. (2013). From model-based control to data-driven control: Survey, classification and perspective. *Information Sciences*, 235:3–35.

[Huang and Kadali, 2008] Huang, B. and Kadali, R. (2008). *Dynamic modeling, predictive control and performance monitoring: a data-driven subspace approach*. Springer.

[Ionita and Antoulas, 2014] Ionita, A. C. and Antoulas, A. C. (2014). Data-driven parametrized model reduction in the loewner framework. *SIAM Journal on Scientific Computing*, 36(3):A984–A1007.

[Jun and Safonov, 2002] Jun, M. and Safonov, M. G. (2002). Controller parameter adaptation algorithm using unfalsified control theory and gradient method. *IFAC Proceedings Volumes*, 35(1):283–287.

[Kammer, 2018] Kammer, C. (2018). Frequency-domain control design in power systems. Technical report.

[Karimi and Galdos, 2010] Karimi, A. and Galdos, G. (2010). Fixed-order h controller design for nonparametric models by convex optimization. *Automatica*, 46(8):1388–1394.

[Karimi and Kammer, 2017] Karimi, A. and Kammer, C. (2017). A data-driven approach to robust control of multivariable systems by convex optimization. *Automatica*.

[Karimi et al., 2002] Karimi, A., Miskovic, L., and Bonvin, D. (2002). Convergence analysis of an iterative correlation-based controller tuning method. In *15th IFAC World Congress*, page 1546.

[Karimi et al., 2018] Karimi, A., Nicoletti, A., and Zhu, Y. (2018). Robust H_∞ controller design using frequency-domain data via convex optimization. *International Journal of Robust and Nonlinear Control*, 28(12):3766–3783.

[Karimi et al., 2007] Karimi, A., Van Heusden, K., and Bonvin, D. (2007). Non-iterative data-driven controller tuning using the correlation approach. In *2007 European Control Conference (ECC)*, pages 5189–5195. IEEE.

[Karlsson et al., 2010] Karlsson, J., Georgiou, T., and Lindquist, A. (2010). The inverse problem of analytic interpolation with degree constraint and weight selection for control synthesis. *IEEE Transactions on Automatic Control*.

[Kergus et al., 2018a] Kergus, P., Demourant, F., and Poussot-Vassal, C. (2018a). Identification of parametric models in the frequency-domain through the subspace framework under lmi constraints. *International Journal of Control*, pages 1–12.

[Kergus et al., 2018b] Kergus, P., Formentin, S., Poussot-Vassal, C., and Demourant, F. (2018b). Data-driven control design in the Loewner framework: Dealing with stability and noise. *European Control Conference*.

[Kergus et al., 2019a] Kergus, P., Olivi, M., Poussot-Vassal, C., and Demourant, F. (2019a). Data-driven reference model selection and Application to Loewner Data-Driven Control. *Arxiv*.

[Kergus et al., 2019b] Kergus, P., Olivi, M., Poussot-Vassal, C., and Demourant, F. (2019b). From reference model selection to controller validation: Application to Loewner Data-Driven Control. *IEEE Control Systems Letters*.

[Kergus et al., 2017] Kergus, P., Poussot-Vassal, C., Demourant, F., and Formentin, S. (2017). Frequency-domain data-driven control design in the loewner framework. *IFAC-PapersOnLine*, 50(1):2095–2100.

[Khadraoui et al., 2013] Khadraoui, S., Nounou, H. N., Nounou, M. N., Datta, A., and Bhattacharyya, S. P. (2013). A measurement-based approach for designing reduced-order controllers with guaranteed bounded error. *International Journal of Control*, 86(9):1586–1596.

[Köhler, 2014] Köhler, M. (2014). On the closest stable descriptor system in the respective spaces rh2 and rh. *Linear Algebra and its Applications*, 443:34–49.

[Kostic, 2004] Kostic, D. (2004). Data-driven robot motion control design. *Technische Universiteit Eindhoven, Netherlands, 2004, Phd Thesis*.

[Landau et al., 1995] Landau, I., Rey, D., Karimi, A., Voda, A., and Franco, A. (1995). A flexible transmission system as a benchmark for robust digital control. *European Journal of Control*.

[Lecchini, 2001] Lecchini, A. Campi, M. C. . S. S. M. (2001). Sensitivity shaping via virtual reference feedback tuning. In *Proceedings of the 40th IEEE Conference on Decision and Control*, volume 1, pages 750–755. IEEE.

[Lee, 2011] Lee, J. H. (2011). Model predictive control: Review of the three decades of development. *International Journal of Control, Automation and Systems*, 9(3):415.

[Lefteriu et al., 2010] Lefteriu, S., Ionita, A. C., and Antoulas, A. C. (2010). Modeling systems based on noisy frequency and time domain measurements. In *Perspectives in Mathematical System Theory, Control, and Signal Processing*, pages 365–378. Springer.

[Liu et al., 1996] Liu, K., Jacques, R. N., and Miller, D. W. (1996). Frequency domain structural system identification by observability range space extraction. *Journal of Dynamic Systems, Measurement, and Control*, 118(2):211–220.

[Ljung, 2010] Ljung, L. (2010). Perspectives on system identification. *Annual Reviews in Control*, 34(1):1–12.

[Lovera and Mercere, 2007] Lovera, M. and Mercere, G. (2007). Identification for gain-scheduling: a balanced subspace approach. In *IEEE American Control Conference*.

[Luenberger, 1967] Luenberger, D. (1967). Canonical forms for linear multivariable systems. *IEEE Transactions on Automatic Control*.

[Luenberger, 1977] Luenberger, D. (1977). Dynamic equations in descriptor form. *IEEE Transactions on Automatic Control*, 22(3):312–321.

[MacFarlane and Karcanias, 1976] MacFarlane, A. and Karcanias, N. (1976). Poles and zeros of linear multivariable systems: a survey of the algebraic, geometric and complex-variable theory. *International Journal of Control*, 24(1):33–74.

[Markusson et al., 2001] Markusson, O., Hjalmarsson, H., and Norrlof, M. (2001). Iterative learning control of nonlinear non-minimum phase systems and its application to system and model inversion. In *Proceedings of the 40th IEEE Conference on Decision and Control (Cat. No. 01CH37228)*, volume 5, pages 4481–4482. IEEE.

[Mårtensson and Hjalmarsson, 2009] Mårtensson, J. and Hjalmarsson, H. (2009). Variance error quantifications for identified poles and zeros. *Automatica*.

[Martínez et al., 2018] Martínez, D., Bose, G., Seyfert, F., and Olivi, M. (2018). Convex optimisation method for matching filters synthesis. In *7th International Workshop on Microwave Filters*.

[Mayo and Antoulas, 2007] Mayo, A. and Antoulas, A. (2007). A framework for the solution of the generalized realization problem. *Linear algebra and its applications*, 425(2):634–662.

[McKelvey, 1995] McKelvey, T. (1995). *Identification of state-space models from time and frequency data*. Department of Electrical Engineering, Linköping University.

[McKelvey et al., 1996] McKelvey, T., Akçay, H., and Ljung, L. (1996). Subspace-based multivariable system identification from frequency response data. *IEEE Transactions on Automatic Control*, 41(7):960–979.

[Miller and De Callafon, 2013] Miller, D. and De Callafon, R. (2013). Subspace identification with eigenvalue constraints. *Automatica*.

[Moore, 1996] Moore, K. (1996). Iterative learning control for deterministic systems. *Automatica*, 6(32):948–949.

[MOR Toolbox, 2018] MOR Toolbox (2018). `http://mordigitalsystems.fr/en/`.

[Nicoletti et al., 2017] Nicoletti, A., Martino, M., and Karimi, A. (2017). A data-driven approach to power converter control via convex optimization. In *2017 IEEE Conference on Control Technology and Applications (CCTA)*, pages 1466–1471. IEEE.

[Panzani et al., 2012] Panzani, G., Formentin, S., and Savaresi, S. M. (2012). Active motorcycle braking via direct data-driven load transfer scheduling. *IFAC Proceedings Volumes*, 45(16):1257–1262.

[Passenbrunner et al., 2012] Passenbrunner, T. E., Formentin, S., Savaresi, S. M., and del Re, L. (2012). Direct data-driven control of internal combustion engine test benches using closed-loop experiments. In *2012 IEEE 51st IEEE Conference on Decision and Control (CDC)*, pages 3765–3770. IEEE.

[Phillips and Allemang, 2003] Phillips, A. W. and Allemang, R. J. (2003). An overview of mimo-frf excitation/averaging/processing techniques. *Journal of Sound and vibration*, 262(3):651–675.

[Piga et al., 2018] Piga, D., Formentin, S., and Bemporad, A. (2018). Direct data-driven control of constrained systems. *IEEE Transactions on Control Systems Technology*, 26(4):1422–1429.

[Pintelon and Schoukens, 2012] Pintelon, R. and Schoukens, J. (2012). *System identification: a frequency domain approach*. IEEE Press.

[Pintelon et al., 2010a] Pintelon, R., Schoukens, J., Vandersteen, G., and Barbé, K. (2010a). Estimation of nonparametric noise and frf models for multivariable systems—part i: Theory. *Mechanical Systems and Signal Processing*, 24(3):573–595.

[Pintelon et al., 2010b] Pintelon, R., Schoukens, J., Vandersteen, G., and Barbé, K. (2010b). Estimation of nonparametric noise and frf models for multivariable systems—part ii: Extensions, applications. *Mechanical Systems and Signal Processing*, 24(3):596–616.

[PISA Toolbox, 2018] PISA Toolbox (2018). INRIA Sophia-Antipolis, `https://project.inria.fr/pisa/`.

[Poussot-Vassal, 2019] Poussot-Vassal, C. (2019). *Large-scale dynamical model approximation and its applications*. PhD thesis, INP Toulouse.

[Pronzato, 2008] Pronzato, L. (2008). Optimal experimental design and some related control problems. *Automatica*, 44(2):303–325.

[Rachah et al., 2016] Rachah, A., Noll, D., Espitalier, F., and Baillon, F. (2016). A mathematical model for continuous crystallization. *Mathematical Methods in the Applied Sciences*, 39(5):1101–1120.

[Rallo, 2017] Rallo, G., F. S. R. C. R. O. T. . S. S. M. (2017). Data-driven $\mathcal{H}_\infty$-norm estimation via expert advice. In *Proceedings of the 56th IEEE Conference on Decision and Control*, pages 1560–1565. IEEE.

[Rapisarda and Antoulas, 2016] Rapisarda, P. and Antoulas, A. C. (2016). A bilinear differential forms approach to parametric structured state-space modelling. *Systems & Control Letters*, 92:14–19.

[Saeki et al., 2010] Saeki, M., Ogawa, M., and Wada, N. (2010). Low-order h controller design on the frequency domain by partial optimization. *International Journal of Robust and Nonlinear Control: IFAC-Affiliated Journal*, 20(3):323–333.

[Safonov and Tsao, 1995] Safonov, M. and Tsao, T.-C. (1995). The unfalsified control concept: A direct path from experiment to controller. In *Feedback Control, Nonlinear Systems, and Complexity*, pages 196–214. Springer.

[Safonov, 2006] Safonov, M. G. (2006). Data-driven robust control design: Unfalsified control. Technical report, UNIVERSITY OF SOUTHERN CALIFORNIA LOS ANGELES DEPT OF ELECTRICAL ENGINEERING.

[Safonov and Tsao, 1994] Safonov, M. G. and Tsao, T.-C. (1994). The unfalsified control concept and learning. In *Proceedings of 1994 33rd IEEE Conference on Decision and Control*, volume 3, pages 2819–2824. IEEE.

[Sala and Esparza, 2005] Sala, A. and Esparza, A. (2005). Extensions to "virtual reference feedback tuning: A direct method for the design of feedback controllers". *Automatica*, 41(8):1473–1476.

[Selvi et al., 2018] Selvi, D., Piga, D., and Bemporad, A. (2018). Towards direct data-driven model-free design of optimal controllers. In *European Control Conference*, pages 2836–2841. IEEE.

[Seron et al., 1997] Seron, M. M., Braslavsky, J. H., and Goodwin, G. C. (1997). *Fundamental limitations in filtering and control*. Springer Science & Business Media.

[Sjöberg, 2005] Sjöberg, J. (2005). *Descriptor systems and control theory*. Linköping University Electronic Press.

[Sjöberg et al., 2003] Sjöberg, J., De Bruyne, F., Agarwal, M., Anderson, B., Gevers, M., Kraus, F., and Linard, N. (2003). Iterative controller optimization for nonlinear systems. *Control Engineering Practice*, 11(9):1079–1086.

[Sjöberg et al., 2009] Sjöberg, J., Gutman, P.-O., Agarwal, M., and Bax, M. (2009). Nonlinear controller tuning based on a sequence of identifications of linearized time-varying models. *Control Engineering Practice*, 17(2):311–321.

[Tóth, 2010] Tóth, R. (2010). *Modeling and identification of linear parameter-varying systems*. Springer.

[Van Helvoort et al., 2005] Van Helvoort, J., De Jager, B., and Steinbuch, M. (2005). Unfalsified control using an ellipsoidal unfalsified region applied to a motion system. *IFAC Proceedings Volumes*, 38(1):157–162.

[Van Helvoort et al., 2007] Van Helvoort, J., de Jager, B., and Steinbuch, M. (2007). Direct data-driven recursive controller unfalsification with analytic update. *Automatica*, 43(12):2034–2046.

[Van Helvoort, 2007] Van Helvoort, J. J. M. (2007). Unfalsified control: data-driven control design for performance improvement. *Technische Universiteit Eindhoven, Eindhoven, Netherlands*.

[Van Heusden, 2010] Van Heusden, K. (2010). Non-iterative data-driven model reference control.

[Van Heusden et al., 2007] Van Heusden, K., Karimi, A., and Bonvin, D. (2007). Data-driven estimation of the infinity norm of a dynamical system. In *2007 46th IEEE Conference on Decision and Control*, pages 4889–4894. IEEE.

[van Heusden et al., 2008] van Heusden, K., Karimi, A., and Bonvin, D. (2008). Data-driven controller tuning with integrated stability constraint. In *2008 47th IEEE Conference on Decision and Control*, pages 2612–2617. IEEE.

[Van Heusden et al., 2009] Van Heusden, K., Karimi, A., and Bonvin, D. (2009). Data-driven controller validation. In *Proceedings of the 15th IFAC Symposium on System Identification*, pages 1050–1055.

[Van Heusden et al., 2011a] Van Heusden, K., Karimi, A., and Bonvin, D. (2011a). Data-driven model reference control with asymptotically guaranteed stability. *International Journal of Adaptive Control and Signal Processing*, 25(4):331–351.

[Van Heusden et al., 2011b] Van Heusden, K., Karimi, A., and Söderström, T. (2011b). On identification methods for direct data-driven controller tuning. *International Journal of Adaptive Control and Signal Processing*, 25(5):448–465.

[Vinnicombe, 1993] Vinnicombe, G. (1993). Frequency domain uncertainty and the graph topology. *IEEE Transactions on Automatic Control*, 38(9):1371–1383.

[Vollmer and Raisch, 2001] Vollmer, U. and Raisch, J. (2001). H-control of a continuous crystallizer. *Control Engineering Practice*, 9(8):837–845.

[Wahlberg et al., 2010] Wahlberg, B., Syberg, M. B., and Hjalmarsson, H. (2010). Non-parametric methods for l2-gain estimation using iterative experiments. *Automatica*, 46(8):1376–1381.

[Wang and Safonov, 2002] Wang, R. and Safonov, M. G. (2002). The comparison of unfalsified control and iterative feedback tuning. *University of Southern California, USA*.

[Xu and Hou, 2009] Xu, J.-X. and Hou, Z.-S. (2009). Notes on data-driven system approaches. *Acta Automatica Sinica*, 35(6):668–675.

[Yin et al., 2014] Yin, S., Gao, H., and Kaynak, O. (2014). Data-driven control and process monitoring for industrial applications—part i. *IEEE Transactions on Industrial Electronics*, 61(11):6356–6359.

[Yin et al., 2015] Yin, S., Gao, H., and Kaynak, O. (2015). Data-driven control and process monitoring for industrial applications—part ii. *IEEE Transactions on Industrial Electronics*, 62(1):583–586.

[Zhou and Doyle, 1998] Zhou, K. and Doyle, J. C. (1998). *Essentials of robust control*, volume 104. Prentice hall Upper Saddle River, NJ.

[Zhou et al., 1996] Zhou, K., Doyle, J. C., Glover, K., et al. (1996). *Robust and optimal control*, volume 40. Prentice hall New Jersey.

[Ziegler and Nichols, 1942] Ziegler, J. and Nichols, N. (1942). Optimum settings for automatic controllers. *trans. ASME*, 64(11).